ESTIMATION OF BIAS-CORRECTED HIGH-RESOLUTION RADAR PRECIPITATION MAPS USING THE RADAR AND RAIN GAUGE NETWORK OVER TURKEY

A THESIS SUBMITTED TO
THE GRADUATE SCHOOL OF NATURAL AND APPLIED SCIENCES
OF
MIDDLE EAST TECHNICAL UNIVERSITY

BY

KAVEH PATAKCHI YOUSEFI

IN PARTIAL FULFILLMENT OF THE REQUIREMENTS
FOR
THE DEGREE OF MASTER OF SCIENCE
IN
CIVIL ENGINEERING

AUGUST 2020

Approval of the thesis:

ESTIMATION OF BIAS-CORRECTED HIGH-RESOLUTION RADAR PRECIPITATION MAPS USING THE RADAR AND RAIN GAUGE NETWORK OVER TURKEY

submitted by **Kaveh Patakchi Yousefi** in partial fulfillment of the requirements for the degree of **Master of Science** i**n Civil Engineering, Middle East Technical University** by,

Prof. Dr. Halil Kalıpçılar
Dean, Graduate School of **Natural and Applied Sciences** _____

Prof. Dr. Ahmet Türer
Head of the Department, **Civil Engineering** _____

Assoc. Prof. Dr. M. Tuğrul Yılmaz
Supervisor, **Civil Engineering, METU** _____

Dr. Kurtuluş Öztürk
Co-Supervisor, **Remote Sensing Department, General Directorate of Meteorology** _____

Examining Committee Members:

Prof. Dr. İsmail Yücel
Civil Engineering, METU _____

Assoc. Prof. Dr. M. Tuğrul Yılmaz
Civil Engineering, METU _____

Assoc. Prof. Dr. Koray Kamil Yılmaz
Geological Engineering, METU _____

Prof. Dr. Elçin Kentel Erdoğan
Civil Engineering, METU _____

Assist. Prof. Dr. Gökçen Uysal
Civil Engineering, Eskişehir Technical University _____

Date: 13.08.2020

I hereby declare that all information in this document has been obtained and presented in accordance with academic rules and ethical conduct. I also declare that, as required by these rules and conduct, I have fully cited and referenced all material and results that are not original to this work.

Name, Last name :

Signature :

ABSTRACT

ESTIMATION OF BIAS-CORRECTED HIGH-RESOLUTION RADAR PRECIPITATION MAPS USING THE RADAR AND RAIN GAUGE NETWORK OVER TURKEY

Patakchi Yousefi, Kaveh
Master of Science, Civil Engineering
Supervisor: Assoc. Prof. Dr. M. Tuğrul Yılmaz
Co-Supervisor: Dr. Kurtuluş Öztürk

August 2020, 123 pages

Meteorological weather radars can provide spatio-temporally high resolution precipitation estimates. Nevertheless, these estimates are prone to systematic and random errors due to the indirect nature of the measurement algorithm of radars. Gauge-based observations are known to be complementary data for reducing the radar-based estimation errors. In this study, the precipitation data retrieved from seventeen C-band meteorological weather radars in Turkey are merged with the station-based precipitation observations to obtain a spatially-continous high accuracy quantitative precipitation estimates (QPE). In contrast to the previous studies which focused on limited methodology, region or number of events, this study impliments, investigates and validates four gauge adjustment [Mean Field Bias (MFB), Local Multiplicative Bias (LMB), Local Additive Bias (LAB), Local Mixed Bias (LMIB)] and four time-independent [Multiple Linear Regression (MLR), Artificial Neural Network (ANN), Cumulative Distribution Function (CDF), Z-R Matching (Z-R)] bias correction methods over all the operating radars during the years 2014-2018. The relative performances of these bias correction methodologies were compared both spatially and temporally in training, and validation datasets.

Among these methodologies, a consistent algorithm (LAB) that generally results in the highest QPE performance was used in producing a high-resolution composite precipitation map. The datasets and maps produced in this study can be used as a significant input and contribution for future hydrology and water resources studies.

Keywords: Radar Precipitation, Bias Correction, Precipitaiton Estimation

ÖZ

TÜRKİYE ÜZERİNDE RADAR VE YAĞIŞ İSTASYON AĞINI KULLANARAK İYİLEŞTİRİLMİŞ YÜKSEK ÇÖZÜNÜRLÜKLÜ RADAR YAĞIŞ HARİTALARININ TAHMİNİ

Patakchi Yousefi, Kaveh
Yüksek Lisans, İnşaat Mühendisliği
Tez Yöneticisi: Doç. Dr. Mustafa Tuğrul Yılmaz
Ortak Tez Yöneticisi: Dr. Kurtuluş Öztürk

Ağustos 2018, 123 sayfa

Meteorolojik hava radarları zamansal ve mekansal açıdan yüksek çözünürlükte yağış tahminleri sağlayabilir. Fakat bu tahminler radarların doğrudan olmayan ölçüm teknikleri sebebiyle sistematik ve rastgele hatalara eğilimlidir. Yer gözlem istasyonlarından elde edilen yağış verileri, radar tabanlı tahmin hatalarını azaltmak amacıyla kullanılan tamamlayıcı veriler olarak bilinmektedir. Bu çalışmada, Türkiye'de bulunan 17 C-bandı meteorolojik hava tahmin radarlarından elde edilen yağış verileri, mekansal olarak sürekli ve yüksek doğrulukta sayısal yağış tahminleri (QPE) elde etmek amacı ile istasyon tabanlı yağış gözlemleri ile birleştirilmiştir. İşlemler sırasında kullanılan metot, bölge ve olay sayısı bakımından sınırlı sayıda olan geçmiş çalışmaların aksine bu çalışma 4 tane ölçüm ayarlama metodu (MFB, LMB, LAB, LMIB), 4 tane de zamandan bağımsız hata düzeltme metodu (MLR, ANN, CDF, Z-R) aracılığıyla 2014-2018 yılları arasında ülkede işletmede olan tüm radarları incelemiş, uygulamış ve doğrulamıştır. Bu hata düzeltme metotlarının göreceli performansları öğrenme, doğrulama ve test veri kümelerinde hem mekansal hem de zamansal açıdan karşılaştırılmıştır. Bu metotlar arasında en yüksek

doğrulukta QPE değerleri veren tutarlı algoritmalar yüksek çözünürlükte birleşik yağış haritası üretiminde kullanılmıştır. Bu çalışma kapsamında üretilen bu veri ve haritalar ülkemizde gerçekleştirilecek hidroloji ve su kaynakları çalışmalarında önemli bir girdi verisi olarak kullanılabilir ve yüksek katkıda bulunabilir.

Anahtar Kelimeler: Radar Yağışı, Hata Düzeltme, Yağış Tahmini

This thesis is dedicated to my wonderful family, my grandmother, and my friends. They have given me all the hope and energy to accomplish my goal.

ACKNOWLEDGMENTS

There are a number of people without whom this thesis might not have been written, and to whom I am greatly thankful.

I would like to express my deepest gratitude to my supervisor, Assoc. Prof. Dr. M. Tuğrul Yılmaz, who was always there when I needed guidance starting from the first moments of my master's study. He taught me how to be an independent researcher. Nevertheless, he would not mind helping me proceed with all my analyses and studies smoothly by arranging in-demand meetings even at the weekend. I could never have wished for a better supervisor, and I look forward to working with him again in the future.

I have greatly benefited from all the supports and feedbacks given by my co-supervisor, Dr. Kurtuluş Öztürk. I am grateful for his knowledge and constructive comments, which have helped me a lot in my master's study. Also, he has patiently provided terabytes of meteorological data used in this study. Without his support, I could not accomplish my study.

I am grateful to my professors Prof. Dr. İsmail Yücel and Assoc. Prof. Dr. Koray Yılmaz, who guided me with their critical and constructive comments in numerous meetings held during my master’s study.

I wish to thank the members of my dissertation committee: Prof. Dr. İsmail Yücel, Assoc. Prof. Dr. Tuğrul Yılmaz, Assoc. Prof. Dr. Koray Yılmaz, Prof. Dr. Elçin Kentel, and Dr. Gökçen Uysal for generously offering their time, support, guidance and good will throughout the preparation and review of this document.

The technical assistance of remote sensing team, especially Alper Çubuk, Canberk Karadavut, and Sema Çil Keydal in General Directorate of Meteorology, are gratefully acknowledged.

Pursuing master’s and living in a foreign country for the first time, comes with its own hardships, which cannot be overcome without moral support. Thanks to my

family for being so morally supportive during my stay out of the home. They have been my motivation in every step of my life, and I honestly could not conquer life challenges without them. I would also like to thank my grandmother, my aunts, and my cousins, for their love and endless support.

I am grateful to my best friend, co-traveler, co-chef, and partner Sonia, for her love and belief in me. She inspires me with her determination and hard work every day, and she backed me up in completing my thesis.

My special gratitude goes for Soheil Pouraltafi, who has been a supportive and best friend of mine not only in ordinary but also in academic steps of life. I am looking forward to seeing his success in every moment of his life.

I would like to thank my research group members: Mehdi Hesami Afshar, Eren Düzenli, Burak Bulut, Muhammed Amjad, Erhan Ersoy, Ipek Karasu, Azar Arghavanian and Farhad Ghiaei for all their assistance and support. I have learned a lot from them, and they have had a substantial positive impact on my academic life.

I would like to acknowledge the financial support of TUBİTAK (PROJECT NO: 117Y118), which funded my entire Master's studies.

TABLE OF CONTENTS

LIST OF TABLES

TABLES

LIST OF FIGURES

FIGURES

LIST OF ABBREVIATIONS

ABBREVIATIONS

AF	Assessment Factor
AFY	Afyon Meteorological Weather Radar
ANK	Ankara Meteorological Weather Radar
ANN	Artificial Neural Network
ANT	Antalya Meteorological Weather Radar
AWOS	Automatic Weather Observation Station
BBF	Beam Blockage Fraction
BLK	Balıkesir Meteorological Weather Radar
BRS	Bursa Meteorological Weather Radar
CBB	Cumulative Beam Blockage
CBB-AV	Average Cumulative Beam Blockage
CDF	Cumulative Distribution Function
COR	Correlation Coefficient
MLR	Multiple Linear Regression
DEM	Digital Elevation Model
ERZ	Erzurum Meteorological Weather Radar
ESD	Error Standard Deviation
FFT	Fast Fourier Transform
GZT	Gaziantep Meteorological Weather Radar

HTY	Balıkesir Meteorological Weather Radar
Hvmin	Minimum Height of Visibility (m)
IDW	Inverse Distance Weighted
IST	İstanbul Meteorological Weather Radar
IZM	İzmir Meteorological Weather Radar
KRM	Karaman Meteorological Weather Radar
LMB	Local Multiplicative Bias
LMIB	Local Mixed Bias
LAB	Local Additive Bias
ME	Mean Error
MGL	Muğla Meteorological Weather Radar
GDM	General Directorate of Meteorology
NEXRAD	Next-Generation Radar
NWP	Numerical Weather Prediction
MFB	Mean Field Bias
OPERA	Operational Program for Exchange of Weather Radar Information
PMM	Probability Matching Method
QPE	Quantitative Precipitation Estimation
RAIN1	Hourly Accumulated Radar Precipitation Estimation
RMSE	Root Mean Squared Error
RQI	Radar Quality Index

SMN	Samsun Meteorological Weather Radar
SRF	Şanlıurfa Meteorological Weather Radar
SRTM	Shuttle Radar Topography Mission
SVS	Sivas Meteorological Weather Radar
TMM	Traditional Matching Method
TRZ	Trabzon Meteorological Weather Radar
VPR	Vertical Profile of Reflectivity
WCMM	Window Correlation Matching Method
WMO	World Meteorology Organization
WPMM	Window Probability Matching Method
ANN	Artificial Neural Network
ZNG	Zonguldak Meteorological Weather Radar

CHAPTER 1

INTRODUCTION

1.1 Motivation

1.1.1 Background

Owing to its role in the water and the energy balances, precipitation is one of the most significant inputs in hydrological and meteorological applications, such as studies related to droughts, floods, climate change, and water potential of basins. High accuracy QPE and their forecasts with high temporal and spatial resolutions are of great interest for many studies, as precipitation has very complex spatiotemporal variability (Berne and Krajewski, 2013). Such estimates are particularly useful in hydrological modeling applications, estimating runoff, and calibrating the parameters that best reflect the characteristics of basins (McKee and Binns, 2016; Arnaud et al., 2011).

Precipitation estimates could be acquired via several different platforms, such as station gauge-based observations, numerical weather prediction (NWP) model-based estimates, and remote sensing-based estimates (e.g., satellite- or ground radar-based). Station-based rain-gauges have long been used for monitoring precipitation (e.g., around a century over Turkey). They typically provide high-accuracy precipitation observations due to their "direct measurement principle" (Bianchi, Van Leeuwen, Hogan, and Berne, 2013), hence regarded as the most accurate precipitation estimates. However, gauge-based observations face various uncertainties and disadvantages associated with the type of precipitation, geographic location, or systematic deficiencies. Measurement errors of these observations

primarily stem from environmental effects such as wind, while shortcomings in maintenance/calibration or systematic/mechanical deficits also exist (Jewell and Gaussiat, 2015; Larson and Peck, 1974; McKee and Binns, 2016; Yilmaz et al., 2005). Even though such uncertainties exist, gauge-based precipitation observations are still regarded as the most accurate estimates, and the other precipitation estimates are almost always validated against gauge-based observations as ground truth (Amjad et al. 2020; Barton et al. 2020; Goudenhoofdt and Delobbe 2009; Mahavik 2017; Sharifi, Steinacker, and Saghafian 2016; Sokol 2003). On the other hand, station gauge-based observations are point-scale datasets; hence, they may yield representativeness errors when spatially average precipitation estimates are needed mainly when the station network is not dense. Moreover, the installation of a high-density gauge network may not be possible over most locations because of installation and maintenance costs. Currently, the gauge density over Turkey is around 500 km^2/station (i.e., around 1500 ground stations for 783.562 km^2 area), while the recommended area per gauge station is 250 km^2/station for mountainous regions and 575 km^2/station for hilly/undulating regions (WMO 2008). Considering Turkey has very complex and mountainous topography, 500 km^2/station is not sufficient to provide high accuracy precipitation estimates over most locations.

Accordingly, the use of spatially and temporally continuous and consistent products (e.g., NWP model- or remote sensing-based) are needed to provide products that represent spatially average estimates. At the same time, such datasets should be validated with the existing station-based observations for the characterization of their accuracies. Satellite-based remote sensing observations are also utilized for estimation of precipitation, while most such products have a relatively lower spatial and temporal resolution (Global Precipitation Measurement precipitation product has ~10 km spatial resolution, Tropical Rainfall Measuring Mission-based products have ~25 km spatial resolution) and temporal resolutions (~1.5 hours revisiting time for GPM, and ~3 hours for other polar-orbiting satellites). NWP models also provide high accuracy estimates of precipitation. However, most NWP models that are currently used have spatial resolutions varying between 4-10 km (Amjad et al. 2020).

While spatial resolutions between 4-25 km could be sufficient for many applications (e.g., studies related with the characterization of drought), higher spatial resolution precipitation estimates ($\leq$ 5 km for stratiform and $\leq$ 1 km for convective events) are particularly desired for hydrological applications focusing on flood runoff estimation under severe weather conditions and for urban hydrology (Schilling 1991; Shakti, Nakatani, and Misumi 2019).

Alternatively, meteorological radar-based products may provide a higher spatial resolution (0.33 km-4 km) and temporal resolution (2.5 min-60 min) precipitation estimates (Barton et al. 2020; Ozkaya and Akyurek 2019; Park, Berenguer, and Sempere-Torres 2019; J. Zhang et al. 2011; X. Zhang and Srinivasan 2010). Radars do not measure the precipitation directly, while their observations of volumetric reflectivity backscattered from particles above the ground are converted into precipitation intensity using various relationships between reflectivity-rainfall (Z-R). Thus, radar-based estimates are prone to various sources of error, either associated with the calculation of reflectivity or calibration of reflectivity-rainfall (Z-R) relationships. Such sources of error are incorporated systematically and randomly into the estimation capability of radars (Berne and Krajewski, 2013).

Combining the advantageous aspects of gauge-based observations and radar-based estimates to eliminate the systematic and the random errors has been the main motivation for many studies that merge radar- and station-based measurements to improve the accuracy of precipitation estimates (Goudenhoofdt and Delobbe, 2009; McKee and Binns, 2016; P. Yousefi et al., 2020; Sinclair and Pegram, 2005). These applications are various depending on the assumptions made on the type of errors in the estimations. The first type of approach concentrates on radar reflectivity measurement before rainfall estimation. Developing correction algorithms for reflectivity-related error sources such as attenuation, ground clutter, beam blockage, anomalous propagation, range effects has long been the main focus in the literature (Marco Gabella, Joss, and Perona 2000; Hunter 1996; Rahimi et al. 2006). Another approach determines different methods to match radar reflectivities with rainfall rates (Z-R relationships) using regression-, and probability-based methods (Ayat,

Reza Kavianpour, Moazami, Hong, and Ghaemi, 2018; Lee, Kim, and Suk, 2015; Piman, Babel, Gupta, and Weesakul, 2007; Rosenfeld, Wolff, and Amitai, 1994; Teschl, Randeu, and Teschl, 2007). Finally, other approaches rely on a static Z-R relationship (mostly Marshal Palmer) and use the rain-gauge measurements as references to correct the radar-based estimates at different time steps (10 minutes, 1-hour, 6-hour, daily). The corrections are implemented by calculating multiplicative/additive radar-gauge pairs for adjustment, or merging methods (M. Gabella and Amitai, 2000; Jewell and Gaussiat, 2015; McKee and Binns, 2016; Sahlaoui, 2019).

In the recent decade, several studies have been published on projects supported by the national weather services of different countries worldwide. SUK et al. (2013) developed an operational QPE correction for ten radars in South Korea. Park et al. (2019) validated a bias correction method initially developed by Brandes (1975) on The Operational Program on the Exchange of Weather Radar Information (OPERA) over a long-term period. Since June 2006, The National Mosaic and Multi-Sensor Quantitative Precipitation Estimation system have been running in real-time. This system produces several products based on merged radar and rain-gauge data in the United States of America (J. Zhang et al. 2011). All of these studies above have proved improved precipitation accumulations on hourly/daily scales.

1.1.2 Problem Statement

Real-time and time-dependent radar-gauge bias correction and merging models developed by researchers have shown promising results in improving the gridded radar-based QPE. This type of approach demands the availability of rain-gauge data. While investigating the opportunities obtained by such methods is very crucial, the real-time correction of the improved radar-based product is highly dependent on the availability of a high-density gauge station network at each time step. In operational practice, it would be very beneficial to examine the time-independent methods, as well. Among the time-independent methods, the majority of the studies have focused

on determining several fitted Z-R relationships on a specific environment or type of precipitation. However, another solution is to link the associated radar estimation errors with three stationary parameters: distance from the radar, height, and the minimum height of visibility. This approach has initially been developed by Gabella et al. (2000), and a great case-study was exemplified by Öztürk and Yilmazer (2007).

Nevertheless, some assumptions made in these studies can be revised. In the previous approaches, the logarithmic errors (referred to as assessment factors) are assumed to be linearly dependent on three time-independent parameters. However, other "non-linear" relationships must also be tested by utilizing other non-linear methods such as Artificial Neural Networks (ANN) in addition to Multiple Linear Regression (MLR). Finally, the effect of Cumulative Beam Blockage (CBB) in calculating one of these stationary parameters, Hvmin, has been neglected. So, Hvmin values must be recalculated by considering the ratio of the radar beam that is blocked.

Operational concerns demand an estimation technique that suits the constraints of each environment temporally and spatially (McKee and Binns, 2016). Therefore, in order to generalize radar-gauge merging techniques for other locations and radar instruments, they must be applied over a long-term period on different forms of topography and settings. Goudenhoofdt and Delobbe (2009) have assessed several radar-gauge merging methods such as kriging with external drift, ordinary kriging, mean field bias correction in a long-term period on a single radar. In a recent study (Park, Berenguer, and Sempere-Torres 2019), a long-term analysis of a simple gauge adjustment method was tested over on a multi-national scale. Large-scale and long-term validation of other gauge adjustment methods and time-independent approaches has not been dealt with in-depth approaches. Even for conventional methods, temporal/geographical/systematic variations demand further research. Considering these variations, and the complexity of the topography in Turkey (Amjad, 2020), the feasibility of such methodologies can be tested over the meteorological radar network in Turkey, so that other countries' meteorological services can take advantage of the outcome.

In Turkey, the General Directorate of Meteorology (GDM) has initially started monitoring the weather using 12 radars installed in various regions since 2000, but after installation of 6 more radars, currently, there are a total of 17 C-band and one X-band meteorological radars. The list of these radars is given in Table 1.1.

Table 1.1 The list of 18 meteorological weather radars in Turkey

CITY	INSTALLATION YEAR	LONGITUDE (DEGREE)	LATITUDE (DEGREE)	BAND	TYPE
ANKARA	2000	32.9714	39.7986	C	Single Pol. Doppler
İSTANBUL	2003	28.355	41.345	C	Single Pol. Doppler
BALIKESIR	2003	27.6183	39.74	C	Single Pol. Doppler
ZONGULDAK	2003	31.6983	41.1819	C	Single Pol. Doppler
ANTALYA	2012	30.4375	36.2664	C	Single Pol. Doppler
İZMIR	2011	27.0011	38.3114	C	Multi Pol. Doppler
HATAY	2011	35.7882	36.318	C	Multi Pol. Doppler
MUĞLA	2010	28.3325	36.8859	C	Multi Pol. Doppler
TRABZON	2012	39.4683	41.0747	C	Single Pol. Doppler
SAMSUN	2012	36.0367	41.3147	C	Single Pol. Doppler
AFYONKARAHISAR	2015	30.4192	38.4017	C	Multi Pol. Doppler
GAZIANTEP	2016	37.1372	37.1372	C	Multi Pol. Doppler
ŞANLIURFA	2017	39.8289	37.7167	C	Multi Pol. Doppler
BURSA	2015	29.9033	40.5383	C	Multi Pol. Doppler
SIVAS	2016	36.8544	39.7656	C	Multi Pol. Doppler
KARAMAN	2015	33.1397	37.3922	C	Multi Pol. Doppler
ERZURUM	2017	41.5567	40.1603	C	Multi Pol. Doppler
MOBILE	2014	40.1247	32.9931	X	Multi Pol. Doppler

The qualitative aspects of meteorological radars have long been studied in Turkey. However, the quality control of QPE is not well-studied yet because most of the practices only cover a particular region and a limited number of events. Even though radar-based estimates need gauge-based corrections, there are only a few studies focused on this aspect. Among these studies, Öztürk and Yilmazer (2007) have proposed a time-independent regression-based method over 48 hours rainfall event for Balıkesir radar over the locations of the gauge stations. Three time-independent parameters (associated with the location of the rain-gauges and the radar) were used

for estimating the amount of error over all rain-gauges. This study was later tested on Istanbul radar and extended to estimating errors in all radar pixels by Ozturk et al. (2012). Ozkaya and Akyurek (2019) developed a Mean Field Bias (MFB) correction using the estimations of Samsun radar only from 8 events observed at 13 rain gauge stations. Thus, all existing literature about the use of radar-observations over Turkey has only focused on some limited events (e.g., over a couple of days/events) or locations (e.g., on a specific radar). In contrast, an algorithm that corrects the entire radar-based records to acquire consistently corrected datasets are needed. Additionally, even though there are 18 weather radars, an algorithm that merges all of these products over Turkey to create a single blended product is needed for the use in various hydrological studies.

The available radar data can only be accessed through a software offered by the manufacturer company and only runs in LINUX environment, which is one of the biggest obstacles faced by researchers and practitioners using long-term time-series analysis of radar data (i.e., many graduate students and researchers in Turkey are more used to Windows operating system). The ability to access the radar data in commonly known operating systems such as Windows will increase the applications related to radar data in our country. This study can be a starting point for large-scale radar-based QPE studies by opening the radar data for easier access for academics (can be requested from GDM) and initializing a study which represents country-wise solutions in finding a consistent method for radar bias correction. The resulting composite maps consisting of the improved radar-based estimations obtained from all 17 C-band radars are expected to be used in many studies, especially hydrology, meteorology, and agriculture, and it is also expected to form a base for many future studies.

1.2 Objectives and Goals of the Study

Given the above problems that exist in the current literature, the objectives of this study are listed as follows:

- Initial analysis and validation of radar-based estimates using gauge-based observations over the entire radar network in Turkey over five years (2014-2018);
- Long-term spatio-temporal validation of the performance of gauge adjustment and time-independent bias correction methods using the training and validation datasets over the years 2014-2018;
- Production and validation of composite high spatial resolution (1 km) precipitation maps over entire Turkey based on bias-corrected radar data over the years 2014-2018;
- Selection of a consistent algorithm for bias correction of the entire radar dataset archive over Turkey.

The above objectives will help to achieve the goal of investigating, developing, and validating various bias correction methods for improving the radar-based precipitation estimations by merging observations made from radar and rain-gauge networks over Turkey and produce a high-resolution precipitation map of Turkey. In order to reach this goal, these questions must be addressed:

- What is the accuracy of the available radar-based observations obtained from GDM in terms of agreement with the rain-gauges over different time scales?
- Which approaches have been previously developed and tested for improving radar-based QPE in the literature?
- Do gauge adjustment methods improve all statistics, including RMSE, mean error, and standard deviation both in the training and validation datasets, and which gauge adjustment performs better in terms of agreement with the rain-gauges?
- What are the limitations of the time-independent bias correction methods available in the literature, and do the new approaches have enough generalization ability, and how well can they improve all error statistics?
- What are the advantages of a composite radar-gauge merged over radar-only product?

1.3 Structure of the Thesis

The structure of the thesis is as follows:

- Chapter 2 provides information about the datasets, bias-correction methodologies, and evaluation of the radar-based datasets.
- Chapter 3 covers the initial investigation of the accuracy of radar-based estimations and evaluation of the bias-corrected radar-based estimations against the rain gauge observations
- Chapter 4 presents a summary of the results and concludes the main findings of the dissertation

CHAPTER 2

METHODOLOGY

2.1 Datasets

Two types of data (Station-Based and Radar-Based) were used in this study. Figure 2.1 shows a preview of the data used in the study. The red circles indicate the locations of 17 C-band radars with a range of 120 km. The maximum range of each radar is variable (e.g., 120, 125, 250 km) dependent on operational policies. Figure 2.2 depicts the position of radars and other stations, assuming all radars have a maximum range of 250 km. However, in this study, only the radar data obtained from an optimum range of 120 km was used (see section 2.1.2.4). All of these radars are currently operating, and their data is available. The locations of the stations (AWOS, Triple-Collocated gauges, and optical disdrometers) are given as well. The AWOS rain gauge data are mainly used for improving radar-based estimations (see 2.2). The collocated gauges are used as test fields (see 2.3.2), and the disdrometers are used for specifying Z-R relationships (see 2.2.2.4).

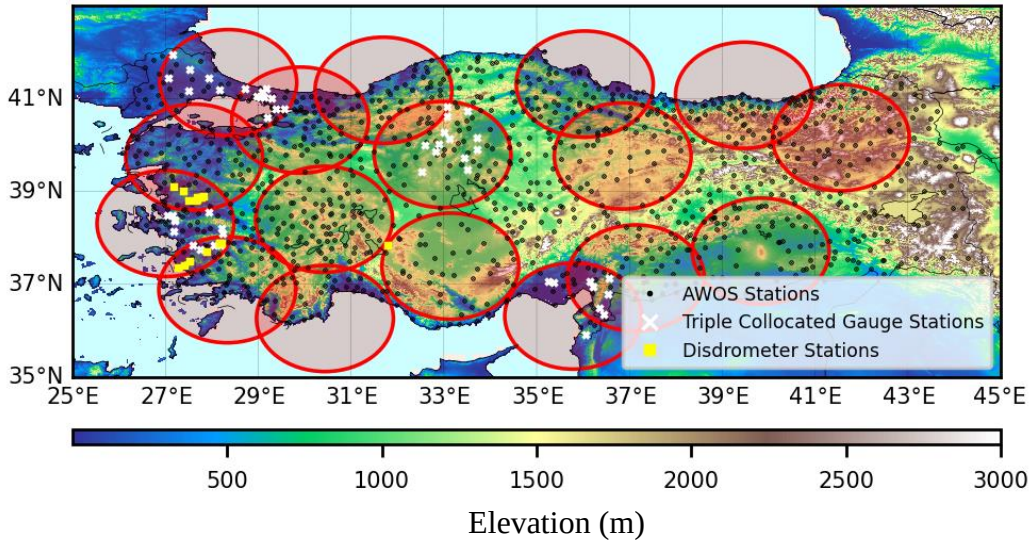

Figure 2.1 AWOS, Triple-Collocated, optical disdrometers stations, and the C-band meteorological weather radar locations plotted over digital elevation map over Turkey. The range of radars is 120 km.

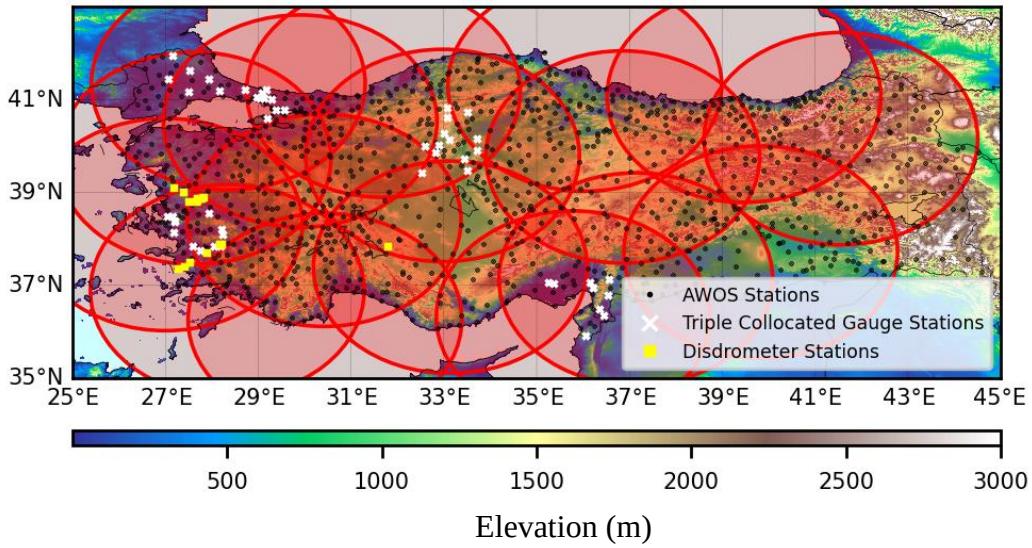

Figure 2.2 AWOS, Triple-Collocated, optical disdrometers stations, and the C-band meteorological weather radar locations plotted over digital elevation map over Turkey. The range of radars shown in this map is 250 km.

2.1.1 Station-Based

2.1.1.1 AWOS

Traditionally, one of the widely used methods for measuring precipitation in hydrology is a rain-gauge. Different types of instruments, such as tipping bucket rain-gauges, weighing rain gauges, optical rain gauges, and disdrometers, are used for recording rainfall activity (McKee and Binns 2016). Rain-gauges generally provide good-quality point observations and a high temporal resolution. Typically, rain-gauges are regarded as instruments that provide the "ground truth" values. However, they can be prone to both random and systematic errors (Jewell and Gaussiat 2015). The majority of automatic weather observation stations (AWOS) in Turkey include both tipping bucket and weighing rain-gauges. The location of AWOS rain gauges is shown as black dots in Figure 2.1.

2.1.1.2 Triple-Collocated

Since 2013, GDM has recorded precipitation at 50 independent stations in four separate regions, three of which are located in overlapping areas between two radars. Each of these stations consists of one weighting and two tipping bucket rain gauges measuring the precipitation independently. The data from these stations were used as an independent observation dataset to test the precipitation estimation accuracy of the composite map over these regions (2.3.2). The locations of these stations are given as white crosses in Figure 2.1.

2.1.1.3 Disdrometer

Disdrometer is an optical device that measures drop size distribution, droplet diameter, and velocity. GDM has installed 16 disdrometers and has been receiving

minutely data from these devices since 2013. The locations of these instruments are marked as yellow squares in Figure 2.1.

2.1.1.4 Quality Control of Rain Gauge Data

The temporal resolution of the final composite maps generated in this study is 1-hour. However, the gauge station data used in this study are minutely accumulated precipitation data. The reason for using minutely accumulated data instead of hourly is to run a more profound quality control procedure, including minutely, hourly and yearly thresholds. The minutely station-based observation data obtained from GDM consists of records from 1742 AWOS stations from the years 2003-2019. These data were converted into hourly accumulated data after four quality control requirements introduced to ensure the accuracy of the rain gauge observations:

1. Any precipitation value greater than 30 mm/min is eliminated (here, this 30mm/min threshold to eliminate datasets as part of quality control is acquired from GDM).
2. If the precipitation data is available in at least 50 minutes out of 60 minutes in one hour, then hourly average precipitation is calculated utilizing these observations; otherwise, the minutely data for the particular hour is neglected.
3. A maximum hourly threshold is chosen. According to GDM, among all extreme events recorded by all gauge stations in Turkey until the year 2019, the highest recorded rate is 131mm/hr. Therefore, any observation data greater than 140 mm/hr is eliminated.
4. A standard deviation criterion was considered for stations that might have a repetition of entries (particularly zero values). A station is eliminated if its hourly standard deviation does not exceed 0.05 mm/hr for at least once in four years.
5. A dynamic maximum yearly limit is also taken into consideration. GDM provides long-term mean records of total annual precipitation based on

observations recorded from 1927 to 2018 according to every region in Turkey. If the yearly accumulated precipitation amount of a gauge station varies more than 60% in comparison with the long-term annual stats for the corresponding region, then it is neglected.

Among these quality control steps, the first three steps can result in removal of precipitation data in one or more stations. None of the first three steps resulted in removing a large ratio (more than half) of the gauge station data, so none of the stations were eliminated in these steps. The final two steps, however, resulted in removing the gauge stations. After these quality control steps, 1153 AWOS stations remained out of 1742 stations. The hourly time series obtained after the above quality control steps are used as "ground truth" dataset in this study for the bias correction and the validation of the merged products.

2.1.2 Radar-Based

2.1.2.1 Raw Datasets

RAIN1 (hourly accumulated precipitation) data is used in this study. The temporal resolution of a full volume scan of the radar data is 15 minutes. In the generation of RAIN1 precipitation estimation, Marshal- Palmer Z-R relationship ($Z = 200\,R^{1.6}$) is used to convert radar reflectivity to precipitation. Before this conversion, the radar reflectivity is clutter-filtered by Doppler filtering or FFT (Fast Fourier Transform) algorithm (Öztürk and Yilmazer, 2007)

2.1.2.2 Dataset Availability

Due to various installation and operational dates of each radar, they have different data availability status. Table 2.1 represents the starting date in which RAIN1 data has been available since.

Table 2.1 The starting dates of RAIN1 radar data availability

Radar Name	Available After (Year-Month)		Radar Name	Available After (Year-Month)
Afyon	2015-12		**İzmir**	2011-02
Ankara	2013-06		**Karaman**	2016-06
Balıkesir	2011-01		**Muğla**	2011-08
Bursa	2015-06		**Samsun**	2012-08
Antalya	2012-01		**Şanlıurfa**	2012-01
Gaziantep	2016-01		**Trabzon**	2013-02
Hatay	2011-08		**Zonguldak**	2007-04
İstanbul	2007-01		**Erzurum**	2017-01
Sivas	2017-01		-	-

The year 2017 is the first year in which RAIN1 data from all 17 radars are available. For the year 2017 and later, the composite precipitation map shall include data from all the radar. However, for years before 2017, not all radar-based data are going to exist on the map. However, the non-existing radar data gaps will be filled by the spatial interpolation of the station-based observations.

2.1.2.3 Reading the Data

The radar data files (RAIN1) need to be decoded by a program to be available on other operating systems such as Windows. Within this project, all radar datasets saved as IRIS binary dataset are extracted and saved as .rdata file (readable through R environment) by writing a program for decoding binary data on R and as .npz files (readable through Python environment) by writing scripts in Python environment and utilizing read_iris function in Wradlib (Heistermann, Jacobi, and Pfaff , 2013) module available in Python.

2.1.2.4 Upscaling and Trimming

During the operation of meteorological weather radars, different policies can be issued on the maximum range of radars according to different scenarios or expectations. Therefore, the maximum range in which each radar measures reflectivity can change from radar to radar and from time to time (e.g., from 120km to 250km). The changes in the range also affect the resolution (e.g., from 0.3km to 0.7km). In qualitative monitoring of the weather and early warning systems, longer ranges can be useful. However, for quantitative precipitation, longer distances are not recommended due to higher rates of inaccuracy (Goudenhoofdt and Delobbe 2009; Lengfeld et al. 2020; Öztürk and Yilmazer 2007). Thus, by trimming the radar images, the radar estimations from a maximum range of 120 km were used for creating a composite precipitation map. Also, all radar images were upscaled into a 1-km scale, which is the resolution of the final composite map. For upscaling, the area-weighted sum of the trimmed radar data with their original resolution was interpolated into 1-km scale grids. For example, if the original resolution is 0.333 km, then the sum of the area from 9 pixels were interpolated into a 1-km scale pixel. Examples of the trimming/upscaling procedure of radar images according to their initial range and resolution is given in Figure 2.3.

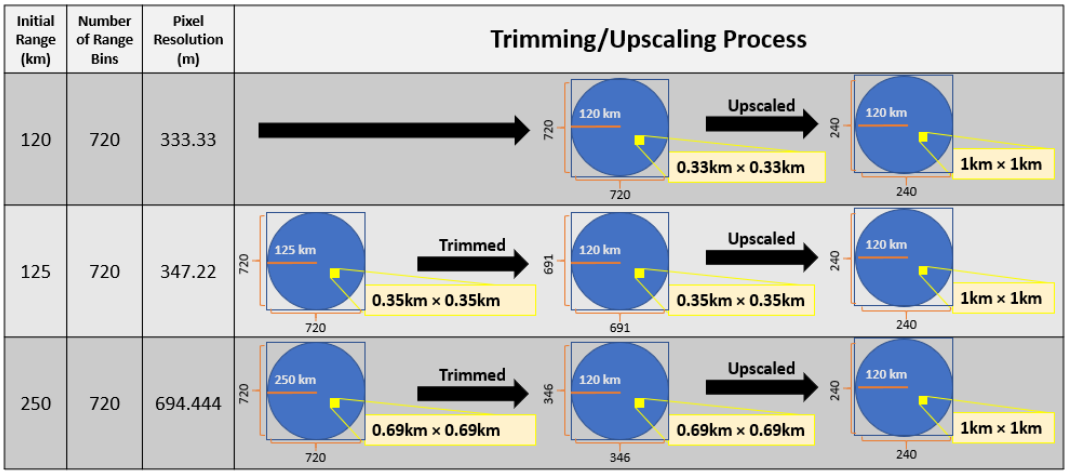

Figure 2.3 Trimming/upscaling procedures of radar images

2.1.3 Radar-Gauge Integration

For determining the radar-gauge pairs, the data from both instruments must be integrated in time and space. The data observed by radar aloft is not directly associated with the rain intensity on the ground, but there is a variable shift in time and space. This shift is dependent on factors such as the velocity of the raindrops and the horizontal advection (Morin et al., 2003). Both the temporal and spatial radar-gauge integration scales have effects on the accuracy of the radar-based estimates compared with the gauge observations. It is recommended to avoid using extremely small space-time integration scales. Also, in very large scales, the measured parameters such as reflectivity and rainfall would have a lower variety, thus highly biased (Morin et al., 2003; Song, Han, and Rico-Ramirez, 2016).

The original spatial resolution of the radars is between 0.3 to 0.7 km. However, all radar data is upscaled into 1-km resolution (see 2.1.2.4). For spatial integration, one choice is to incorporate the pixel, which is the closest to the rain gauge plus nine neighborhood pixels. In this case, the sampling size representing a precipitation event would be $9km^2$. This sampling size is too large for representing the convective precipitation. Therefore, the nearest pixel from the gridded radar data was chosen and paired with the point observation from the rain gauges (Figure 2.4a).

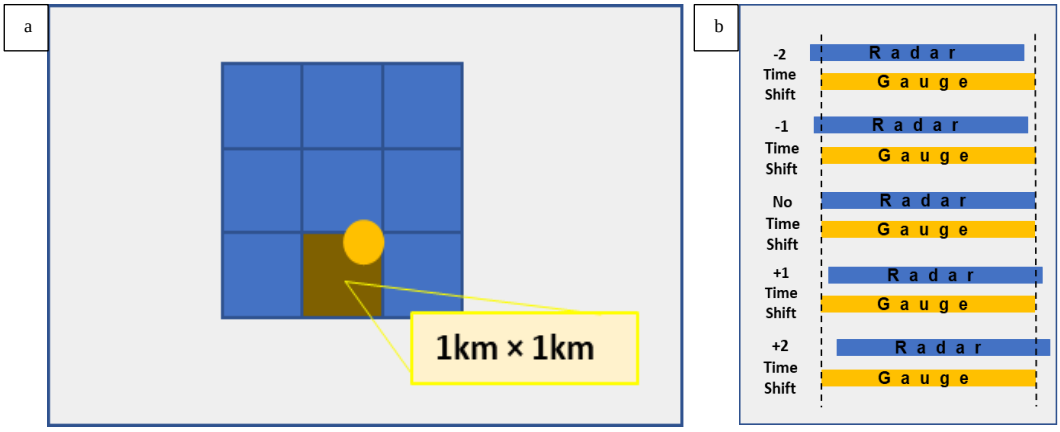

Figure 2.4 How the radar and gauge data are integrated spatially (a) and temporally (b)

The temporal resolution of the original radar data used in this study is 1-hour (2.1.2.1). The minutely gauge observations were accumulated and integrated with radar on an hourly time scale. However, there is a difference between the time conventions of radar and gauges. In the radars, the accumulated precipitation within an hour is recorded as in the next timestamp. In rain gauges, however, the accumulated precipitation within an hour is recorded as in the previous timestamp. Several time shifts were analyzed (Figure 2.4b) for choosing the best time shift, in which both instruments are in a relatively better consistency with each other. The results regarding the consistency of radar-gauge data are given in section 3.1.1.

2.2 Gauge Adjustment and Time-Independent Bias Correction Methods

The bias correction methodology in this section will be introduced in two parts: Hourly gauge adjustment methods, and time-independent bias correction methods.

2.2.1 Gauge Adjustment Methods

The basic concept of Gauge Adjustment methods is to correct gridded radar estimations using point-based gauge observations considered as "ground truth" by defining a correction factor. Among various methods, different assumptions are made on the distribution of the correction factor (e.g., local or global), and its type (e.g., multiplicative or additive). In this study, *wradlib* (Heistermann et al., 2013) module was used in implementing the gauge adjustment methods:

- Mean Field Bias (MFB) Correction
- Local Multiplicative Bias (LMB) Correction
- Local Additive Bias (LAB) Correction
- Local Mixed Bias (LMIB) Correction

2.2.1.1 Mean Field Bias

Mean Field Bias (MFB) Correction assumes the existence of a uniform multiplicative error in the radar field. This method is computationally and operationally functional due to its simplicity. The correction factor in this method is defined as the ratio of the sum of the gauge observations to the radar estimations:

$$C_{MFB,t,r} = \sum_{s=1}^{n} G_{t,s,r} / \sum_{s=1}^{n} R_{t,s,r} \quad (1)$$

$$R_{MFB,t,x,y,r} = C_{MFB,t,r} . R_{t,x,y,r} \quad (2)$$

where x and y represent the location of the pixel over the radar image, the r represents the ID number of radars (total 17 radars available), t represents the time step of correction which ranges between 1 to 8760 over a year. s represents the number of gauge station around each radar which ranges between 1 to the total number of stations within 120 km range of each radar. In equation (1), $C_{MFB,t,r}$ is the MFB correction factor calculated for the radar field for every time step t. $G_{t,s,r}$ is the value of gauge measurement at time step t and in station s. For dealing with the spatial variability of radar measurements, rather than measuring the radar estimation only in the pixel corresponding the gauge station, $R_{t,x,y,r}$ is chosen as the mean of radar precipitation estimation values within the $5 * 5$ pixels neighboring each gauge station s for every time step of t. In all the gauge adjustment methods the radar-gauge pairs which both represent a precipitation value of greater than 0.2mm/hr is considered in calculating the correction factors. According to equation (2), adjusted radar image ($R_{MFB,t,x,y,r}$) is calculated by multiplying the entire domain of raw radar image ($R_{t,x,y,r}$) by the correction factor value ($C_{MFB,t,r}$).

2.2.1.2 Local Multiplicative Bias

This method is based on a multiplicative model initially proposed by Brandes (1975). The multiplicative correction factor is assumed to be locally various for each station. Thus, an individual multiplicative correction factor is measured for every gauge station in the radar field as shown in this equation:

$$C_{LMB,t,s,r} = \frac{G_{t,s,r}}{R_{t,s,r}} \tag{3}$$

$$C_{LMB,t,x,y,r} = IDW\left(C_{LMB,t,s,r}\right) \tag{4}$$

$$R_{LMB,t,x,y,r} = C_{LMB,t,x,y,r}.R_{t,x,y,r} \tag{5}$$

where $C_{LMB,t,s,r}$ represents the value of multiplicative correction factor for every gauge station at every time step, and $C_{LMB,t,x,y,r}$ represents the value of multiplicative correction factor for each pixel over the radar image that is calculated using Inverse Distance Weighting (IDW) methodology utilizing $C_{LMB,t,s,r}$ values. The LMB corrected radar ($R_{LMB,t,x,y,r}$) is then found by multiplying the interpolated matrix ($C_{LMB,t,x,y,r}$) to the raw radar ($R_{t,x,y,r}$) as shown in equation (5).

2.2.1.3 Local Additive Bias

This method is similar to 2.2.1.2, but rather than considering a multiplicative error local to each rain gauge, it assumes that the error is additively and spatially variable. Thus, its correction factor is defined as the subtracted difference between the radar estimation and gauge observation precipitation values:

$$C_{LAB,t,s,r} = G_{t,s,r} - R_{t,s,r} \tag{6}$$

$$C_{LAB,t,x,y,r} = IDW\left(C_{LAB,t,s,r}\right) \quad (7)$$

$$R_{LAB,t,x,y,r} = C_{LAB,t,x,y,r} + R_{t,x,y,r} \quad (8)$$

In equation (6), $C_{LAB,t,s,r}$ is the value of additive correction factor for every gauge station s at every time step of t in radar r. Consistent with the multiplicative error model, this correction factor is then interpolated using the IDW technique to obtain an image matrix of the correction factor for the whole radar field (equation (7)). Finally, as shown in equation (8), the LAB corrected radar ($R_{LAB,t,x,y,r}$) then is calculated by multiplying the interpolated matrix of correction factors ($C_{LAB,t,x,y,r}$) by the raw radar matrix ($R_{t,x,y,r}$).

2.2.1.4 Local Mixed Bias

There are some considerable disadvantages in using additive-only or multiplicative-only models (Pfaff, 2010) such as obtaining huge correction factors when the amount of the denominator is considerably lower than the nominator in the multiplicative error model (Equation 3) or occurrence of negative values in the correction factor of the additive error model (Equation 6). The Local Mixed Bias (LMIB) model assumes there is either a multiplicative or an additive error for the gauge-radar pairs, depending on its scale. For large-scaled errors, this model matches the multiplicative error model, whereas, in the small-scaled errors, it can be related to the additive error model. The difference between real precipitation observation at each gauge station and the corresponding radar estimated precipitation ($G_s - R_s$) is simultaneously related to an additive (ε) and multiplicative (δ) errors as follows (M. Heistermann et al, 2013):

$$G_{t,s,r} - R_{t,s,r} = \delta_{t,s,r} * R_{t,s,r} + \varepsilon_{t,s,r} \quad (9)$$

By adding one more restriction to equation (9), minimization of the sum of the error squares ($\delta^2 + \epsilon^2$), the values of δ and ϵ are obtained as:

$$\varepsilon_{t,s,r} = \frac{G_{t,s,r} - R_{t,s,r}}{{R_{t,s,r}}^2 + 1} \tag{10}$$

$$\delta_{t,s,r} = \frac{G_{t,s,r} - \varepsilon_{t,s,r}}{R_{t,s,r}} - 1 \tag{11}$$

$$\varepsilon_{t,x,y,r} = IDW(\varepsilon_{t,s,r}) \tag{12}$$

$$\delta_{t,x,y,r} = IDW(\delta_{t,s,r}) \tag{13}$$

Both errors measured for each gauge station location at every time step ($\varepsilon_{t,s,r}$ and $\delta_{t,s,r}$) is interpolated within the radar field using the IDW method. $R_{LMIB,t,x,y,r}$ local mixed bias-corrected radar image is given in equation (14):

$$R_{LMIB,t.x,y,r} = \left(1 + \delta_{t,x,y,r}\right).R_{t,x,y,r} + \varepsilon_{t,x,y,r} \tag{14}$$

2.2.2 Time-Independent Methods

In time-independent methods, radar estimations and gauge observations are compared in a long-term period. The availability of gauge-based observations is not necessary for correcting the radar estimations at every time step. These methods are expected to reduce the radar QPE bias and resolve the radar underestimation problem.

2.2.2.1 Multiple Linear Regression

This method, proposed by Gabella et al. (2000), consists of the following four steps:

1. Obtaining the gauge station observations (G) and radar precipitation estimations (R) over all the gauge stations within the field of the radar (120km),

2. Calculation of an assessment factor ($AF = R/G$) for every gauge station,

3. Using these AFs and three other parameters [the distance between the radar and the gauge station (D), minimum height of visibility (HV_{min}) and height of gauge (HG)] for establishing a multiple linear relationship (Equation 16),

4. Obtaining AFs for all of the other pixels in the radar field ($AF_{x,y,r,s}$) by utilizing the coefficients obtained from the linear regression model.

The corrected radar QPE is then calculated as follows:

$$R_{C,t,r} = R_{R,t,r}.AF_{x,y,r,s} \tag{15}$$

In this equation, $R_{C,t,r}$ and $R_{R,t,r}$ represent the corrected and raw radar QPEs respectively, and $AF_{x,y,t,r}$ represents the assessment factor over the pixel location x, y, radar r and season s. t is the time step associated with the regarding season s $AF_{x,y,t,s}$ is estimated using the regression model:

$$AF_{x,y,r,s}(dB) = a_0 + a_D.log(D_{x,y,r}) + a_{HV}.(HV_{\min})_{x,y,r} + a_{HG}.(HG_{x,y,r}) \tag{16}$$

In this equation, a_0, a_D, a_{HV}, and a_{HG} represent the coefficients to be obtained as a result of multiple regression.

AF is defined as "the ratio between radar- and gauge-based precipitation amounts (R/G)" (Gabella et al., 2000). AF value greater than 1 indicates that the radar-based estimations are on average greater than gauge-based observations (overestimation), while AF value less than 1 indicates radar underestimation on average.

The integration of the radar and rain gauge measurements for comparing their values is necessary. The length of the integration time between radar and gauge depends on factors that affect the variability of these instruments. Longer integration time

increases the representativeness of the rain gauges and reduces the AF fluctuations (Gabella et al., 2000). For example, integration time selections of 4, 20, 48 hours were used in similar studies over a limited number of events (Öztürk & Zeybek (2013), M. Gabella & Amitai (2000)).

For an operational approach, we used an extended integration time: $\mathrm{AF} = \frac{\sum_{t=1}^{S} R_{S,r}}{\sum_{t=1}^{S} G_{S,r}}$, where S represents the total number of hours in each season. Due to the dominance of different precipitation types for different seasons, we assessed four different seasonal AFs for each rain gauge station. Thus, four different correction matrices were generated for each radar. Total hourly accumulated precipitation was measured for radars and gauges over each season and year with a criterion of having at least five radar-gauge pairs greater than 0.1 mm in the summer and 20 events in other seasons. For each season, the AF value is defined as the mean of the associated season over the years 2014-2018. The results regarding the measurement of AF for MLR and ANN models are presented in 3.1.4.

2.2.2.2 Cumulative Distribution Function

Probabilistic bias correction methods based on Cumulative Distribution Function (CDF) have long been used for scaling and improving estimations based on a reference dataset. Afshar & Yilmaz (2017) have used the CDF matching method for rescaling soil moisture data. For meteorological weather radar data, CDF matching is mainly used to eliminate precipitation estimation bias by using gauge stations as reference. Initially, some studies have attempted to relate synchronous radar reflectivity directly with measured precipitation intensity on the ground by fitting them using a regression model (Calheiros and Zawadzki, 1987; Rosenfeld, Atlas, and Short, 1990). This method had some drawbacks, such as the discrepancy between the sampling volumes of the rain gauges and the radar, geometric and timing mismatches, and errors due to different precipitation types (Piman et al., 2007). These probability matching methods are referred to as traditional matching method

(TMM). The drawbacks of this matching method were the initial motivation in using the probability function for matching non-synchronous radar reflectivity and ground observation. These methods are referred to as probability matching methods (PMM), which come up with a more synchronized Z-R relationship than TMM by eliminating the sampling volume discrepancy problem.

Other probabilistic methods were proposed later, such as window probability matching method (WPMM) (Rosenfeld, Wolff, and Amitai, 1994) and window correlation matching method (WCMM) (Piman et al., 2007). Other studies have focused on matching radar precipitation estimation values with the rain gauge corresponding values over shorter time scales. Rabiei and Haberlandt (2015) have used a quantile matching method for matching precipitation values between radar estimations and rain gauge observations for hourly time step and interpolating this to other pixels using two different merging methods applied for each time step.

Our CDF-based proposed method also uses the assumption of equal CDF for both measured and estimation precipitation rates. However, in order to come up with a time-independent solution, we have implemented the CDF correction for each hour over each station for a long-term period (2014-2018), and then used the CDF correction coefficient curves to fix radar underestimation problem independent from the time of the event. Then, using IDW interpolation method, these coefficients are estimated over all radar pixels. The rain gauge observations are selected as the reference data, and the radar estimations over the gauge stations are corrected by matching the CDF of the reference data into the radar pixel values. Equation (17) formulates this method:

$$R_{CDF,s,t,r} = F^{-1}_{G,s,t,r}(F_{R,s,t,r}(R_{s,t,r})) \quad (17)$$

$R_{s,t,r}$ is the estimated value of radar over station s at time t over radar r. $F_{R,s,t,r}$ is the CDF for radar data, and $F^{-1}_{G,s,t,r}$ is the inverse CDF derived from the gauge station measurement. This function inverses the probability estimated by $F_{R,s,t,r}$ back to CDF-corrected radar precipitation intensities, $R_{CDF,s,t,r}$.

In order to implement this bias correction over all radar pixels, firstly a correction coefficient function ($CCF_{s,t,r}$) is needed. This function was defined for each gauge station by dividing the ranked CDF-corrected radar (i.e., ordered by intensity) values to the uncorrected radar values, and fitting these points using a third-degree polynomial function. $CCF_{s,t,r}$ function gives the multiplicative correction coefficient in every station based on the initial intensity of the radar estimation over the same station. For correcting the radar estimations at each time step for all pixels, first, the intensity of the radar estimations over each gauge station and four nearby gauges at that time step are obtained. Later, these coefficients are interpolated inversely weighted according to their distance from the four nearby gauge stations. Finally, a matrix of multiplicative CDF-based bias correction coefficient is obtained. This matrix can be used to correct every pixel in the radar at each time step according to the initial intensity of radar estimations over that pixel. The results regarding the CDFs of radar and their rain gauges are presented in 3.1.5.

2.2.2.3 Artificial Neural Network

ANN is a computer simulation of the human brain capable of learning from experiences and organize itself for potentially predicting outcomes in new conditions. Similar to the human brain, ANN consists of interconnected neurons able to perform challenging operations and perceive intricate patterns with a high generalization ability. Non-linearity, tolerance to noise, and generalization capability are the main superior contributions of ANNs in bias-correction studies focusing on satellite/radar precipitation or other parameters (Afshar and Yilmaz 2017; Liu, Chandrasekar, and Xu 2001; Moghim and Bras 2017; Teschl, Randeu, and Teschl 2007).

Majority of ANN applications in studies related to meteorological radar QPE can be divided into two main approaches:

A. Establishing Complex Nonlinear Z-R Relationships:

Meteorological radars measure the hydrometeor reflectivity aloft, and these reflectivities are eventually transformed into values reflecting the amount of precipitation on the ground and projected into a two-dimensional space resulting in QPE. Z-R relationships used for converting reflectivity into precipitation highly depend on a specific drop-size distribution, which can change in various climates and precipitation types. Thus, the temporal variability in the type of precipitation systems, observation noise in radars, and several other error sources such as beam blockage makes it a demanding task to rely on a specific Z-R relationship for estimating the surface precipitation with high accuracy.

Several studies have focused on establishing ANNs to determine complex Z-R relationships that utilize radar-based reflectivity extracted from various altitudinal/latitudinal/longitudinal layers/points as inputs and the rain gauge observation as the target output (Aditya Sai Srinivas et al. 2019; Liu, Chandrasekar, and Xu 2001; Teschl, Randeu, and Teschl 2007; Tiron and Gosav 2010; Wei and Hsieh 2020; Xiao, Chandrasekar, and Liu 1998). The concept behind these studies is to utilize the information about the nature of precipitation from various dimensions of reflectivity or other inputs such as terminal velocity and horizontal advection to determine the precipitation intensity on the ground using the weights obtained from training the model. Using complex relationships established by ANN using the vertical profile of reflectivity, it is possible to differentiate between convective events (e.g., reaching up to 10 km), and stratiform events.

These studies have shown that ANN-based Z-R relationships are more consistent than conventional Z-R relationships. However, training such ANN relationships is highly dependent on the diversity and completeness of the training dataset (Chiang et al. 2007) over various event types, and demands the availability of vertical profile of reflectivity in most cases.

B. Hydrometeor Classification & Clutter Removal:

Other studies have utilized ANN mainly for obtaining an understanding of the type of hydrometeors, thus reflecting an understanding of the type of precipitation

(Anagnostou 2004; Jing et al. 2008; Lazri et al. 2012; Wang et al. 2017). Hydrometeor classification by ANN is much feasible and accurate than traditional deterministic or statistic methods (Jing et al. 2008). Part of hydrometeor classification also consists of the detection and removal of non-meteorological echoes (Gürbüz and Oğuz 2015). Even though the determination of hydrometeor types is useful in selecting a suitable Z-R relationship, the QPE accuracy still depends on the accuracy of the classification process and the Z-R model, which represents a transformation route from reflectivity measured from a particular hydrometeor type into the precipitation intensity on the ground.

In this methodology, we developed a novel solution for improving radar-based QPE using ANN, which does not require the availability of layers of reflectivity data nor other complex inputs (such as horizontal advection). The concept behind this method is to use three time-independent parameters obtained from each radar pixel to predict the potential bias in the corresponding pixel. This approach is similar to MLR modeling of AF values (see 2.2.2.1 and 3.1.4) initially established by Gabella et al. (2000), and developed by Öztürk and Yilmazer (2007). In these studies, the associated radar estimation errors are assumed to be linearly dependent on three stationary parameters: distance from the radar, the elevation of the gauge from mean sea level, and the minimum height of visibility. However, depending on the precipitation type (e.g., convective or stratiform), the complexity of the topography and climate, "non-linear" relationships may result in a better correlation between the named time-independent parameters (D, HG, and Hvmin) and the AF values. Thus, non-linear relationships must also be tested by utilizing machine learning methods such as ANN. A summary of the input variables and the framework of MLR and ANN models is represented in Figure 2.5.

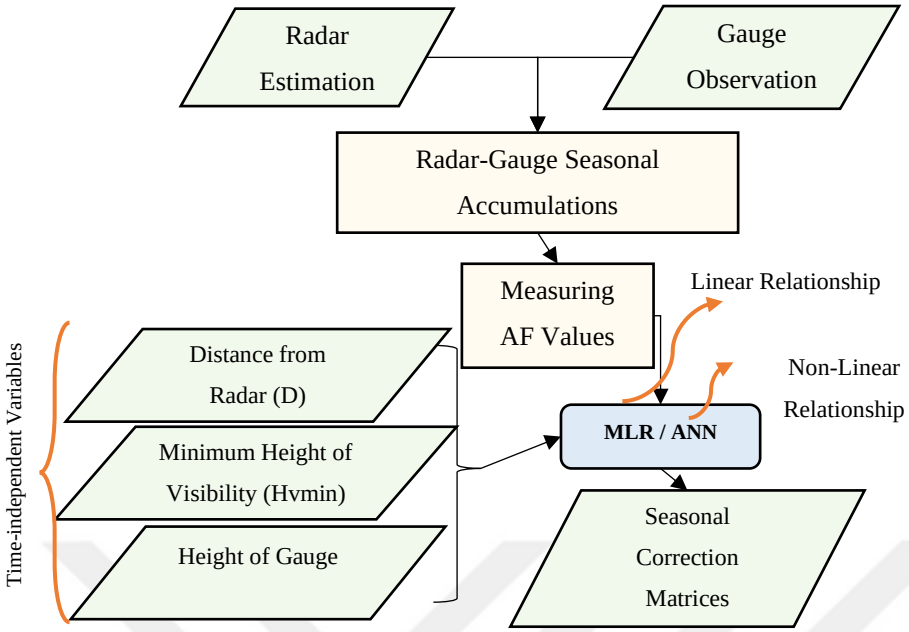

Figure 2.5 ANN & MLR Bias Correction Framework

Four different ANN structures (Multilayer Perceptron, Radial Basis Function, Elman Network, Jordan Networks) were examined in this study for predicting the AF values based on three time-independent variables. The general types of named ANN functions are categorized as feed-forward, radial basis function, and recurrent networks. Keras package in Python was used to structure ANN networks. Each ANN network consists of an input layer, (a) hidden layer(s), and an output layer. The input layer in this study consists of three time-independent variables (D, HG, and Hvmin) measured for different stations, so the dimension of the input layer is three, and the length of the input layer is the number of training stations. The output layer is one-dimensional and consists of the target AF values for each station. It is important to note that unlike MLR, the input values have been normalized before running the ANN model.

Except for the default built-in parameters, the majority of the ANN structure was optimized for this study. For choosing the optimized ANN parameters, a systematic search was conducted by altering the number of hidden layers and neurons, type of activation functions, amount of learning rate, and type of the loss function. The domain of this search for the number of neurons and hidden layers was 1-64. The type of activation functions tested consist of sigmoid, Tanh, and Rectified Linear Unit (ReLU). The learning rate varies from 0.00001 to 0.0001. Finally, the loss functions tested include Mean Squared Error (MSE) and Mean Squared Logarithmic Error (MSLE).

For testing the accuracy of the independent validation of each model, three stations were used as validation, and the remaining were used to train the model. For training the model, the number of epochs (the number of times model re-adjusts its weights by running one cycle through the training dataset) was chosen based on the variations of the loss function. If there was minor change or no significant change in loss function variation, then the model stops training and measures the error metrics. The maximum number of epochs (in case the loss function does not change) was set as 256. After each loop, MSE was measured for both validation and training stations. The mean of MSE for both station types was compared with other structures, and the ANN structure, which yields the least MSE, was chosen as the best. Refer to 3.1.4 for reading the results regarding the measurement and estimation of AF values by both MLR and ANN models.

2.2.2.4 Z-R Relationships

Meteorological radars measure the average backscattered electromagnetic beam, which is dependent on the hydrometeor characteristics such as precipitation type, drop size, shape, and distribution (Wang et al. 2017), and radar characteristics such as frequency, antenna characteristics and the distance to the antenna. Both the radar reflectivity (Z) and precipitation intensity (R) are dependent on drop size distribution (DSD) and measured as follows according to Battan (1973):

$$Z = \sum [N(D) \,.\, D^6 \,.\, \Delta D] \tag{18}$$

$$R = (6\pi/10^4) \,.\, \sum [N(D) \,.\, D^3 \,.\, v(D) \,.\, \Delta D] \tag{19}$$

where D is the drop diameter, $N(D)$ shows the drop size distribution (DSD) (m^{-3} mm^{-1}), $v(D)$ is the falling velocity, and the units of Z and R are mm^6/m^3 and mm/hour, respectively. The properties of the scattered electromagnetic wave depend on the variables $N(D)$, $v(D)$, and ΔD. These variables can be observed on the ground using disdrometers, while such observations are only representative at the specific locations of the disdrometers. However, since radars scan much larger areas, it is impractical to observe all radar-covered hydrometers via disdrometers (many disdrometers are required).

Additionally, assuming that there is a sufficient number of disdrometers to measure the droplet characteristics, there are complications associated with the representativeness of precipitation type and intensity with drop size distribution and diameter. Since the reflectivity measured by disdrometers is dependent on the drop size distribution and sixth power of drop diameter, the reflectivity and volume of 1 droplet of 3 mm diameter and 729 droplets of 1 mm are equal. However, the precipitation falling on the ground is naturally different (Öztürk and Çubuk 2015). Thus, a relationship is required to transform the Z values measured by radar into R. Marshall and Palmer (1948) presented an empirical power-law relation (Z-R relationship) which is widely used today and produces better results in mid-latitudes for stratiform type precipitation:

$$Z = a \,.\, R^b \tag{20}$$

In this equation, Z is generally used as a unit of dBZ: $dBZ = 10 \,.\, \log(Z)$. The experimental coefficients a and b in this relation vary depending on the type of precipitation (Table 2.2):

Table 2.2 Empirical equations obtained between Z and R in different precipitation types (Collier, 2016)

Z-R Relationship	Precipitation Type	Reference
$\boldsymbol{Z = 140R^{1.5}}$	Drizzle	Joss (1970)
$\boldsymbol{Z = 250R^{1.5}}$	Large-Scale Rainfall	Joss (1970)
$\boldsymbol{Z = 200R^{1.6}}$	Stratiform Rainfall	Marshall and Palmer (1948)
$\boldsymbol{Z = 31R^{1.71}}$	Orographic Rainfall	Blanchard (1953)
$\boldsymbol{Z = 500R^{1.5}}$	Stormy Rainfall	Joss (1970)
$\boldsymbol{Z = 485R^{1.37}}$	Stormy Rainfall	Joss (1970)
$\boldsymbol{Z = 2000R^{2}}$	Snowfall	Gunn and Marshall (1958)
$\boldsymbol{Z = 1780R^{2.21}}$	Snowfall	Sekhon and Srivastava (1970)

There are several methods proposed for establishing a Z-R relationship. In one of these methods initially proposed in the project, the disdrometer data is used for derivation of a and b parameters from the power-law relationship (Equation 20). Disdrometer is an optical device that measures DSD, droplet diameter, and final velocity of the hydrometeors. Disdrometers can measure reflectivity and rainfall using these parameters (Equations 18-19). There are some limitations involved with utilizing disdrometers in assigning a suitable Z-R relationship for obtaining an accurate radar-based QPE.

The first limitation is related to the representativeness of the disdrometers. For example, there are a total of 32 disdrometers and 17 radars installed in Turkey. The disdrometers are located either within the range or in the overlapping areas between radars. The droplet diameter and final falling velocity measured by disdrometers can be obtained as a 32*32 matrix with a nominal sampling area of 54 cm^2. Each radar, however, provides reflectivity data as a 240*240 matrix from a total sampling area of 57600 m^2. The variable characteristic of precipitation in space and lack of sufficient disdrometers, which can represent the reflectivity over the entire radar field, is one of the biggest limitations in assessing an appropriate Z-R relationship using optical disdrometers (Cyr, 2014).

Other limitations associated with the use of disdrometers for Z-R relationship establishment involves the reliability of the disdrometer data. According to Hazer and Afacan (2016), there are a few issues regarding the limitations of the disdrometer data in obtaining a radar Z-R relationship with better consistency with the ground observations. The first one is that the disdrometers can record meaningless data (missing values) during their operation, and they need quality-control processes in order to provide reliable data. Since there are only one or two disdrometers around each radar, these missing data can have a substantial effect on the accuracy of the Z-R relationship coefficients. Another quality-related problem is the repetition of individual data with more than once. Although these data are corrected using a software written in PHP language (Hazer and Afacan, 2016), these data are then eliminated, resulting in more missing values. For investigating the accuracy of disdrometer data, the precipitation values obtained from disdrometer data were compared with the observations obtained by three collocated nearby gauges, and the results are presented in 3.1.8.

Hazer & Kara (2017) studied data retrieved from 12 disdrometers and ten radars and determined five different Z-R relationships (a and b coefficients) for convective, stratiform, general, summer and winter precipitation events using linear regression. The daily precipitation values from KDP, Marshall Palmer, and five different Z-R relationships developed in the study were compared with the Triple-Collocated rain-gauges located near the disdrometers. However, newly established Z-R estimates were proved not to outperform the original Z-R relationship (Marshall-Palmer) estimates when compared against the gauge observations. In order to prevent the replication of the Z-R studies focused on disdrometer data in Turkey and the drawbacks associated with disdrometer representativeness and data accuracy, we opted for the use of data collected from AWOS gauges instead of disdrometer data. Considering the variability of the precipitation, and the large area scanned by radars, the representativity of the Z-R relationship will be limited to the representativity of the limited number of gauges. Unlike disdrometers, several numbers of gauge stations are located within the range of each radar. However, despite having more

than one rain gauge, one representative seasonal Z-R relationship for all stations will be established based on long-term observation of reflectivity-rainfall relationships over each radar.

In this method, the best values of a and b parameters are determined through a relationship. This relationship can be established using machine learning techniques. Linear regression is established between radar reflectivity values and rain gauge precipitation observations. It is important to note that. Equation (20) can be written as:

$$Z_r = \text{a}.\ R_g{}^b \tag{21}$$

where Z_r is the reflectivity measured by the radar and R_g is the amount of precipitation observed by the rain gauges. By taking the logarithm of both sides of this equation, a linear relationship can be formed as:

$$log\ (Z_r) = \ log(a) + b.\ log\ (R_g) \tag{22}$$

In this equation $X = log\ (Z_r)$, and $Y = \ log\ (R_g)$. Therefore*:*

$$Y = (X - log(a))/b \tag{23}$$

$$Y = \ \alpha\ .X + \ \beta \tag{24}$$

Equation (23) can be regarded as a linear equation with an intercept of $\beta = -log(a)/b$, and slope coefficient of $\alpha = \ 1/b$ in Equation (24).

For training the regression model for the new Z-R relationship, the gauge observations and radar estimations are extracted over four years (2014-2018) and categorized into four seasons. For a consistent relationship, and elimination of the outliers, the gauge observations were extracted from the gauges that have a correlation coefficient of higher than 0.2 against the radar precipitation rates in each season. The stations which have a beam blockage value of higher than 30% were

also eliminated. The radar estimations were transformed back to reflectivity. 90 percent of the data were randomly sampled for model training, and the remaining 10 percent was separated for validation purposes.

The goal of the regression model is to find α and β coefficients, which produces the best relationship between $X = log\ (Z_r)$ and $Y = log\ (R_g)$. These coefficients are then used to predict a and b values in the power-law relationship (equation 3), resulting in the newly established Z-R relationship. The regression-based Z-R relationship was used to produce new radar-based estimations, and these values were compared with the gauge observations. Two error metrics were considered to investigate the performance of the new Z-R relationship against Marshall-Palmer's relationship ($a = 200, b = 1.6$) for each radar and season: RMSE and mean absolute error (MAE). If the regression-based Z-R relationship performs better in terms of both validation and training datasets based on the mentioned error metrics, then new parameters (a and b) from the regression model are used to estimate precipitation for all radar pixels in the associated radar and season. Otherwise, no changes are applied in terms of the parameters of the Z-R relationship. The results regarding the a and b values obtained based on regression-based Z-R relationships over various seasons is shown in detail in 3.1.6.

2.3 Evaluation of Datasets

2.3.1 Beam Blockage Effect

Beam blockage is an inevitable collision of radar beams with the surrounding terrain surface (Figure 2.6). It can result in the weakening or complete loss of the radar signals, thus affecting the radar-based QPE accuracy. In radar-based precipitation maps, the beam blockage fraction (BBF) is used in determining a radar quality index (RQI) because of its significant role in evaluating the radar quality (Crisologo et al., 2018; Zhang et al., 2012). It can be used for determining other parameters affected by obstruction of beams such as Hvmin. Due to its complex topography, a significant

fraction of radar error sources is expected to be drawn by (partial) beam blockage in Turkey. Still, the impacts of this source of error were overlooked amongst the studies which evaluated the improved radar-based precipitation products in hydrometeorological applications over Turkey (Ozkaya and Akyurek 2019; Öztürk and Yilmazer 2007).

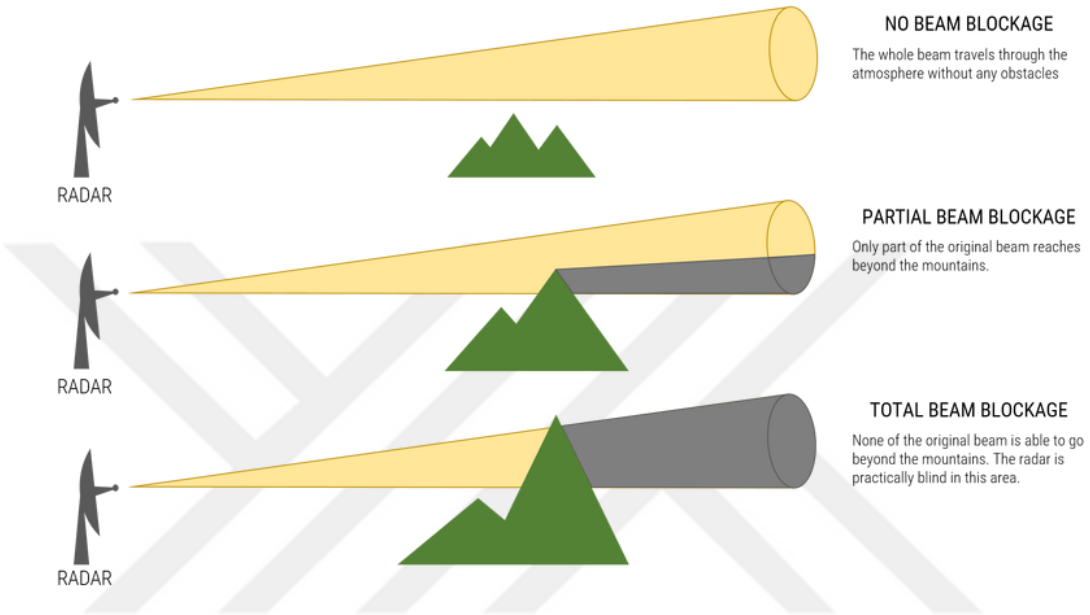

Figure 2.6 Partial or total beam blockage (Crisologo, 2016)

CBB is the cumulative fraction of beam blockage along a beam starting from the location of the antenna up to the final bin in the maximum range. In this study, CBB maps were generated according to the algorithm proposed by Bech et al. (2003). The resolution of the Digital Elevation Model (DEM) is expected to affect the estimation of CBB fraction (Crisologo et al., 2018; Kucera, Krajewski, and Young, 2004). DEM data with the highest available resolution (approximately 30m) from the Shuttle Radar Topography Mission (SRTM) was used in this study. Each radar scans reflectivity from specific elevation angles. The list of the elevation angles for all radars is given in Table 2.3. The CBB maps were created for all elevation angles for each radar and all radar pixels. Later, CBBs measured over all elevation angles of each radar are averaged and defined as CBB-AV. 0% CBB-AV represents no beam blockage in all elevation angles, while a 100% CBB-AV indicates a complete beam

blockage over all elevation angles. Figure 2.7 represents the CBB-AV map plotted for all radars. CBB-AV is also used as a quality filter in the composite map. The results regarding the effect of CBB-AV is given in 3.1.2.

Table 2.3 Elevation angles for calculating CBB, and CBB-AV for all radars

Radar Name	**Elevation Angles (degree)**		**Radar Name**	**Elevation Angles (degree)**
Afyon	-0.2, 0.5, 1.3, 4, 7, 10, 15, 25		İzmir	-0.2, 0.5, 1.3, 3, 5, 7, 10, 15, 25
Ankara	-0.2, 0.5, 1.3, 3, 5, 7, 10, 15, 25		Karaman	-0.2, 0.5, 1.3, 4, 7, 10, 15, 25
Balıkesir	0.5, 1.3, 3, 5, 7, 10, 15		Muğla	0, 0.7, 1.5, 3, 5, 7, 10, 15, 25
Bursa	-0.2, 0.5, 1.3, 3, 5, 7, 10, 15, 25		Samsun	0, 0.7, 1.5, 3, 5, 7, 10, 15, 25
Antalya	-0.2, 0.5, 1.3, 3, 5, 7, 10, 15, 25		Şanlıurfa	-0.2, 0.5, 1.3, 3, 5, 8, 15, 25
Gaziantep	-0.2, 0.5, 1.3, 4, 7, 10, 15, 25		Trabzon	0.2, 0.9, 1.7, 3, 5, 7, 10, 15, 25
Hatay	0, 0.7, 1.5, 3, 5, 7, 10, 15, 25		Zonguldak	0.5, 1.3, 3, 5, 7, 10, 15
İstanbul	0.5, 1.3, 3, 5, 7, 10, 15		Erzurum	-0.2, 0.5, 1.3, 4, 7, 10, 15, 25
Sivas	-0.2, 0.5, 1.3, 3, 5, 7, 10, 15, 25		-	-

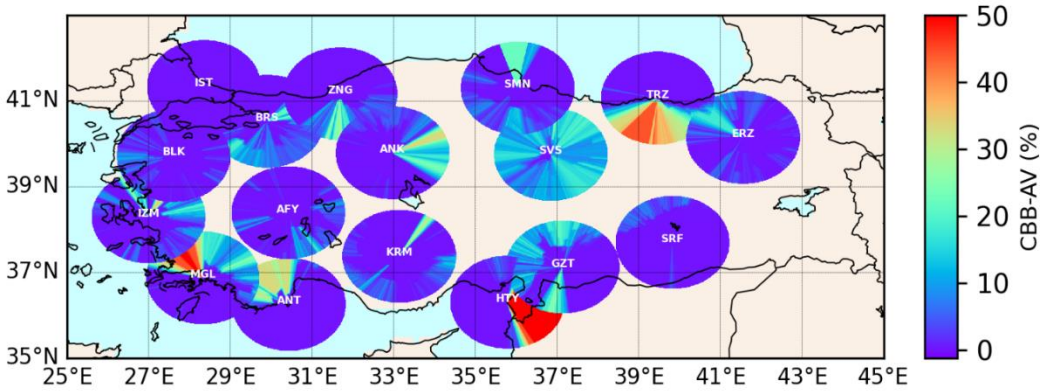

Figure 2.7 The Average Cumulative Beam Blockage (CBB-AV) as a radar quality index (RQI)

2.3.2 Training and Validation Datasets

The performance of bias correction methods is assessed using hourly precipitation accumulations. Three various datasets that represent the accuracy of the bias-corrected radar estimations are analyzed separately (Figure 2.8). These three sets include the number of gauge stations used for calibration, three stations within the range of each radar that are randomly picked for validation, and 50 independent collocated rain gauges for additional validation. In Figure 2.8-2.11, the locations of training and validation stations is given over various years. The availability of radar data changes, as described in 2.1.2.2. The training stations are marked as black dots, whereas validation stations are shown as triangles marks. Also, Figure 2.13 illustrates the location of the Triple-Collocated rain gauge stations over four additional validation regions.

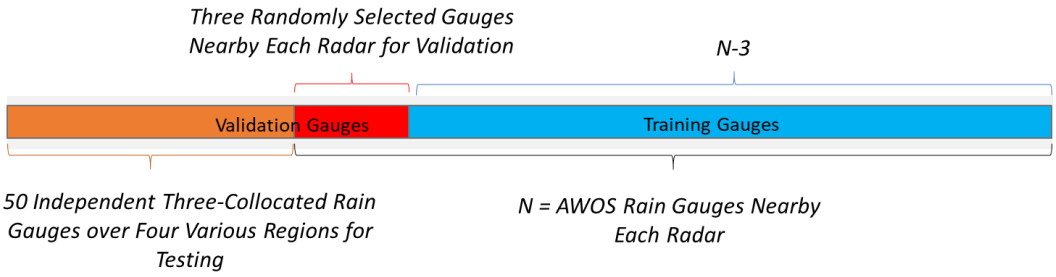

Figure 2.8 A schematic illustration of training and validation datasets

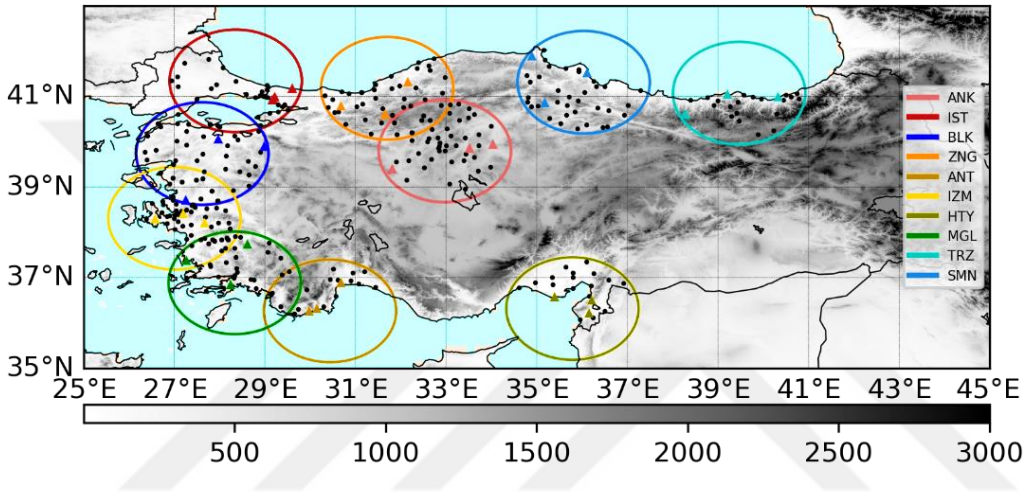

Figure 2.9 The available radar data and training/validation gauge stations in year 2014

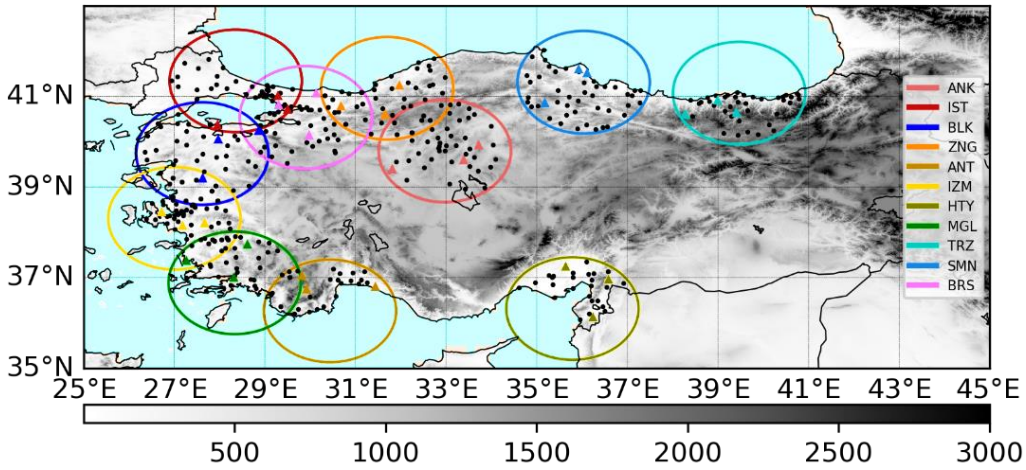

Figure 2.10 The available radar data and training/validation gauge stations in year 2015

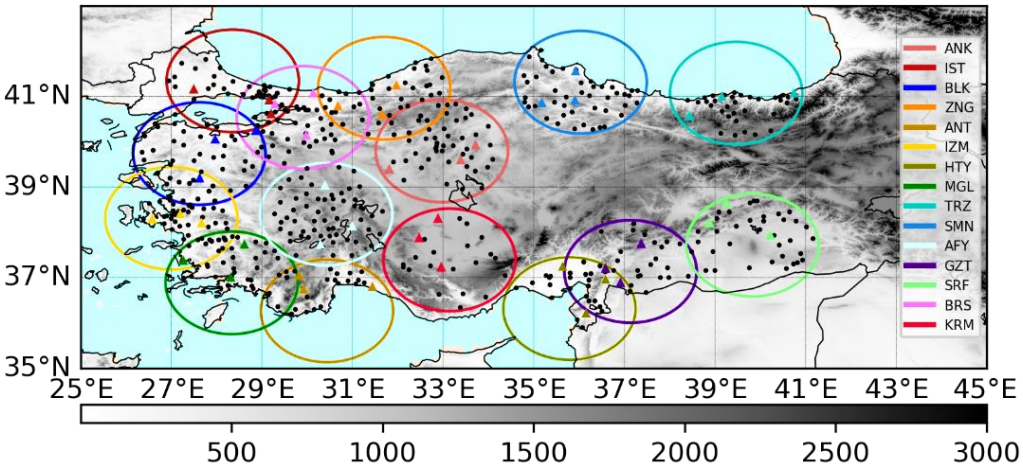

Figure 2.11 The available radar data and training/validation gauge stations in year 2016

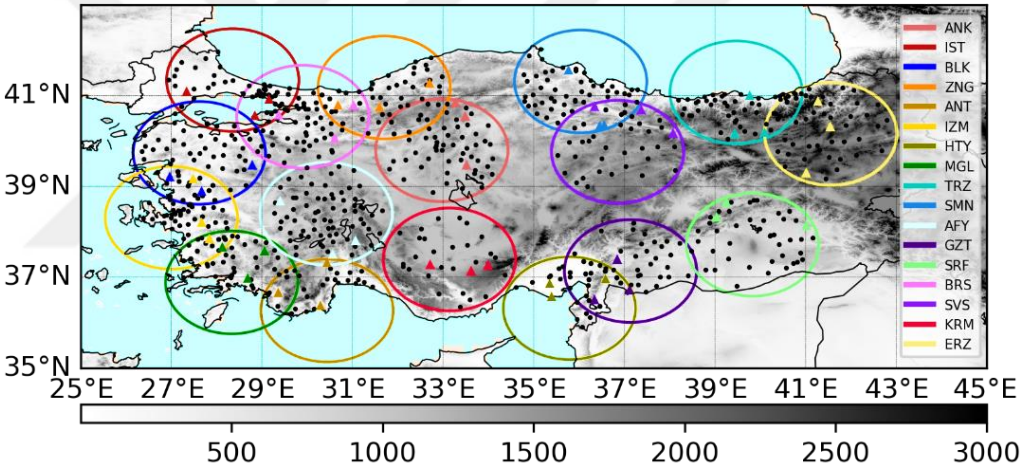

Figure 2.12 The available radar data and training/validation gauge stations in year 2017 and after

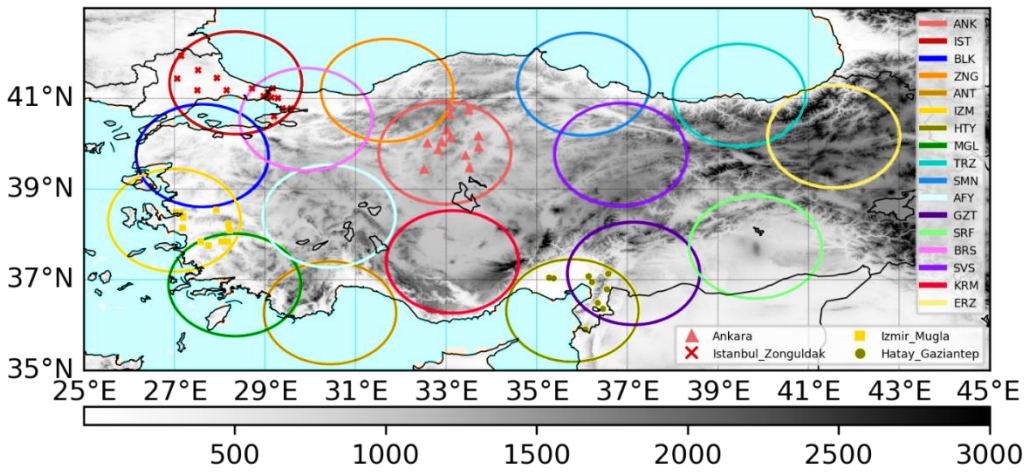

Figure 2.13 Locations of independent Triple-Collocated gauge stations in the additional validation fields located at four various regions: Ankara, Istanbul_Zonguldak, Izmir_Muğla, and Hatay_Gaziantep

2.3.3 Error Statistics

The description of the error metrics used for evaluating the radar-based estimation accuracy is described in this subsection.

2.3.3.1 Mean Error (ME)

ME is used for showing the average of all biases between the radar estimations and gauge observations. Although this error statistic cannot represent the bias and uncertainty due to the cancelation of negative and positive values in averaging the biases, it is a good representative of a general underestimation or overestimation between the radar estimates and gauge measurements:

$$ME = \sum_{i=1}^{N} \frac{R_i - G_i}{N} \quad (25)$$

Where R_i is the radar-based estimation over each gauge station, G_i is the station-based observation, and N is the number of gauge stations.

2.3.3.2 Root Mean Square Error (RMSE)

RMSE is the most famous error metric used in precipitation and rainfall verification studies (A Wardhana1, 2017; Gilewski and Nawalany, 2018; Park et al., 2019; Sharifi et al., 2016). RMSE is the standard deviation of the residuals, showing how spread-out are the radar estimations from gauge observations:

$$RMSE = \sqrt{\frac{\sum_{i=1}^{N}(R_i - G_i)^{\,2}}{N}} \tag{26}$$

2.3.3.3 Correlation Coefficient (COR)

The correlation coefficient (COR) is a measure of the linear relationship between two variables, in this case, radar estimations and gauge observations. COR lies between -1 and 1 values. A CC of 1 means there is a strong positive relationship between two variables. A COR of -1 indicates a strong negative relationship, and a COR of zero indicates no relationship. The COR is determined with the following expression:

$$\mathrm{COR} = \frac{\sum_{i=1}^{N}(R_i - \bar{R})\,(G_i - \bar{G})}{\sqrt{\sum_{i=1}^{N}(R_i - \bar{R})^{\,2}}\sqrt{\sum_{i=1}^{N}(G_i - \bar{G})^{\,2}}} \tag{27}$$

Where $\bar{G}$ is the mean gauge precipitation accumulation, and $\bar{R}$ is the mean radar precipitation accumulation.

2.3.3.4 Error Standard Deviation (ESD)

The standard deviation indicates the amount of dispersion of a variable from the mean. ESD indicates the amount of variability of the bias from the mean bias. In this case, it shows the amount of variability of the differences between radar-based and gauge-based observation as follows:

$$ESD = \sqrt{\frac{\sum_{i=1}^{N}(E_i - \bar{E})^2}{N-1}} \quad (28)$$

Where E_i is the amount of error measured as:

$$E_i = R_i - G_i \quad (29)$$

And $\bar{E}$ is equivalent to the mean error or ME.

2.3.3.5 Percent Bias (Pbias)

Percent bias is the average of percentage error which calculates the mean percentage difference between the radar estimates and gauge observations as follows:

$$ME = \sum_{i=1}^{N} \frac{R_i - G_i}{G_i} . 100 \quad (30)$$

2.3.3.6 Mean Absolute Error (MAE)

The MAE measures the mean absolute difference between the rain gauge observation and the radar estimates following:

$$ME = \sum_{i=1}^{N} \frac{|R_i - G_i|}{N} \quad (31)$$

CHAPTER 3

RESULTS

3.1 Initial Analysis of Radar and Rain Gauge Data

3.1.1 Temporal Consistency of Radar-Gauge Observations

Figure 3.1 and Figure 3.2 show the best time shift used for temporal integration of radar and gauges. The effect of time shift is significantly higher in COR values than the RMSE values. Overall, with the lowest RMSE and the highest COR values among all radars, -1 time shift has proved to be the best for radar-gauge integration. This time shift is also in agreement with the time convention difference between these two instruments.

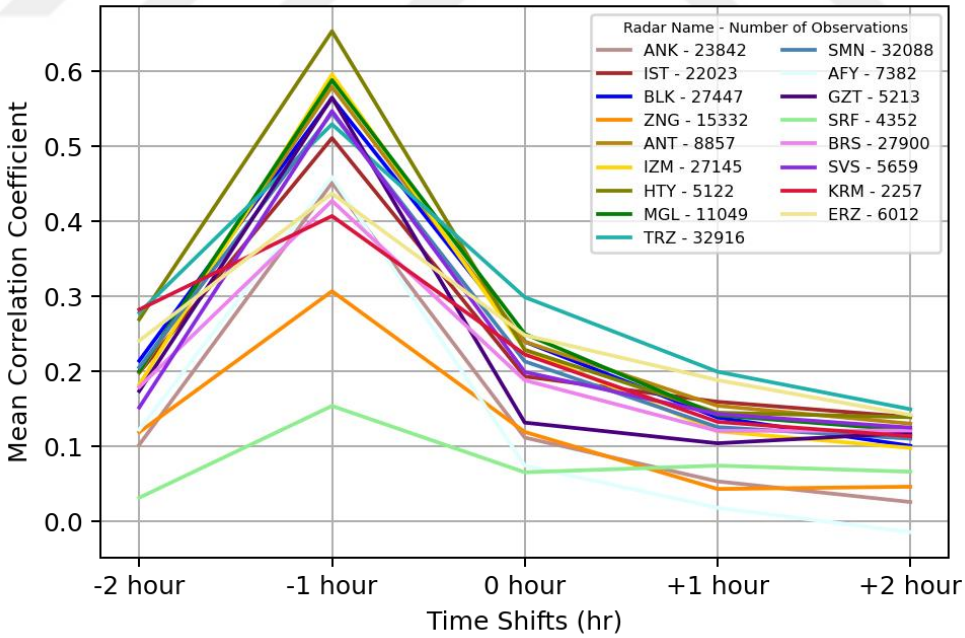

Figure 3.1 The comparison of the effects of time shifts in radar estimations and gauge observations by means of Correlation Coefficient.

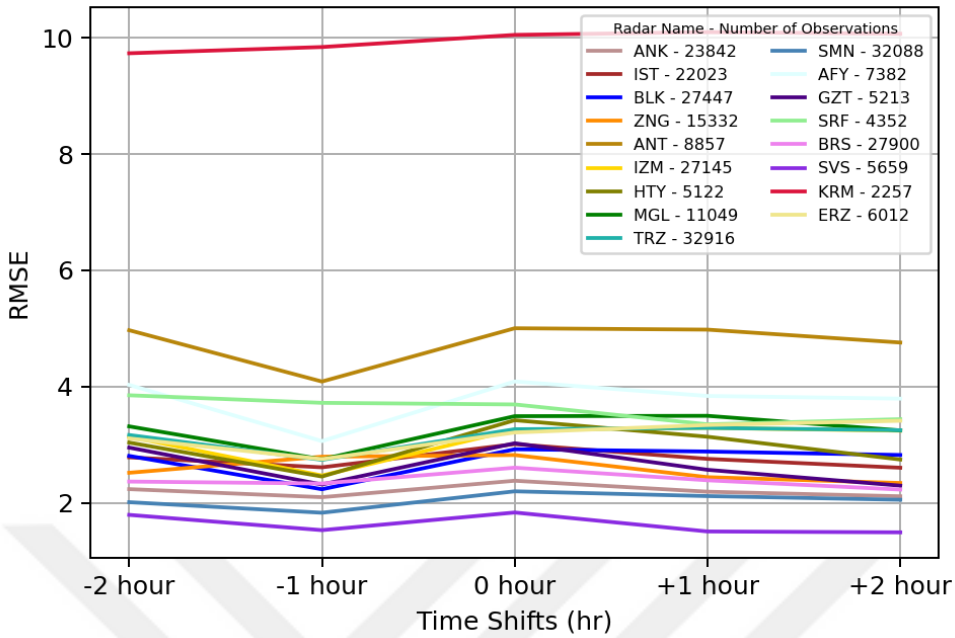

Figure 3.2 The comparison of the effects of time shifts in radar estimations and gauge observations by means of RMSE.

3.1.2 Beam Blockage Analysis

For assessing the underestimation effects caused by Beam Blockage, the stations were categorized according to various CBB-AV rate intervals starting from 0% to 30%. For each category, the number of stations and the percent bias (Pbias) associated with each rate is given in Table 3.1. It can be observed that Pbias generally decreases as the CBB-AV increases. Also, the number of stations associated with lower CBB-AV is higher than the number of stations with higher CBB-AV values. In order to sustain a balance between losing the radar data and reducing the underestimation effects, a subjective CBB-AV threshold of 30% was chosen as a quality mask in the composite maps. If any radar pixel has a CBB-AV of higher than 30%, it is discarded, and the merged product only depends on the gauge-based observations for measuring precipitation in the corresponding pixel.

Moreover, for the overlapping areas, the estimated merged product is dependent on the radar, which has a lower CBB-AV than 30%. For example, in the overlapping

regions between Muğla and İzmir radars (see Figure 2.7), only the estimations from İzmir radar represents the amount of precipitation in this region. However, in the overlapping areas between Istanbul and Balıkesir radars, the average precipitation estimated by both radars are given as the representative amount of precipitation.

Table 3.1 The number of stations and percent biases associated with the given CBB-AV values

CBB-AV (%)	**>= 0.5**		**>= 1**		**>= 2.5**		**>= 5**		**>= 7.5**	
	Number of Stations	**Pbias (%)**	**Number of Stations**	**Pbias (%)**	**Number of Stations**	**Pbias (%)**	**Number of Stations**	**Pbias (%)**	**Number of Stations**	**Pbias (%)**
ANK	37	-8.0	33	-10.6	27	-21.4	16	-22.8	15	-25.3
IST	0	-	0	-	0	-	0	-	0	-
BLK	30	-0.4	25	-3.2	16	-7.5	6	-46.2	2	-69.2
ZNG	28	-72.9	27	-74.7	25	-78.3	16	-79.3	10	-86.5
ANT	14	-75.5	14	-75.5	13	-81.7	12	-87.6	11	-94.9
IZM	49	-40.1	45	-40.2	33	-43.7	21	-53.3	18	-53.4
HTY	24	-68.0	24	-68.0	23	-70.7	20	-78.5	18	-86.8
MGL	40	-74.1	39	-75.7	38	-77.5	37	-78.3	36	-79.2
TRZ	47	22.8	42	25.6	42	25.6	40	31.2	40	31.2
SMN	36	11.1	34	11.9	30	12.7	16	-2.3	8	-16.7
AFY	24	-56.8	21	-60.7	14	-64.6	9	-68.4	6	-71.5
GZT	26	-55.1	25	-56.1	21	-61.8	20	-62.1	17	-63.3
SRF	11	-43.0	11	-43.0	10	-45.1	5	-55.0	2	-49.0
BRS	48	-22.1	43	-23.1	35	-24.4	26	-39.0	17	-54.1
SVS	42	-64.4	42	-64.4	42	-64.4	42	-64.4	41	-65.1
KRM	6	64.1	6	64.1	5	82.7	2	47.7	1	309
ERZ	33	-40.5	32	-42.2	24	-55.9	18	-67.3	13	-77.7

Table 3.1 (continued)

CBB (%)	>= 10		>= 15		>= 20		>= 25		>= 30	
	Number of Stations	Pbias (%)	Number of Stations	Pbias (%)	Number of Stations	Pbias (%)	Number of Stations	Pbias (%)	Number of Stations	Pbias (%)
ANK	14	-25.7	10	-26.7	5	-10	2	-16	0	-
IST	0	-	0	-	0	-	0	-	0	-
BLK	0	-	0	-	0	-	0	-	0	-
ZNG	9	-90.3	7	-92.9	4	-92	1	-96	0	-
ANT	11	-94.9	10	-97.2	9	-98	9	-98	8	-100
IZM	13	-53.2	12	-55.1	8	-47	5	-59	4	-70
HTY	18	-86.8	18	-86.8	18	-86	17	-92	16	-97
MGL	32	-82.0	27	-86.5	23	-86	21	-87	19	-89
TRZ	39	5.8	34	18.4	30	23	27	-83	24	-89
SMN	4	-32.2	1	-27.1	1	-27	0	-	0	-
AFY	3	-79.4	1	-69.9	0	-	0	-	0	-
GZT	10	-73.0	4	-79.9	0	-	0	-	0	-
SRF	0	-	0	-	0	-	0	-	0	-
BRS	11	-64.3	8	-63.4	4	-62	0	-	0	-
SVS	33	-71.4	15	-81.1	3	-85	0	-	0	-
KRM	0	-	0	-	0	-	0	-	0	-
ERZ	11	-79.4	4	-73.0	0	-	0	-	0	-

3.1.3 Karaman Radar

All radars have shown to estimate relatively lower values than gauge observations. As seen in Table 3.1, even over stations with a very slight amount of beam blockage (e.g., <1 percent CBB), the corresponding percent bias values are less than or equal to zero. Radar underestimation is a common problem discussed in many studies which have compared radar QPE with rain gauge observations (e.g., see Goudenhoofdt and Delobbe 2009; Hunter 1996; Overeem, Holleman, and Buishand

2009; Sahlaoui and Mordane 2019). Radar underestimation often happens due to beam blockage or beam overshooting.

However, over Karaman radar, the percent bias (Pbias) values have always shown to be higher than zero, disregarding the amount of beam blockage. Remarkably, over a station with a CBB value of higher than 7.5, Pbias is measured greater than 300%. Figure 3.3 shows the seasonal time-series of radar, gauge, and AF accumulations from 2016 until the end of 2018. These observations are obtained from 31 gauge stations within the range of the radar. It can be observed that Karaman radar's calibration was more stable after 2017. However, yet in winter and fall seasons, a very high mean AF value (e.g., greater than 5 in winter 2018) can be observed, which proves there is a systematic overestimation problem in this radar.

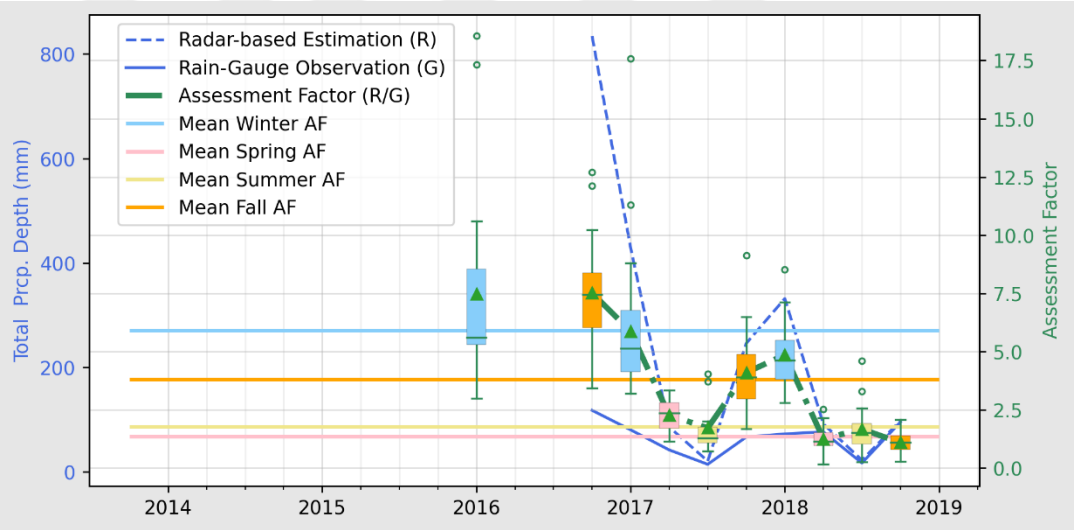

Figure 3.3 Seasonal radar and gauge precipitation accumulations, and AF values of Karaman radar

3.1.4 AF Measurement and Estimation

3.1.4.1 AF Measurement

Among all the stations within the range of each radar, only stations that represent reliable AF ratios (e.g., not having excessive AF fluctuations, underestimation, and

providing enough data for seasonal modeling) are chosen. Other stations were not used in ANN and MLR models. Following are the criteria for choosing reliable stations:

1. Excessive AF fluctuations may represent rain gauge errors. Thus, stations with AF standard deviation above 0.6 were filtered.
2. The stations associated with excessive radar underestimation were filtered. Stations that represent mean AF of less than 0.2 were eliminated.
3. Rain gauge stations that provide data (both radar-based and gauge-based) less than ten seasons (2.5 years out of 5 years) were filtered out.

Table 3.2 The number of stations left nearby each radar before and after considering each criterion in reliable station selection, respectively. The first number indicates the total number of nearby gauge stations (A), whereas the three following numbers (B, C, D) indicate the filtered stations in each criterion. The remaining stations were used in MLR (2.2.2.1) and ANN (2.2.2.3) models.

RADAR NAME	NUMBER OF STATIONS	RADAR NAME	NUMBER OF STATIONS
	A B C D		A B C D
ANKARA	67 44 44 38	**TRABZON**	59 40 38 36
İSTANBUL	56 47 47 45	**SAMSUN**	63 52 52 50
BALIKESİR	66 41 41 41	**AFYON**	77 16 16 13
ZONGULDAK	58 36 32 27	**GAZIANTEP**	49 35 34 33
ANTALYA	28 20 12 11	**ŞANLIURFA**	46 7 7 3
İZMİR	73 51 50 49	**BURSA**	90 41 41 37
HATAY	32 19 16 15	**SİVAS**	43 28 28 25
MUĞLA	51 37 30 29	**ERZURUM**	54 15 14 8
KARAMAN	31 0 0 0		

After selecting the reliable stations, four seasonal AF values were specified for each station except for Karaman radar due to its extreme AF fluctuations and inconsistent data over the studied years (no reliable station). Additionally, there is not a sufficient

number of available stations (three stations) for training and validating models for Şanlıurfa radar, as well. Figure 3.4-3.8 represent seasonal radar estimations, gauge observations, and AF values of radars with a sufficient number of reliable stations.

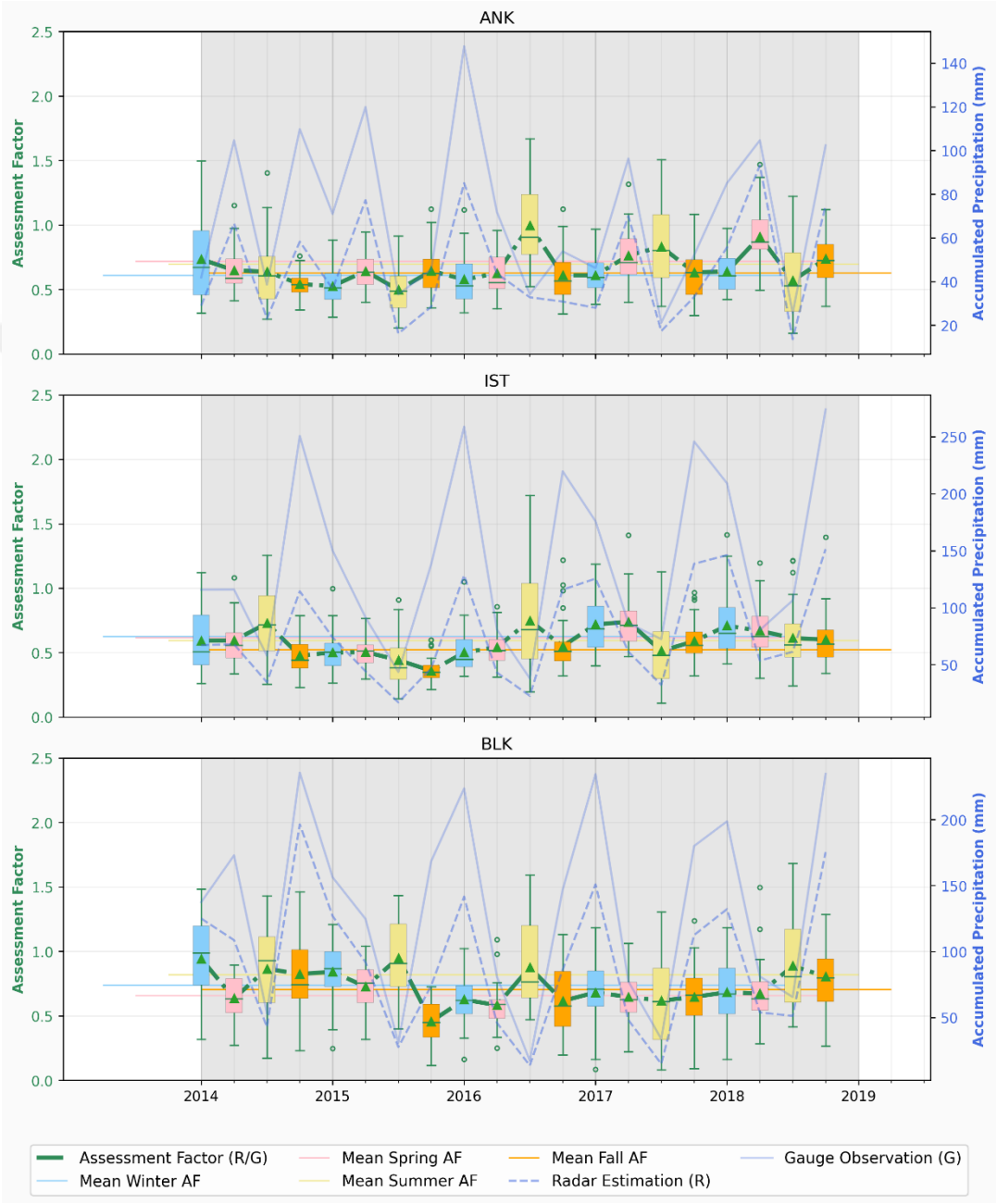

Figure 3.4 Seasonally accumulated radar estimations, gauge observations, and AF values (R/G) time-series for Ankara, Istanbul and Balıkesir radars

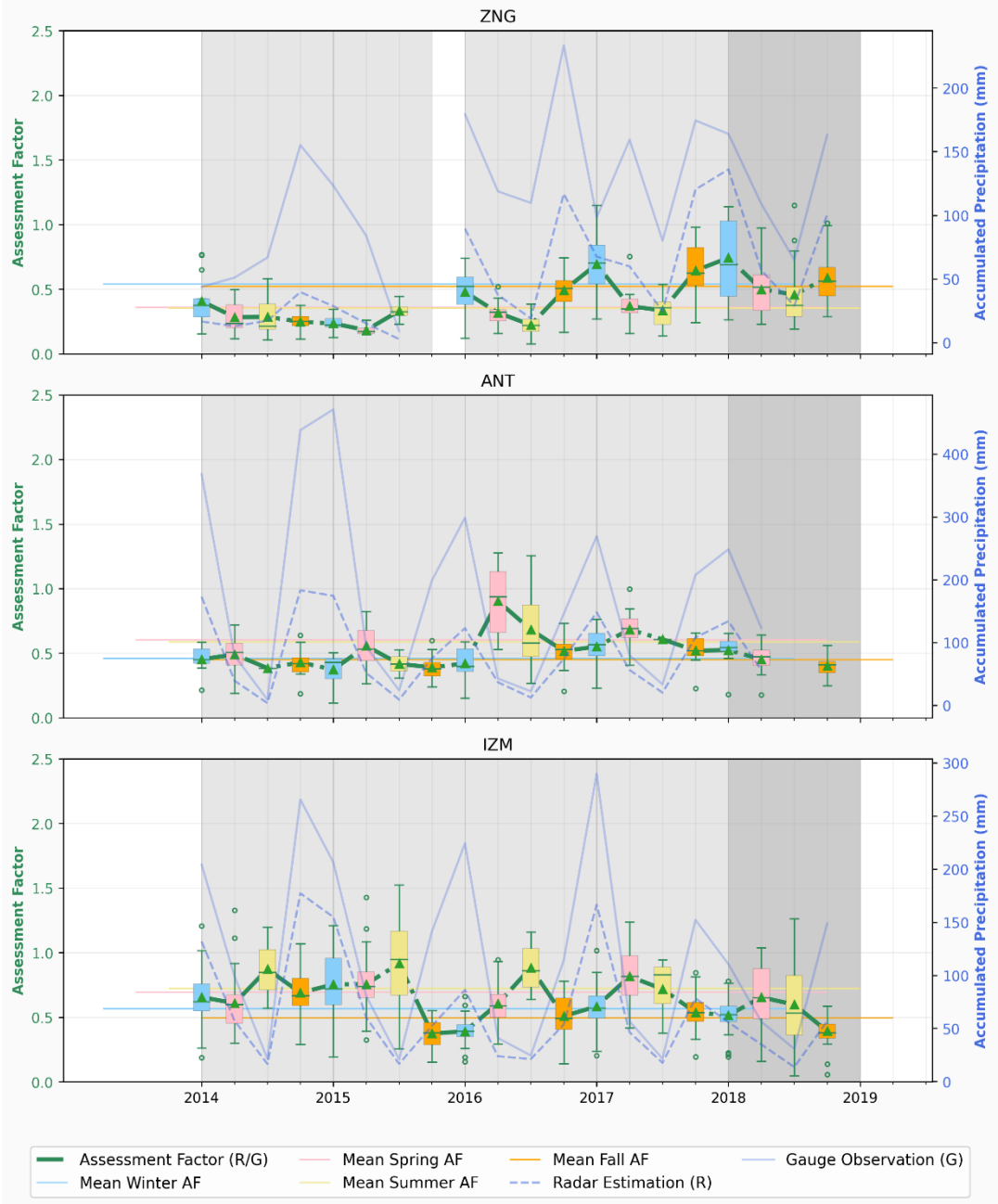

Figure 3.5 Seasonally accumulated radar estimations, gauge observations, and AF values (R/G) time-series for Zonguldak, Antalya and Izmir radars

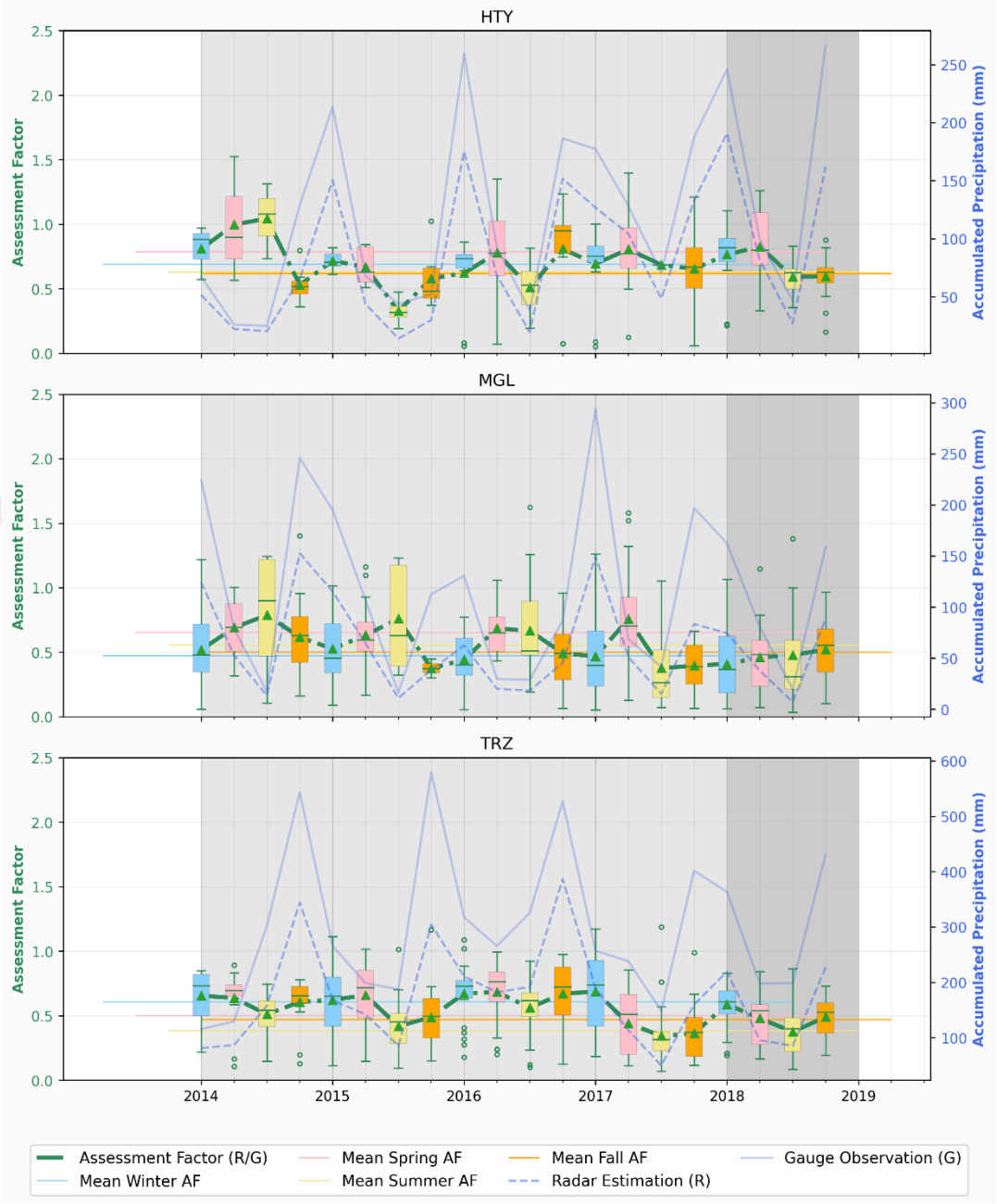

Figure 3.6 Seasonally accumulated radar estimations, gauge observations, and AF values (R/G) time-series for Hatay, Muğla and Trabzon radars

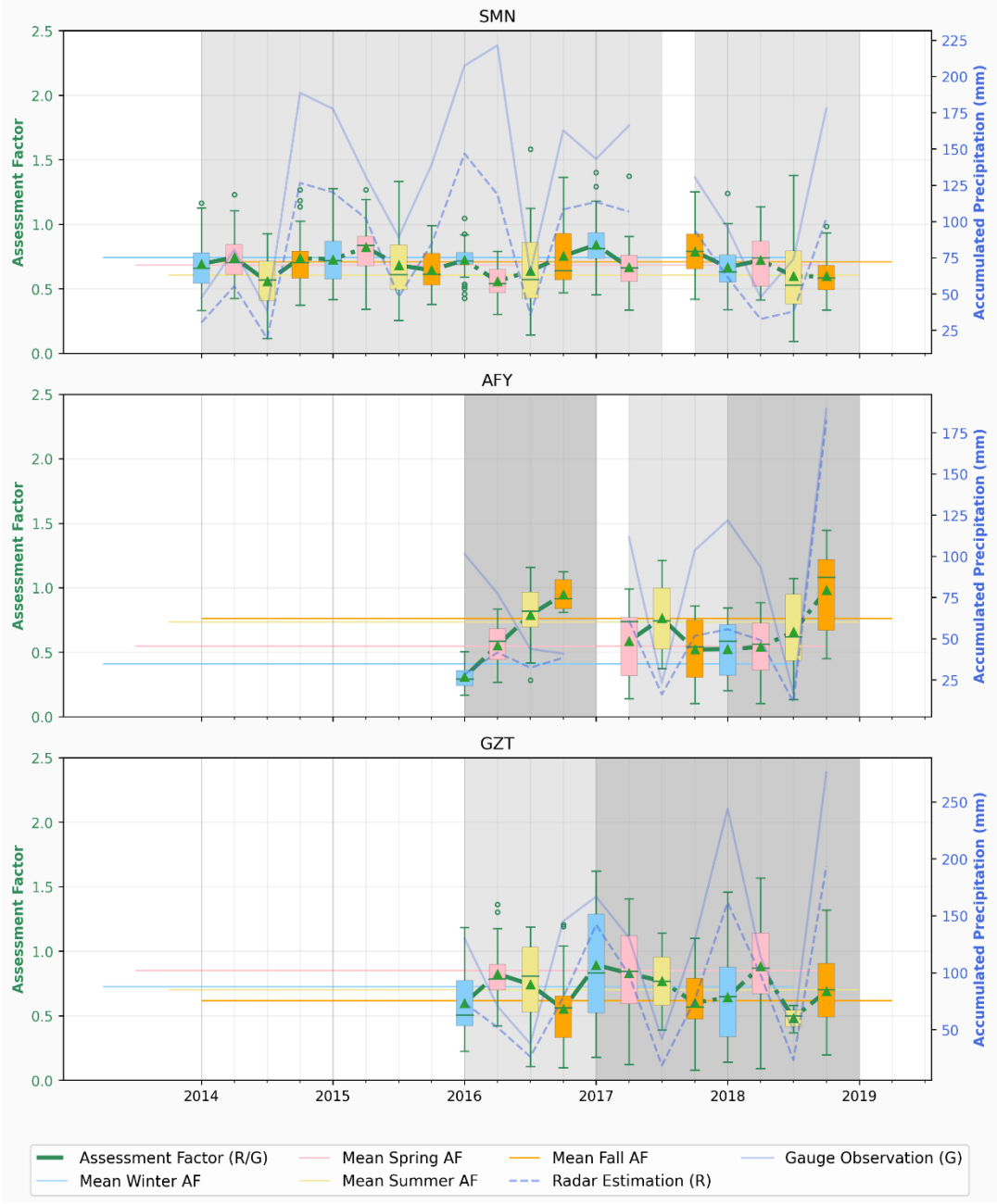

Figure 3.7 Seasonally accumulated radar estimations, gauge observations, and AF values (R/G) time-series for Samsun, Afyon and Gaziantep radars

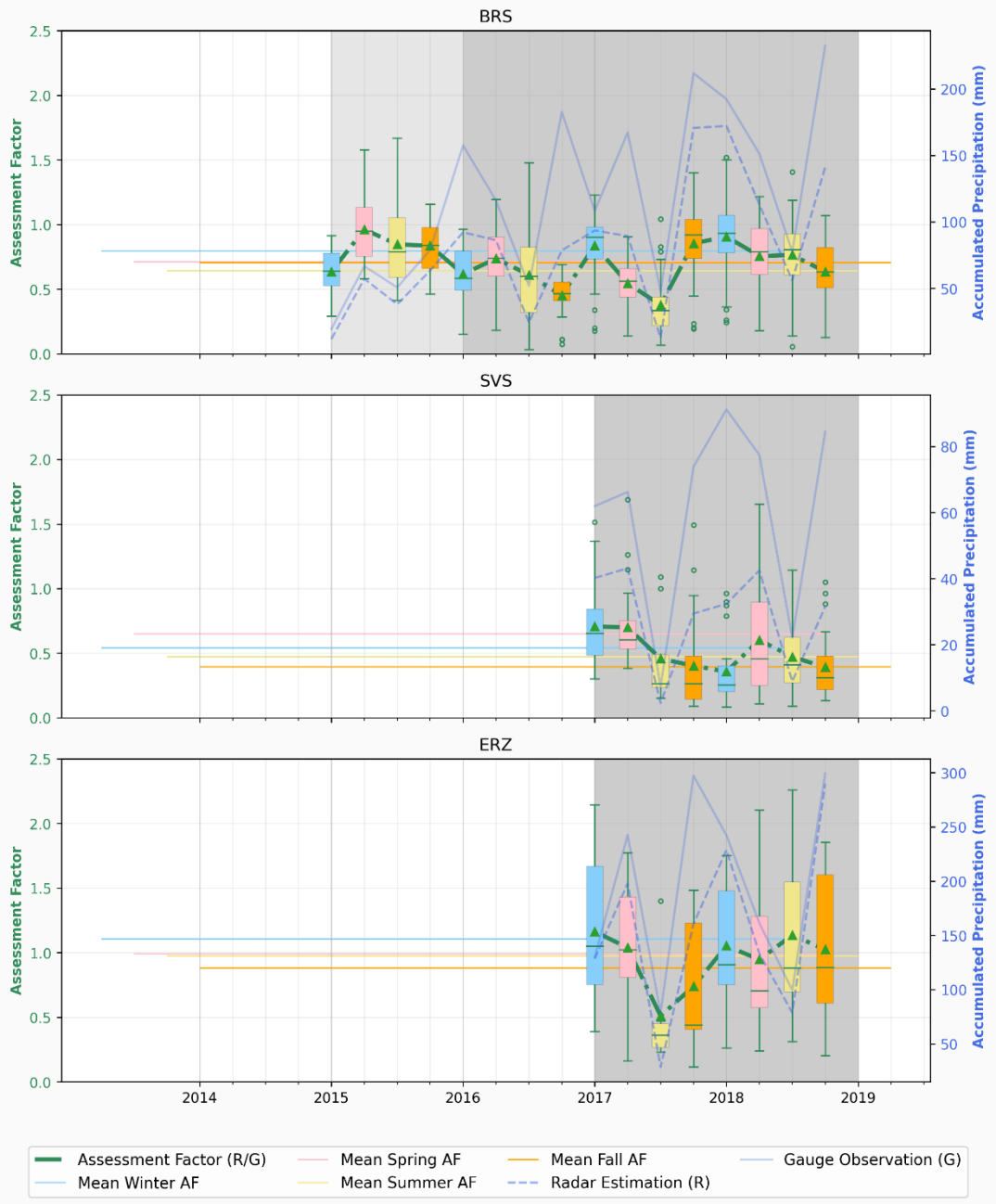

Figure 3.8 Seasonally accumulated radar estimations, gauge observations, and AF values (R/G) time-series for Bursa, Sivas and Erzurum radars

In Figure 3.4-3.8, the periods which the initial range of radar is 120 km is shown with light-colored grey, whereas the periods with radar initial range of greater than 120 km is highlighted with dark-colored grey. During periods where there is no

radar data available, the background is colored as white. Although all the data is trimmed and upscaled into 120 km and 1km resolution (see 2.1.2.4), it can be observed that data trimming and upscaling from higher ranges into smaller ranges have had no significant effect on AF and seasonal radar accumulations.

3.1.4.2 AF Estimation

According to Figure 3.9-3.23, the estimated AF values by both MLR and ANN models have shown to be in close agreement with the measured AF values over BLK, IZM, SMN, GZT, BRS radars with a slight difference in the distribution of the points. It is expected that the improved radar QPE using MLR and ANN models over these locations will have a better agreement with the gauge-based observations. This will be validated after using comparing the corrected radar estimations with the gauge observations (3.3.1). The relationship established in these models only considers time-independent systematic errors, so the effects of random errors on the AF values cannot be determined. Over some radars (e.g., ANT, SVS), there is not a good agreement between the measured and predicted AFs. This poor predictive capacity can be due to the existence of a higher rate of random errors in these radars. Some differences can be observed in how the data are scattered in various seasons and methods. For example, in GZT, the distribution of ANN validation points in fall seasons is sparser than MLR. In TRZ, however, MLR distribution in fall seasons is sparser than ANN, which means either of these models can perform differently regarding the season and type of events, so both of them must be tested and compared.

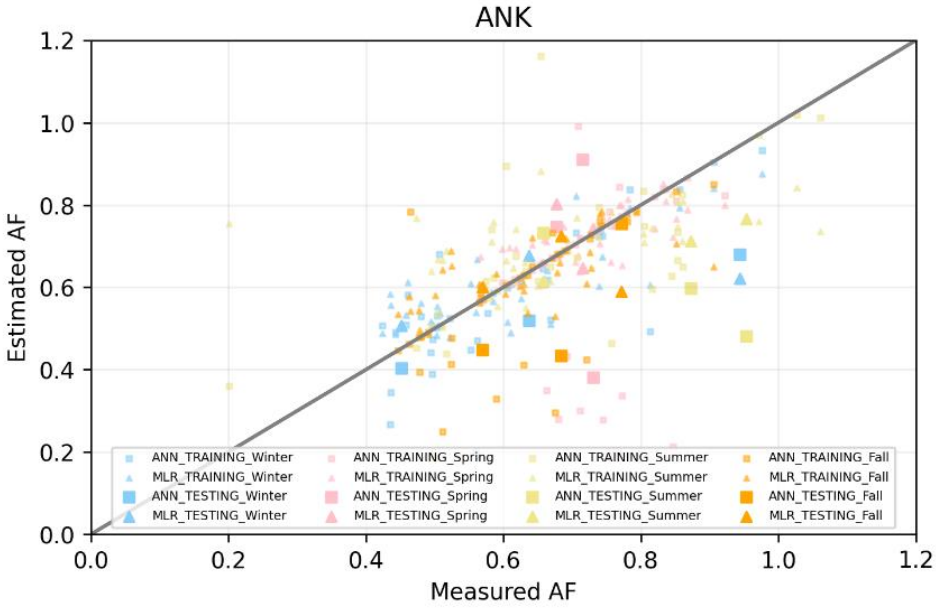

Figure 3.9 AF Estimation-ANK

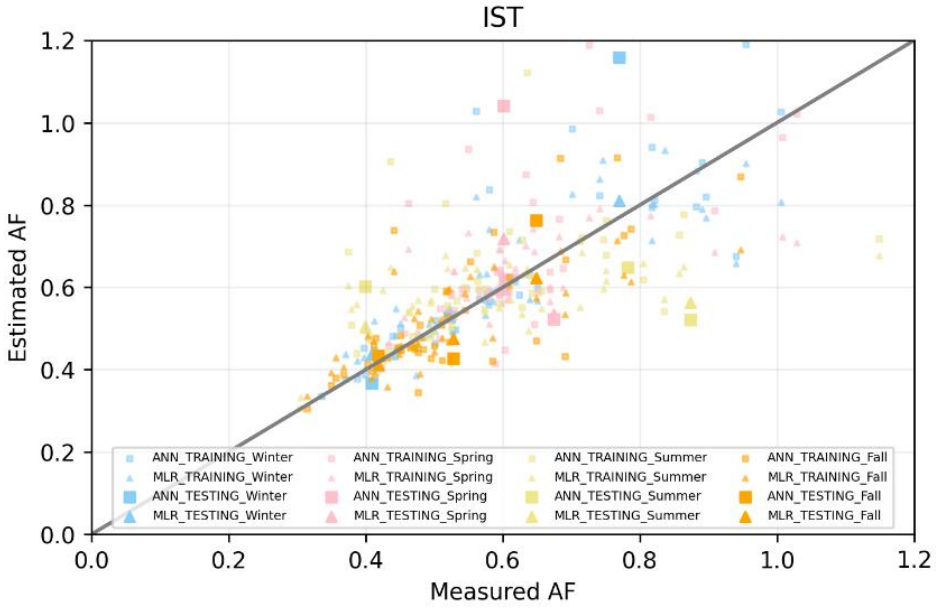

Figure 3.10 AF Estimation-IST

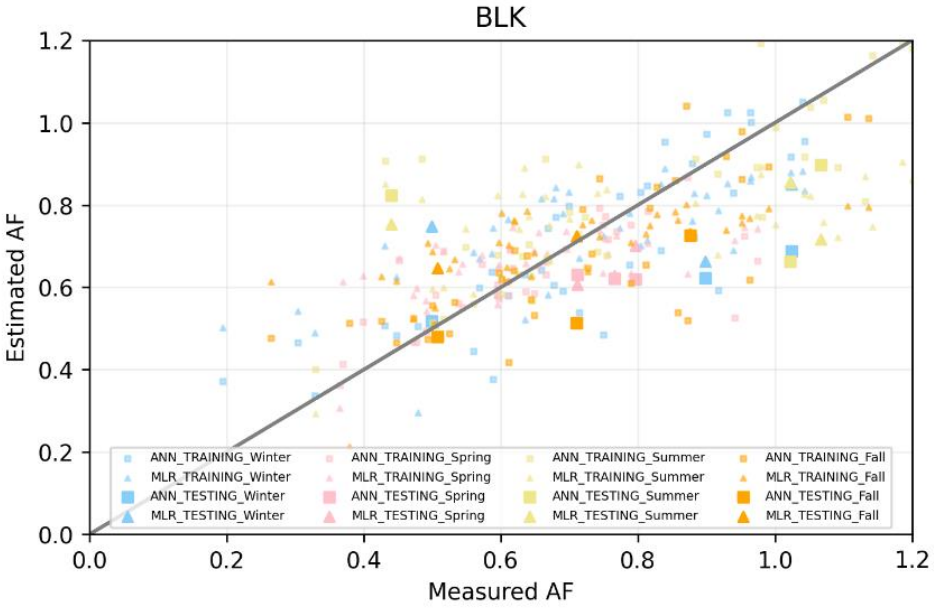

Figure 3.11 AF Estimation-BLK

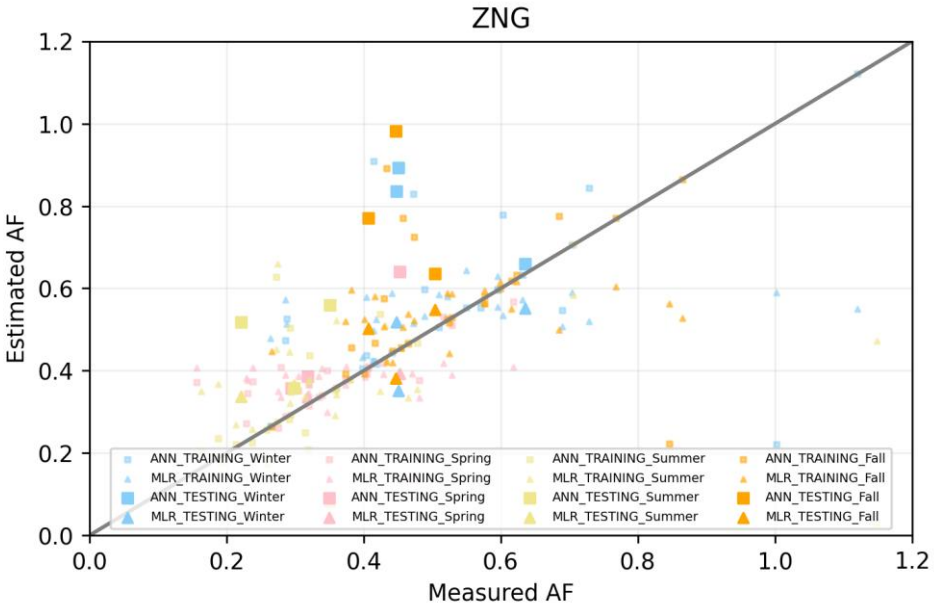

Figure 3.12 AF Estimation-ZNG

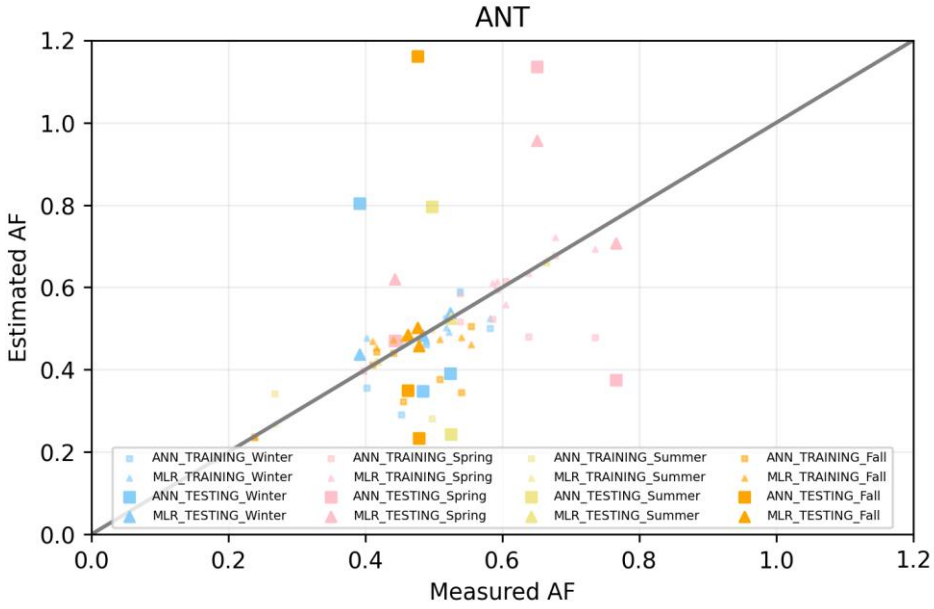

Figure 3.13 AF Estimation-ANT

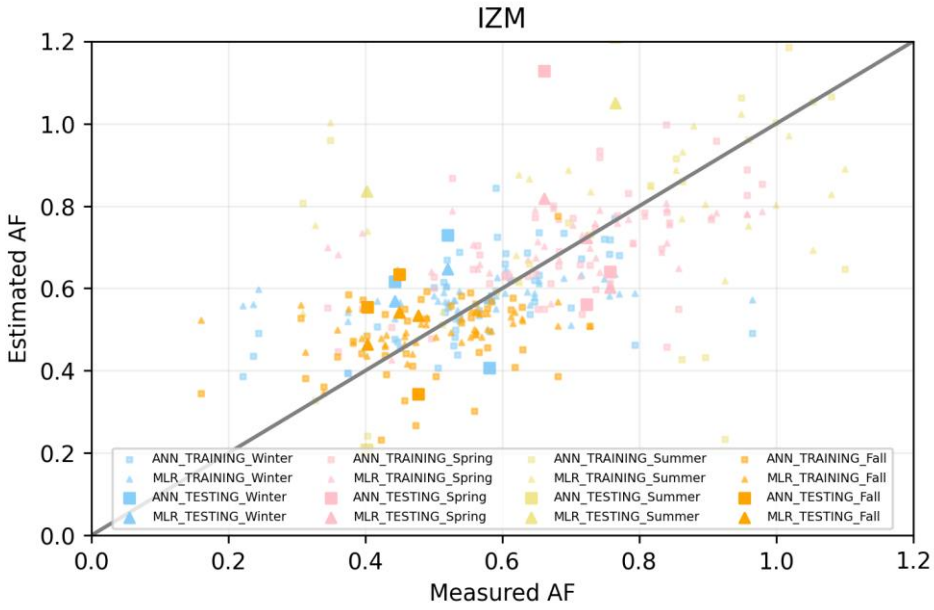

Figure 3.14 AF Estimation-IZM

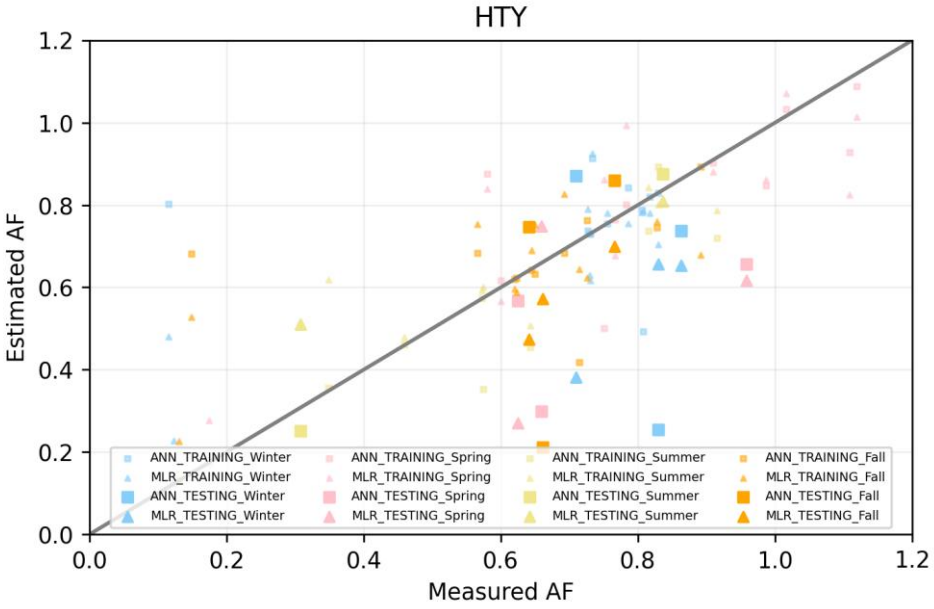

Figure 3.15 AF Estimation-HTY

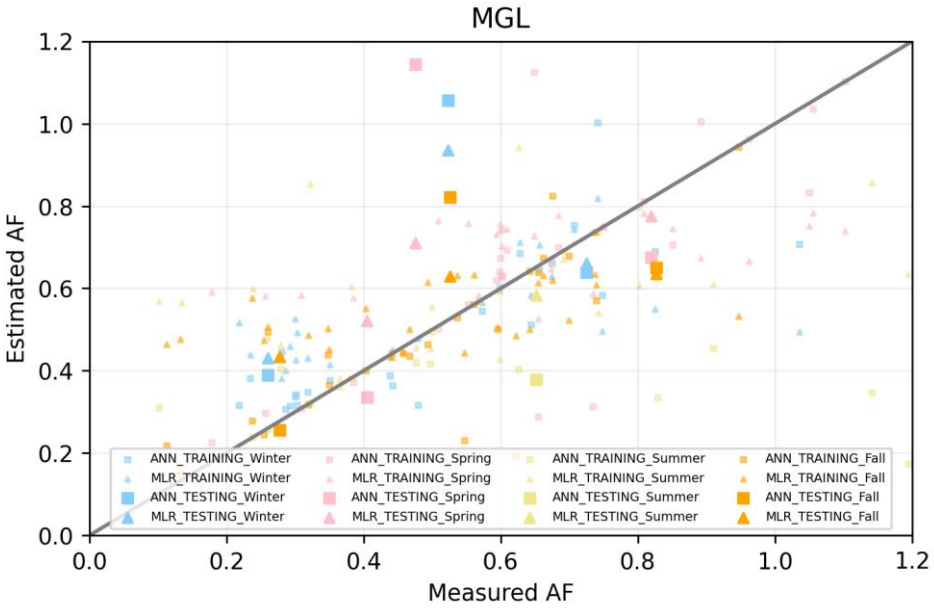

Figure 3.16 AF Estimation-MGL

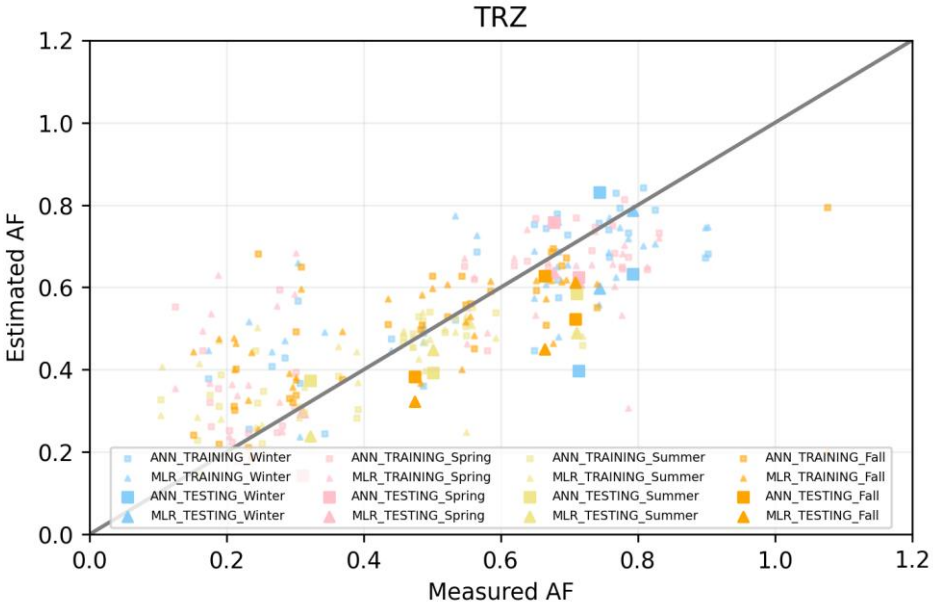

Figure 3.17 AF Estimation-TRZ

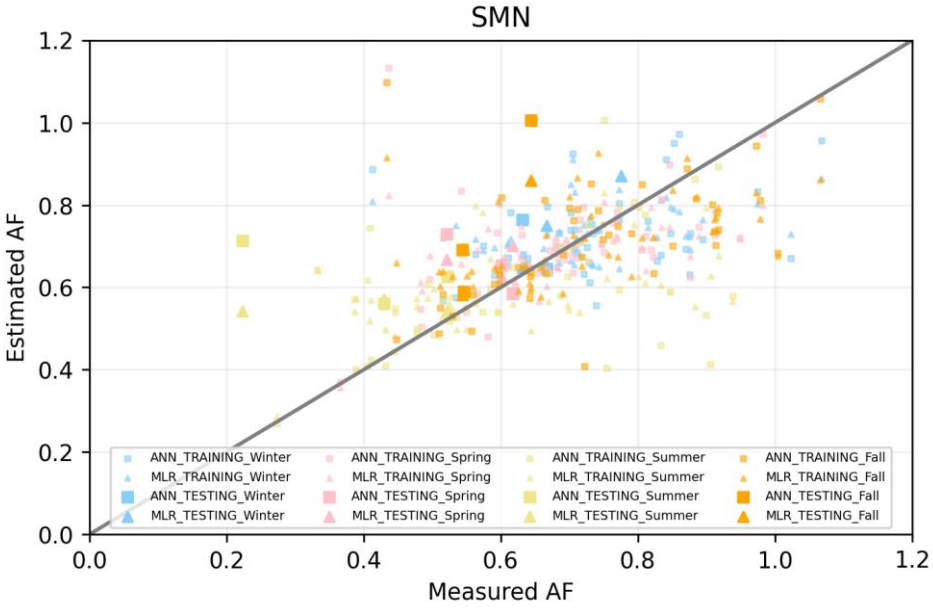

Figure 3.18 AF Estimation-SMN

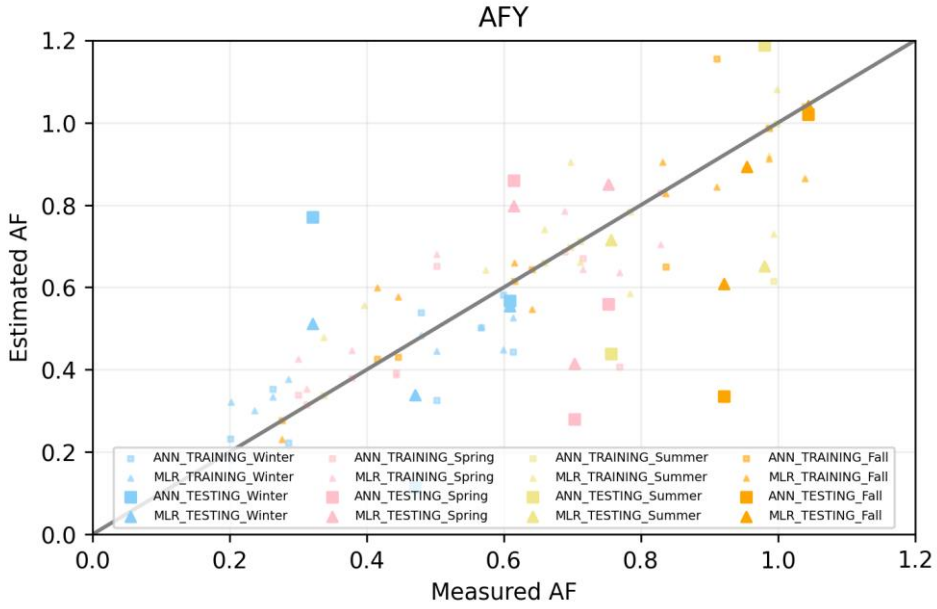

Figure 3.19 AF Estimation-AFY

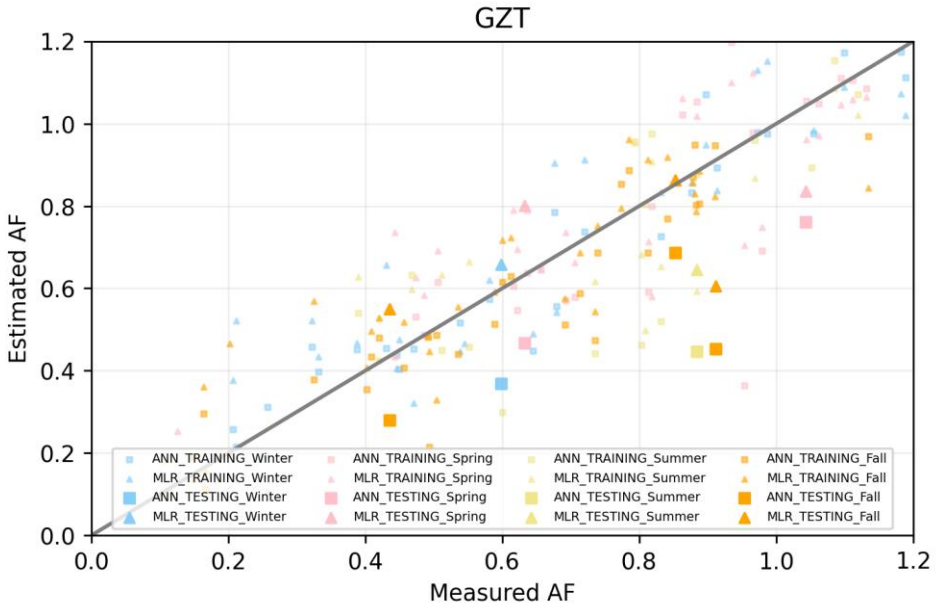

Figure 3.20 AF Estimation-GZT

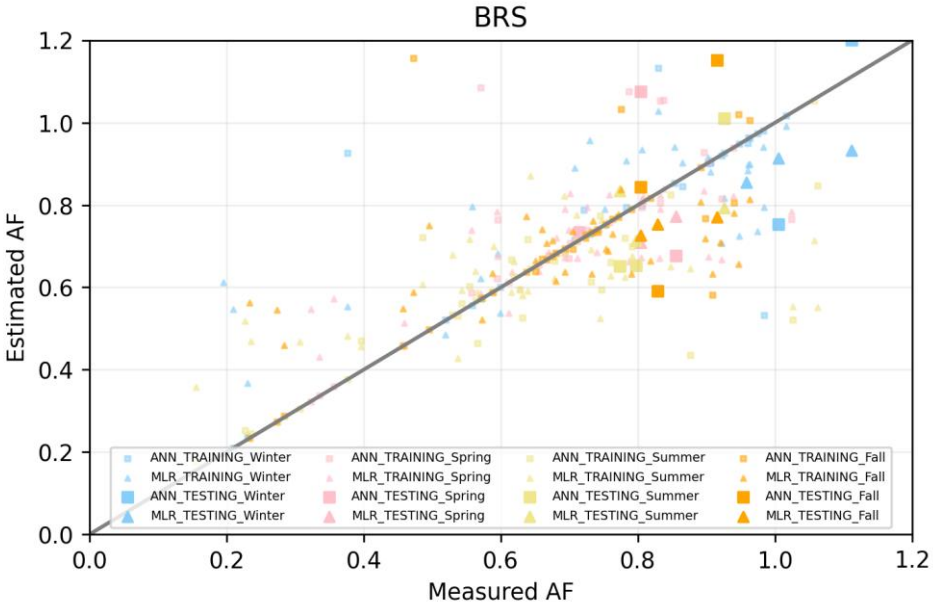

Figure 3.21AF Estimation-BRS

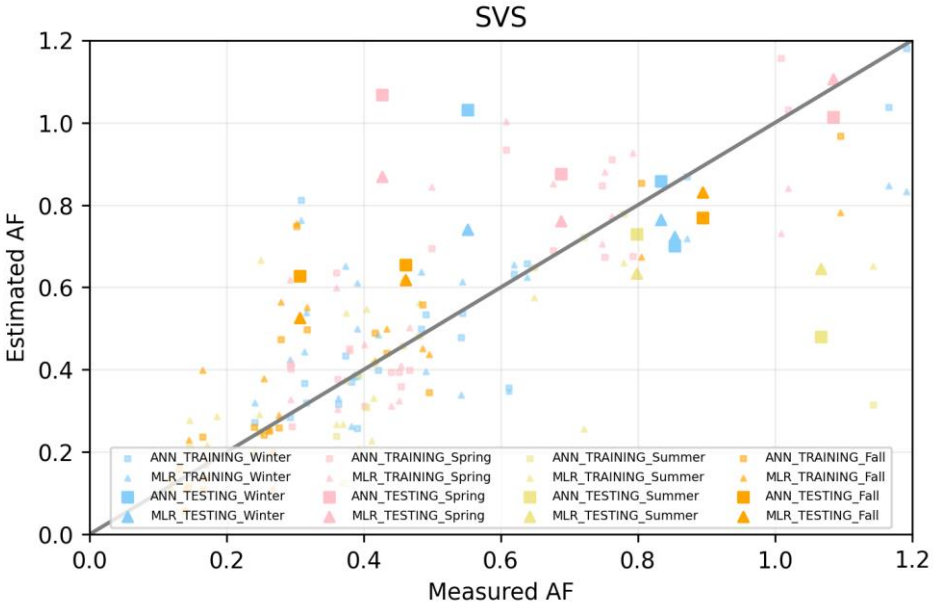

Figure 3.22 AF Estimation-SVS

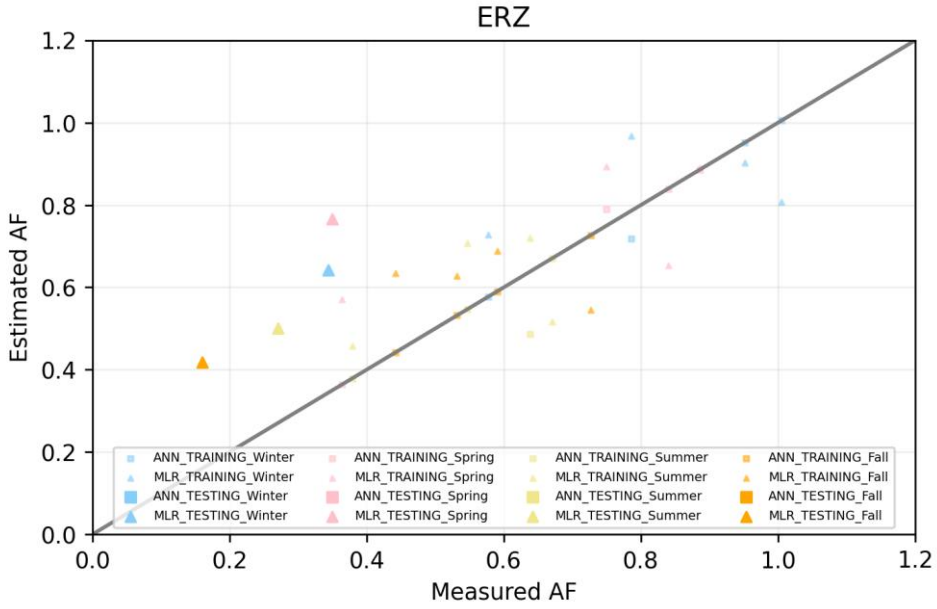

Figure 3.23 AF Estimation-ERZ

3.1.5 Radar-Gauge CDFs

Figure 3.24 shows the CDF of radar-based and station-based precipitation values measured over all stations within the range of each radar. Each line in these plots represents the CDF of radar-based (shown with red color) or station-based (blue color) precipitation observed over a particular station. For a better comparison, only precipitation rates of up to 30mm/hr is shown in this figure. It can be noticed that over Erzurum and Karaman radars, the CDF of radar-based estimations lies below the CDF of gauge-based observations. Therefore, the probability of precipitation with a higher intensity is greater in radar-based estimations than the gauge-based observations. In the contrary, over the rest of the radars (e.g., Ankara, Istanbul, Balıkesir, Muğla), gauge-based observations with higher precipitation intensity are more expected than the radar-based observations with the same intensity. Over some radars (e.g., Hatay, Şanlıurfa, Bursa) the CDFs are very nearly met. However, this does not suggest that the bias is lower in these radars because matched CDFs

represent the relative closeness of the ranked (by intensity) radar estimations and gauge observation values disregarding the time of the precipitation events.

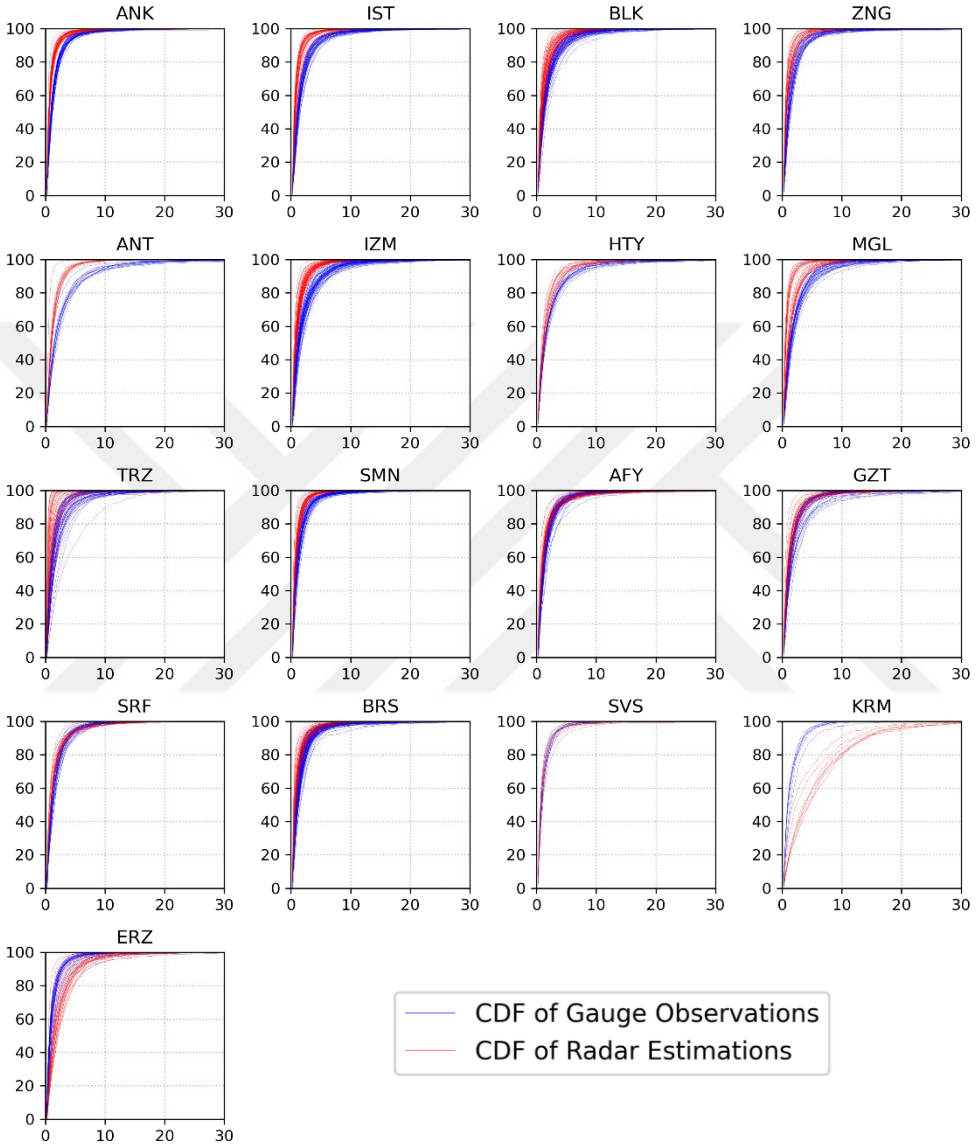

Figure 3.24 CDF of radar-based and station-based precipitation values over all stations within the range of each radar. In these plots, X axis represents the precipitation intensity (mm/hr) and Y axis represents the cumulative probability (%).

3.1.6 Estimation of A and B Parameters in Z-R Relationships

In the following tables, $\Delta \boldsymbol{RMSE}$ (mm/hr) and $\Delta \mathbf{MAE}$ (mm/hr) represent the value of RMSE and MAE obtained from the new Z-R relationship minus the corresponding error values obtained from the original Z-R relationship ($a = 200, b = 1.6$). Negative error values represent better performance of the new Z-R relationship, whereas – sign indicates there is no improvement in the new Z-R relationship and use of the original Marshall-Palmer relationship.

Table 3.3 a and b values obtained based on regression-based Z-R relationship assigned for various radars for the Winter season

	$\boldsymbol{a}$	$\boldsymbol{b}$	$\Delta \boldsymbol{RMSE}$ (mm/hr)	$\Delta \mathbf{MAE}$ (mm/hr)
ANKARA	311.2	3.23	-0.06	-0.06
İSTANBUL	79.80	2.75	-0.11	-0.27
BALIKESİR	200	1.6	-	-
ZONGULDAK	200	1.6	-	-
ANTALYA	62.82	1.98	-0.27	-0.63
İZMİR	87.78	2.23	-0.10	-0.28
HATAY	200	1.6	-	-
MUĞLA	70.20	2.24	-0.11	-0.34
TRABZON	200	1.6	-	-
SAMSUN	200	1.6	-	-
AFYON	200	1.6	-	-
GAZIANTEP	200	1.6	-	-
ŞANLIURFA	200	1.6	-	-
BURSA	200	1.6	-	-
SİVAS	200	1.6	-	-
KARAMAN	5930.5	3.50	-6.17	-4.18
ERZURUM	200	1.6	-	-

Table 3.4 a and b values obtained based on regression-based Z-R relationship assigned for various radars for the Spring season

	a	b	$\Delta RMSE$ (mm/hr)	ΔMAE (mm/hr)
ANKARA	124.42	2.37	-0.17	-0.07
İSTANBUL	93.08	2.26	-0.05	-0.22
BALIKESİR	105.02	2.21	-0.06	-0.16
ZONGULDAK	200	1.6	-	-
ANTALYA	155.12	1.75	-0.03	-0.09
İZMİR	90.53	2.21	-0.04	-0.23
HATAY	200	1.6	-	-
MUĞLA	99.95	2.06	-0.06	-0.22
TRABZON	200	1.6	-	-
SAMSUN	200	1.6	-	-
AFYON	200	1.6	-	-
GAZIANTEP	200	1.6	-	-
ŞANLIURFA	200	1.6	-	-
BURSA	200	1.6	-	-
SİVAS	200	1.6	-	-
KARAMAN	713.28	2.49	-0.69	-0.27
ERZURUM	765.13	2.70	-0.37	-0.01

Table 3.5 a and b values obtained based on regression-based Z-R relationship assigned for various radars for the Summer season

	a	b	$\Delta RMSE$ (mm/hr)	ΔMAE (mm/hr)
ANKARA	111.34	2.31	-0.12	-0.06
İSTANBUL	57.38	2.06	-0.25	-0.60
BALIKESİR	122.47	1.98	-	-
ZONGULDAK	25.42	3.05	-0.18	-0.53

Table 3.5 (continued)

ANTALYA	**200**	**1.6**	**-**	**-**
İZMİR	200	1.6	-	-
HATAY	200	1.6	-	-
MUĞLA	200	1.6	-	-
TRABZON	54.11	2.10	-0.18	-0.45
SAMSUN	200	1.6	-	-
AFYON	200	1.6	-	-
GAZIANTEP	200	1.6	-	-
ŞANLIURFA	200	1.6	-	-
BURSA	200	1.6	-	-
SİVAS	200	1.6	-	-
KARAMAN	200	1.6	-	-
ERZURUM	200	1.6	-	-

Table 3.6 a and b values obtained based on regression-based Z-R relationship assigned for various radars for the Fall season

	$\boldsymbol{a}$	$\boldsymbol{b}$	$\Delta\boldsymbol{RMSE}$ (mm/hr)	$\Delta\mathbf{MAE}$ (mm/hr)
ANKARA	160.03	2.62	-0.02	-0.11
İSTANBUL	70.28	2.40	-0.11	-0.35
BALIKESİR	127.81	2.46	-0.03	-0.03
ZONGULDAK	200	1.6	-	-
ANTALYA	79.59	1.95	-0.18	-0.46
İZMİR	73.51	1.94	-0.22	-0.48
HATAY	200	1.6	-	-
MUĞLA	59.56	2.19	-0.14	-0.46
TRABZON	119.48	2.71	-	-
SAMSUN	191.64	2.73	-0.01	-0.05

Table 3.6 (continued)

AFYON	**200**	**1.6**	-	-
GAZIANTEP	138.06	2.23	-	-
ŞANLIURFA	147.74	2.51	-	-
BURSA	163.72	2.88	-0.06	-0.03
SİVAS	179.89	2.71	-0.06	-0.09
KARAMAN	200	1.6	-	-
ERZURUM	200	1.6	-	-

It can be inferred that the estimation of an appropriate Z-R relationship by fitting the seasonal observations (disregarding the system or nature of the precipitation) using linear regression is an efficient way to reduce the radar estimation errors. However, the estimation skill of the linear regression in predicting a and b values can significantly vary depending on the studied season. Table 3.5 is a clear indication that a regression-based Z-R relationship establishment is less likely a suitable method to be used in summer precipitation events. The new Z-R relationship has performed successfully in 4 out of 17 radars in the summer events. In contrast, in the fall season, 9 out of 17 radars presented a better performance with the new Z-R relationship (Table 3.6).

In this method, a single seasonal Z-R relationship is defined for each radar based on observations made by all stations. Meanwhile, the precipitation type may vary by station. The predominance of convective events in summer may be a significant source of restriction of this method in summer seasons. Not only are convective precipitation events of a very small vertical and horizontal scale, but also higher intensity. The Z-R relationship, which is assigned for larger-scale events recorded in the majority of the stations, might not represent well a station that has a convective precipitation system, which most likely has higher intensity resulting in higher error values.

3.1.7 Analysis of Triple-Collocated Rain Gauge Data

The Triple-Collocated rain gauge stations measure precipitation intensity over three different gauges at one location. In order to choose a representative value for each station to be compared with the radar estimations in each location, we compared the mean and median of the three gauges at each station with the closest AWOS rain gauge. Using the mean of three observations can be helpful when all three gauges have closer values to each other. However, if one of the gauges malfunctions, the mean would be significantly affected by the bias induced by the malfunctioning gauge.

In Figure 3.25-3.6, the RMSE and COR of the mean or median of the Triple-Collocated gauge observations against the nearest AWOS gauge observation are presented.

The median has shown to provide a better agreement with the nearby gauges. Therefore, In the evaluation of methods, the median of the observations from three gauges located at each additional validation station will be used in order to test radar-based estimation accuracy.

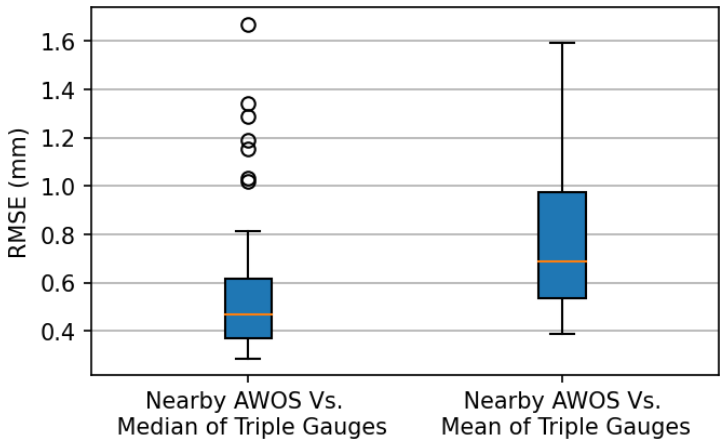

Figure 3.25 Comparison of mean and median of Triple-Collocated gauge observations as a representative value against the nearest AWOS station based on RMSE (mm)

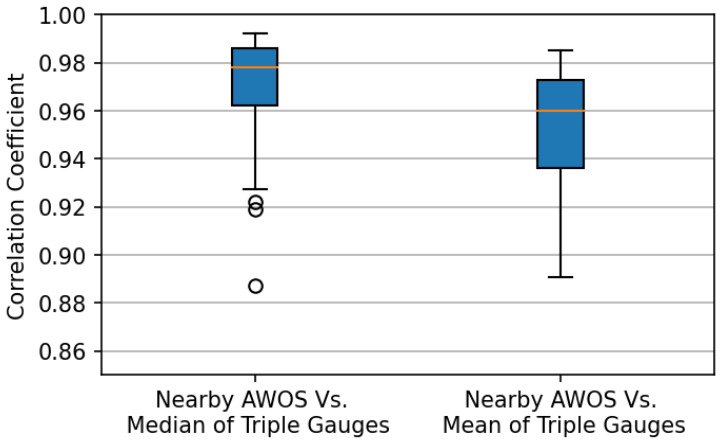

Figure 3.26 Comparison of mean and median of Triple-Collocated gauge observations as a representative value against the nearest AWOS station based on Correlation Coefficient

3.1.8 Analysis of Disdrometer Data

For investigating the accuracy of the disdrometer data, the precipitation observations obtained from disdrometer data were compared with the corresponding observations recorded by three rain gauges located almost at the same location as the disdrometer. This comparison is made for the data observed during the years 2015-2018. The data is obtained from 16 stations, which are located in overlapping areas within 120 km distance from the Balıkesir-Izmir or Muğla-Izmir radars.

The results regarding the consistency of the disdrometer data with the other three gauges as well as the inconsistency of the three gauges are given in the following figures. According to Figure 3.27, except for 6 stations, the correlation of disdrometer-based precipitation is significantly high comparing against the other three gauges in the other 10 stations. The cross RMSE values are generally high (roughly 2.2 mm/hr in average), but lower in 3 stations (less than 1.5 mm/hr), and considerably high in 4 stations (greater than 2.5mm/hr). However, there is no significant difference in cross RMSE values of disdrometer with other gauges.

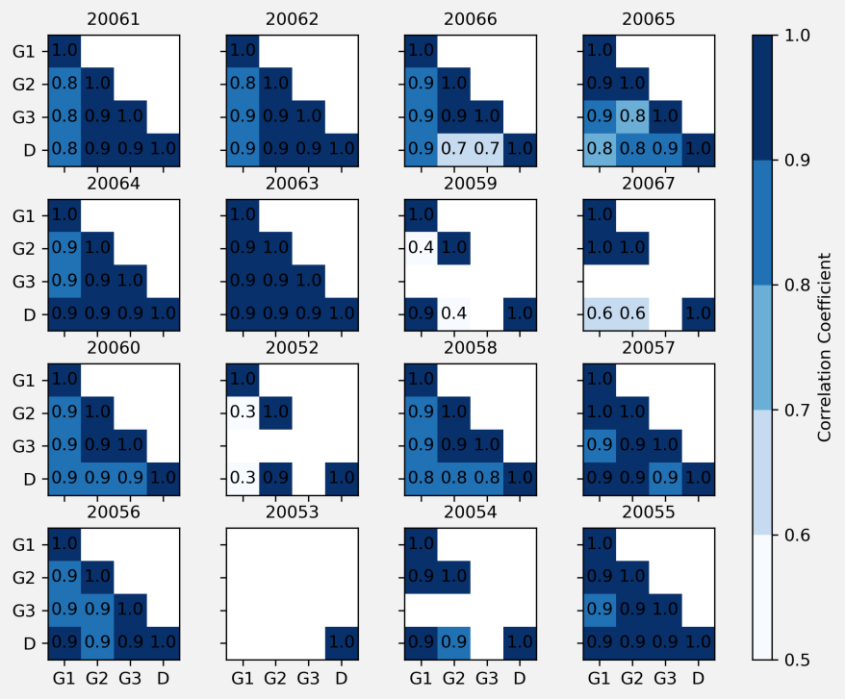

Figure 3.27 Cross correlation of precipitation obtained from each disdrometer (D) and three nearby collocated rain gauges (G1, G2, G3) over 16 various stations

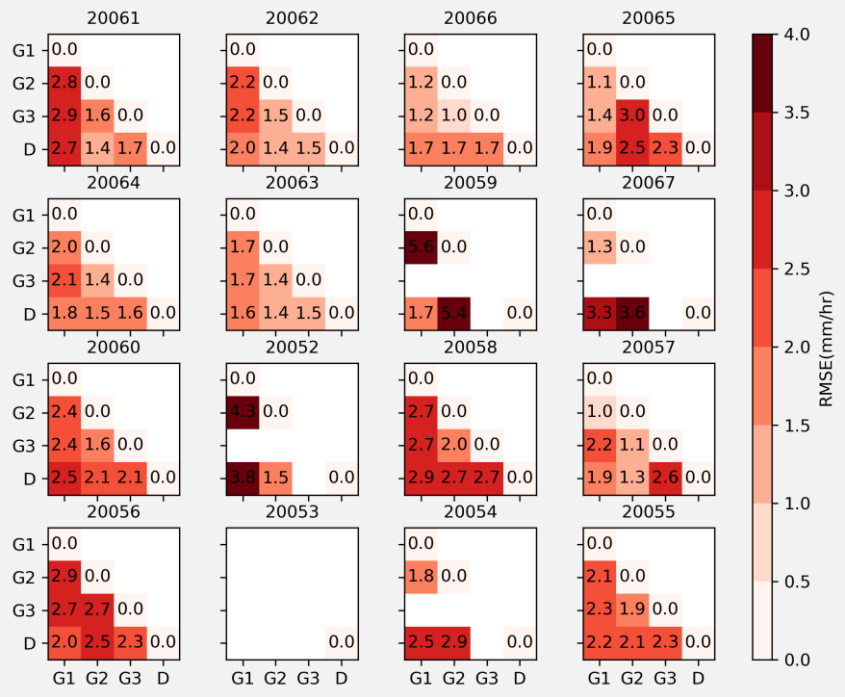

Figure 3.28 Cross RMSE of precipitation obtained from each disdrometer (D) and three nearby collocated rain gauges (G1, G2, G3) over 16 various stations

Figure 3.29-3.31 show the monthly precipitation accumulation time-series plotted for disdrometer and three gauges over 16 stations. The precipitation observed by the disdrometer is shown to be consistently underestimating against the nearby weighing or tipping bucket rain gauges over 12 stations (stations 20058, 20057, 20056, 20054, 20055, 20061, 20062, 20066, 20065, 20064, 20063, 20059). Therefore, using the disdrometer reflectivity data for improving radar-based observations which are prone to underestimation against the ground observations, would not be a good choice with the given data in this particular study.

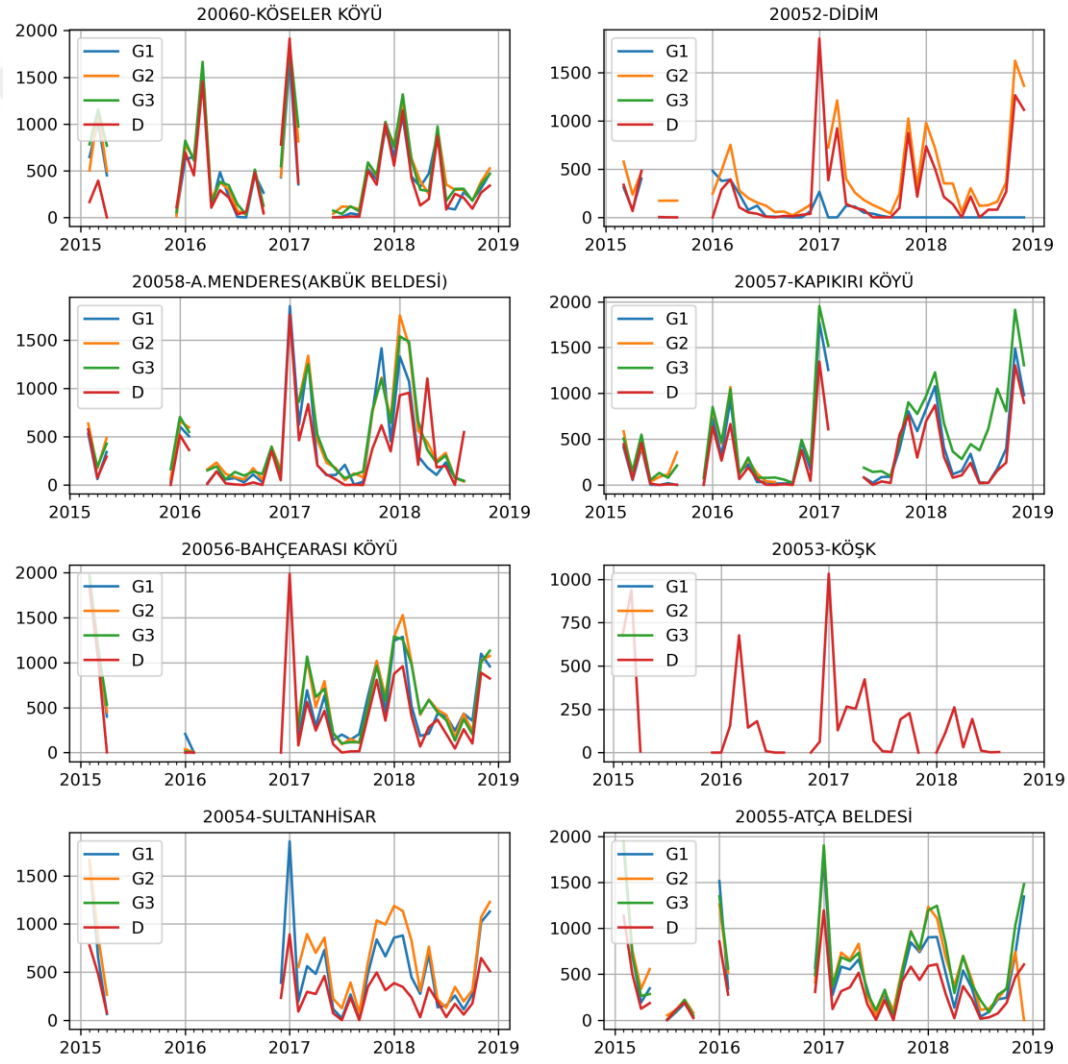

Figure 3.29 Monthly time-series of precipitation observed using disdrometers (D) and three nearby collocated rain gauges (G1, G2, G3)

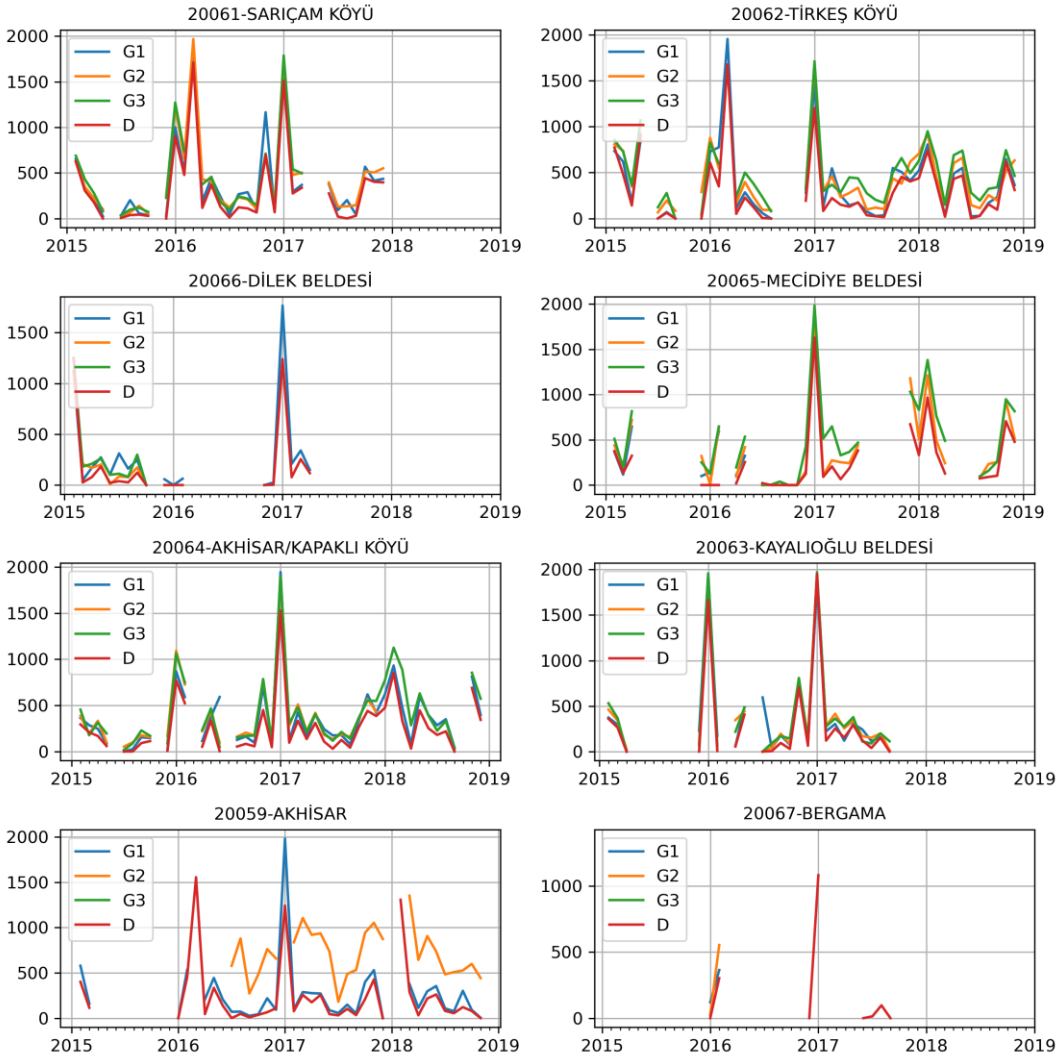

Figure 3.29 (continued)

3.2 Merged Precipitation Maps

The following figures represent two various composite maps produced based on the radar-based estimations merged with the gauge observations through all bias correction methods. In the first set of figures (Figure 3.30-3.34) only radar-gauge merged maps are shown. In the second set of figures (Figure 3.38-3.42), the areas in which there is no available data from the radars (gaps) are filled in with the gauge interpolation data using IDW interpolation method. The figures are generated based on mean total accumulated seasonal precipitation through the years 2014-2018.

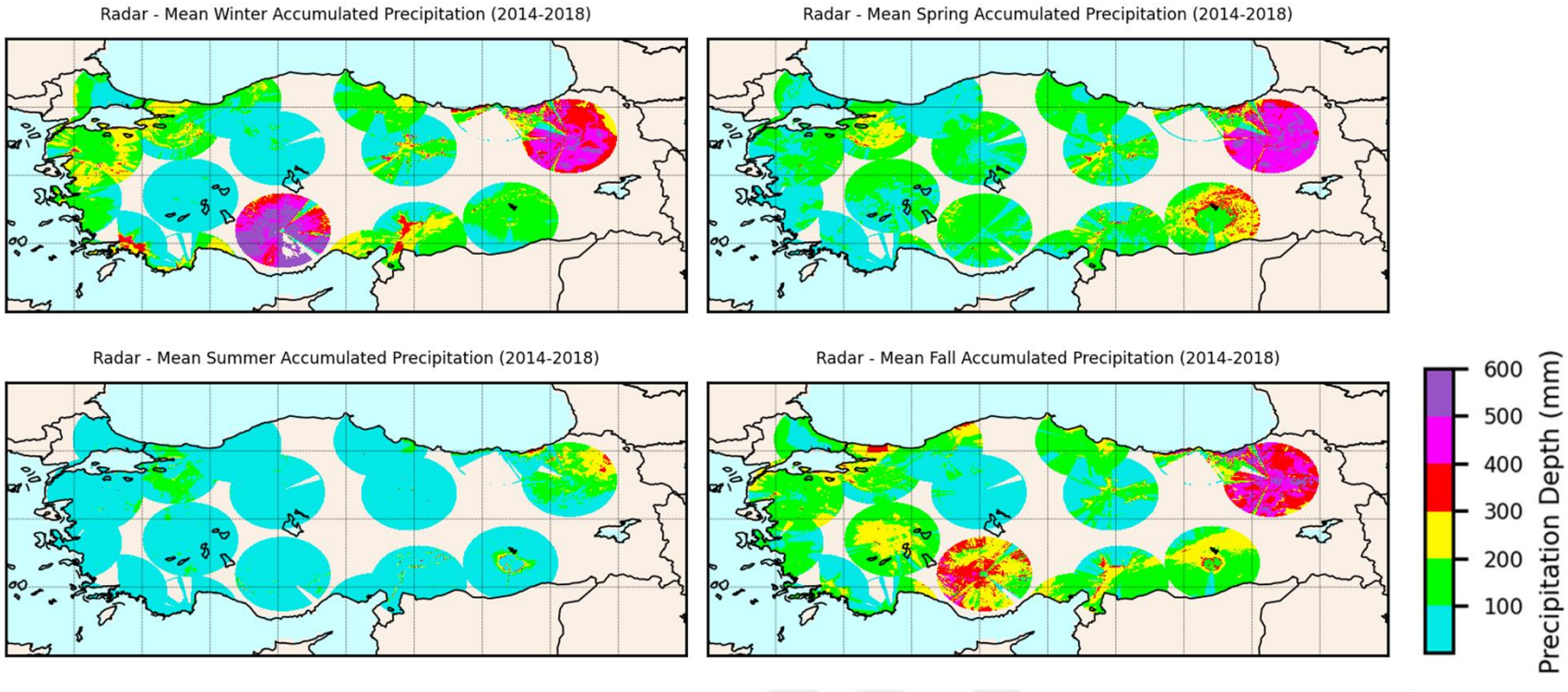

Figure 3.30 Seasonal composite maps for uncorrected radar (Radar) estimations

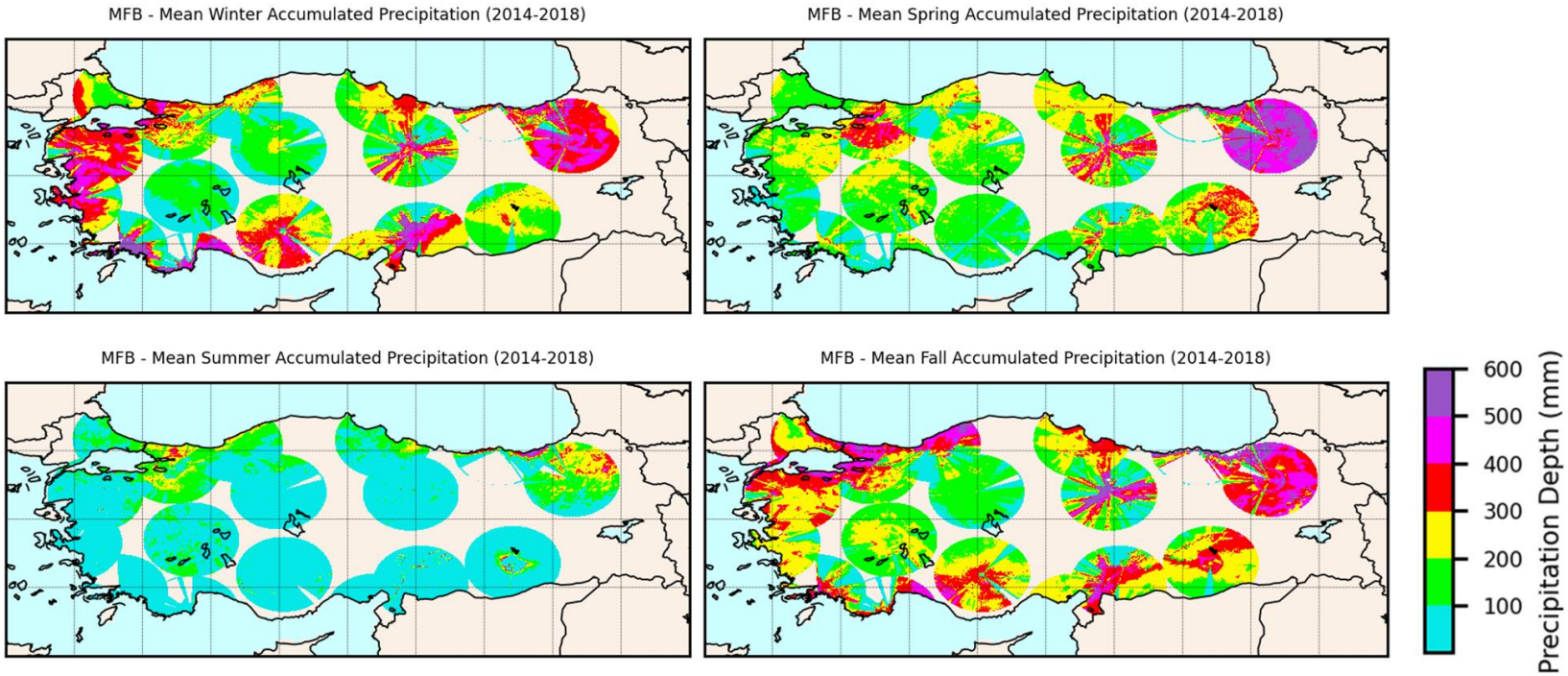

Figure 3.31 Seasonal composite maps for Mean Field Bias (MFB) corrected radar estimations

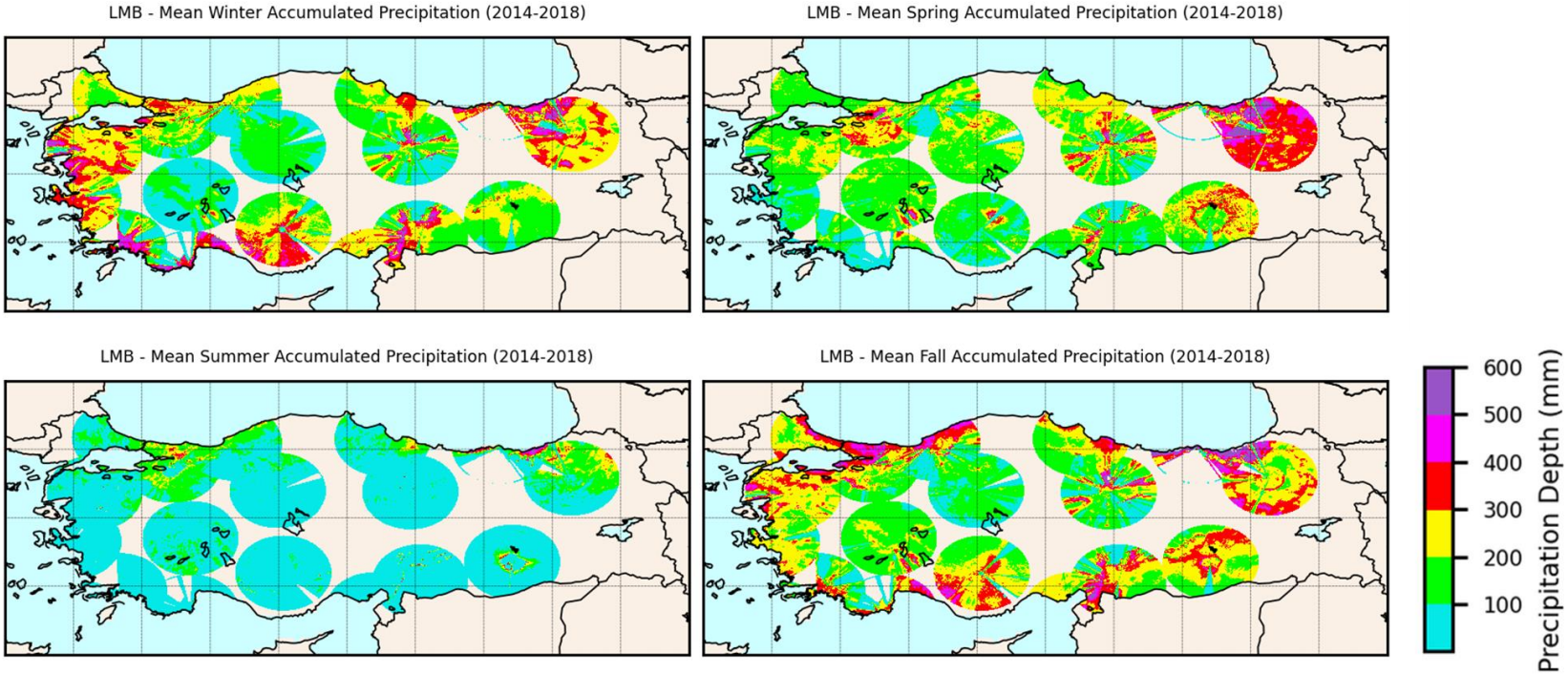

Figure 3.32 Seasonal composite maps for Local Multiplicative Bias (LMB) corrected radar estimations

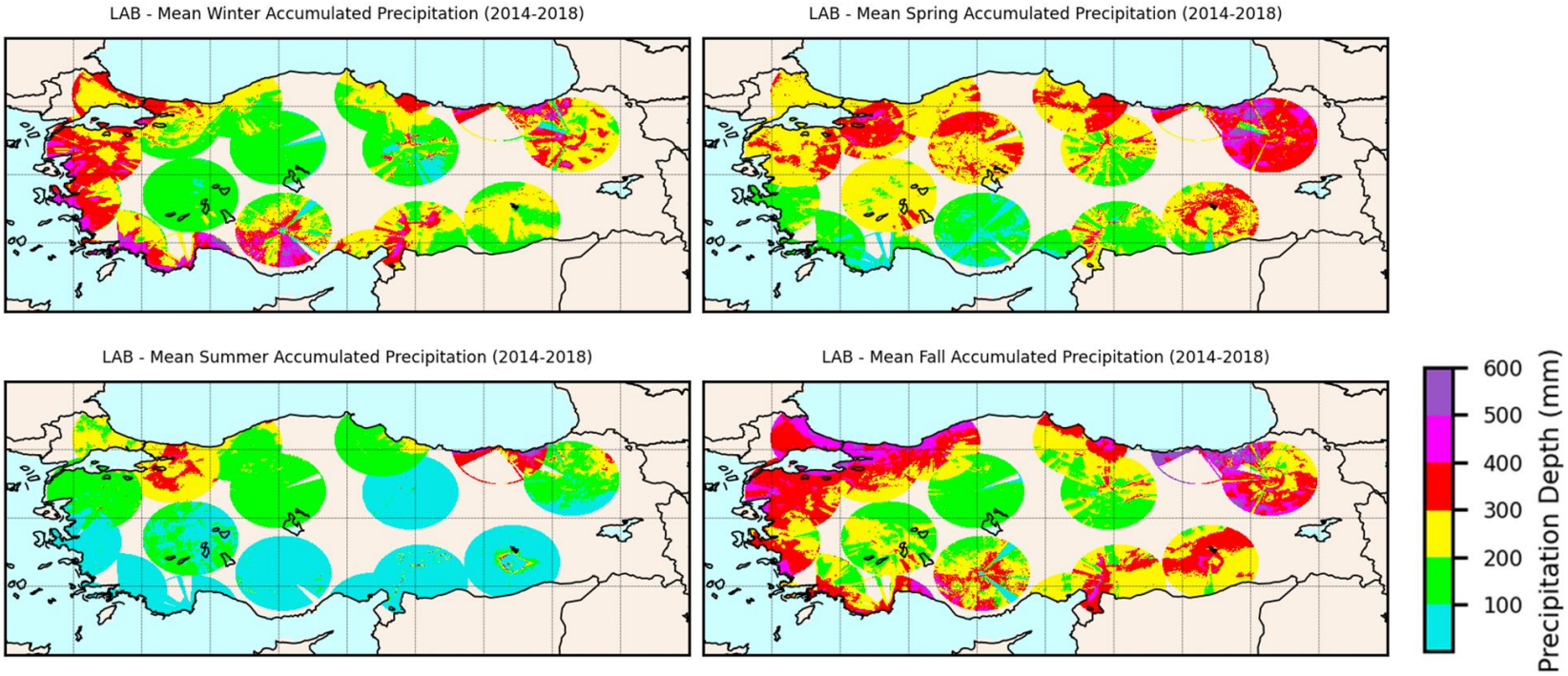

Figure 3.33 Seasonal composite maps for Local Additive Bias (LAB) corrected radar estimations

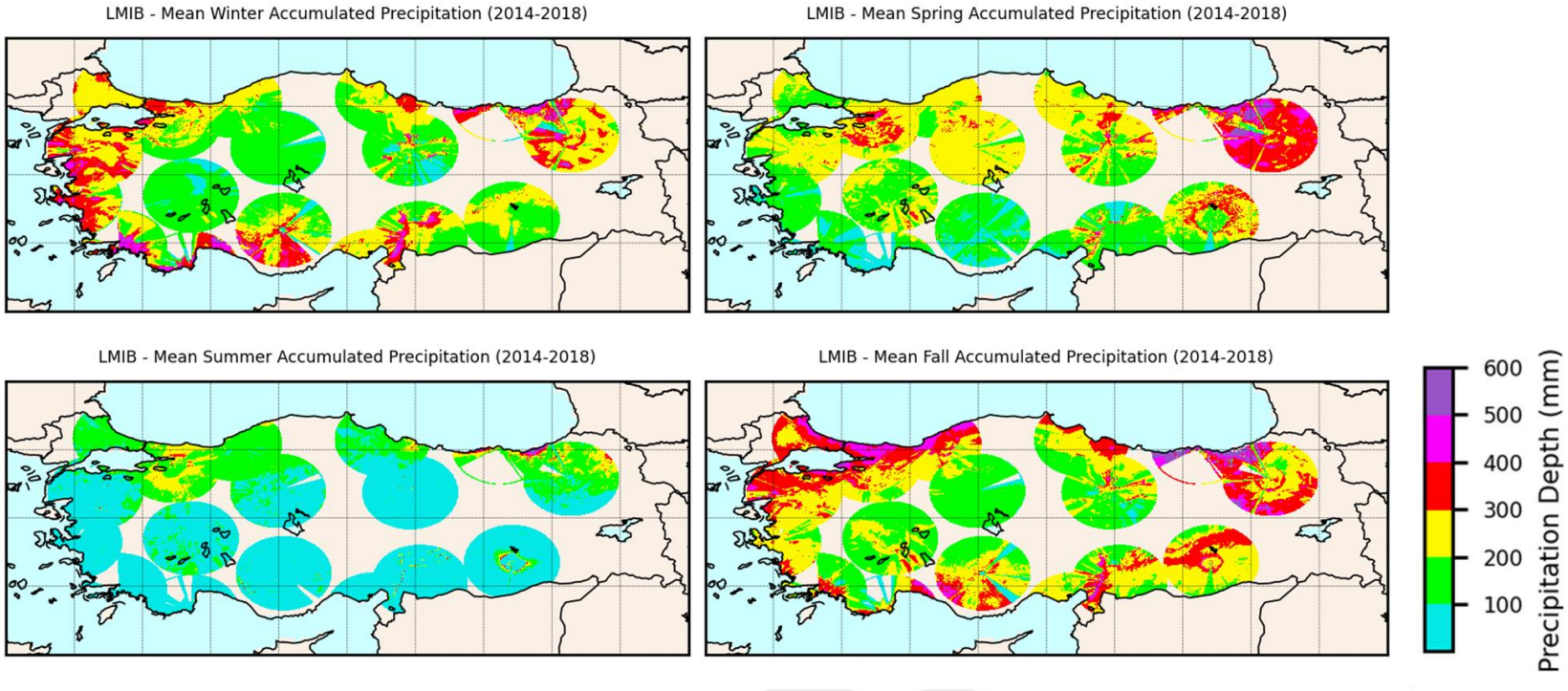

Figure 3.34 Seasonal composite maps for Local Mixed Bias (LMIB) corrected radar estimations

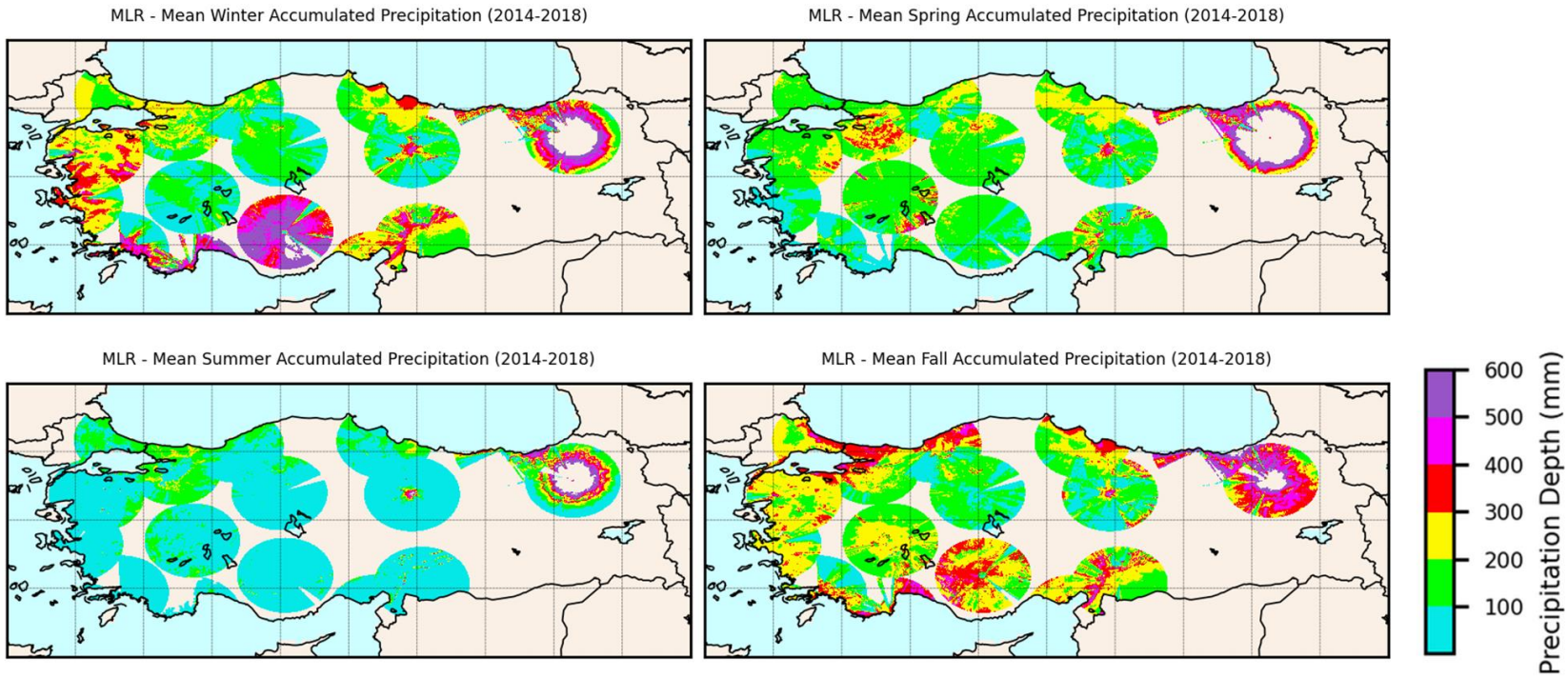

Figure 3.35 Seasonal composite maps for Multiple Linear Regression (MLR) corrected radar estimations

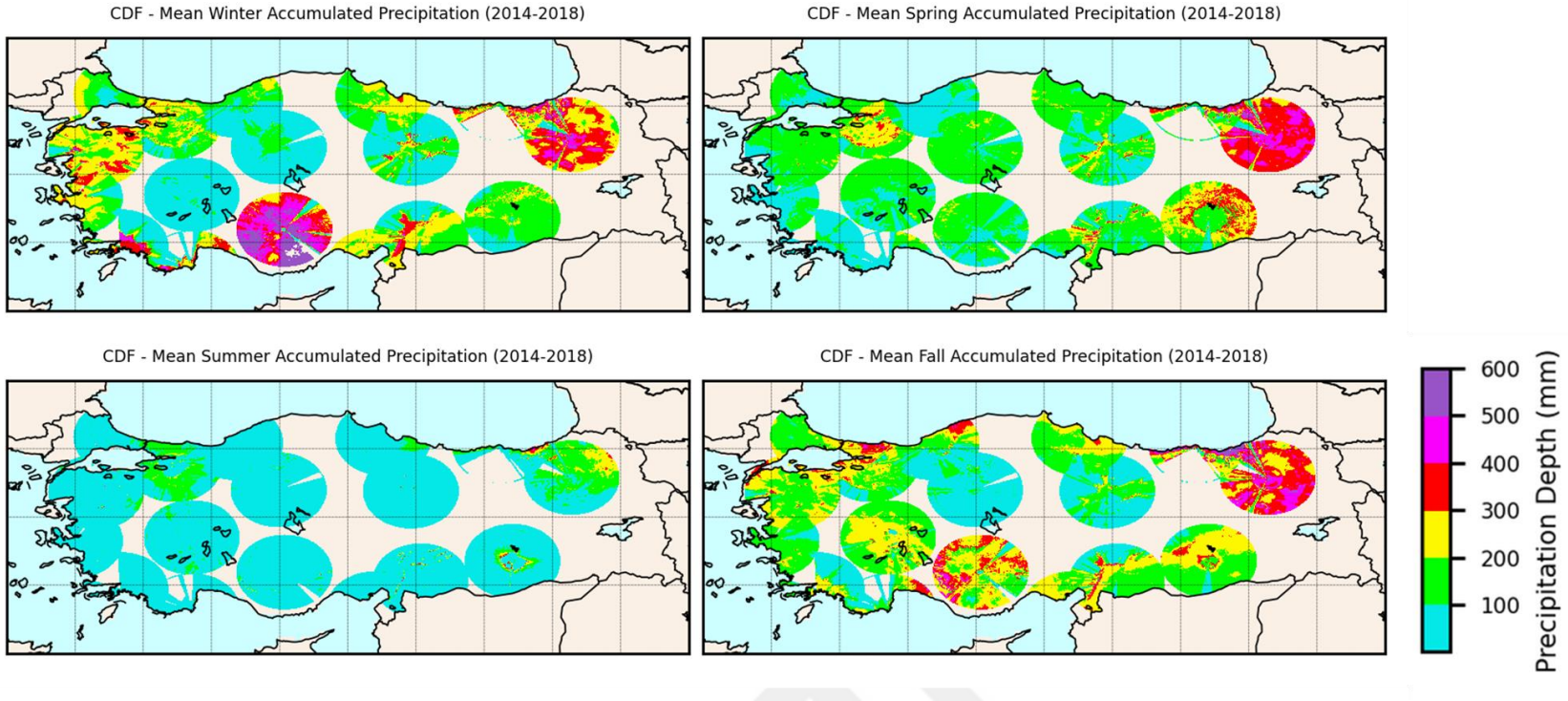

Figure 3.36 Seasonal composite maps for Cumulative Distribution Function (CDF) corrected radar estimations

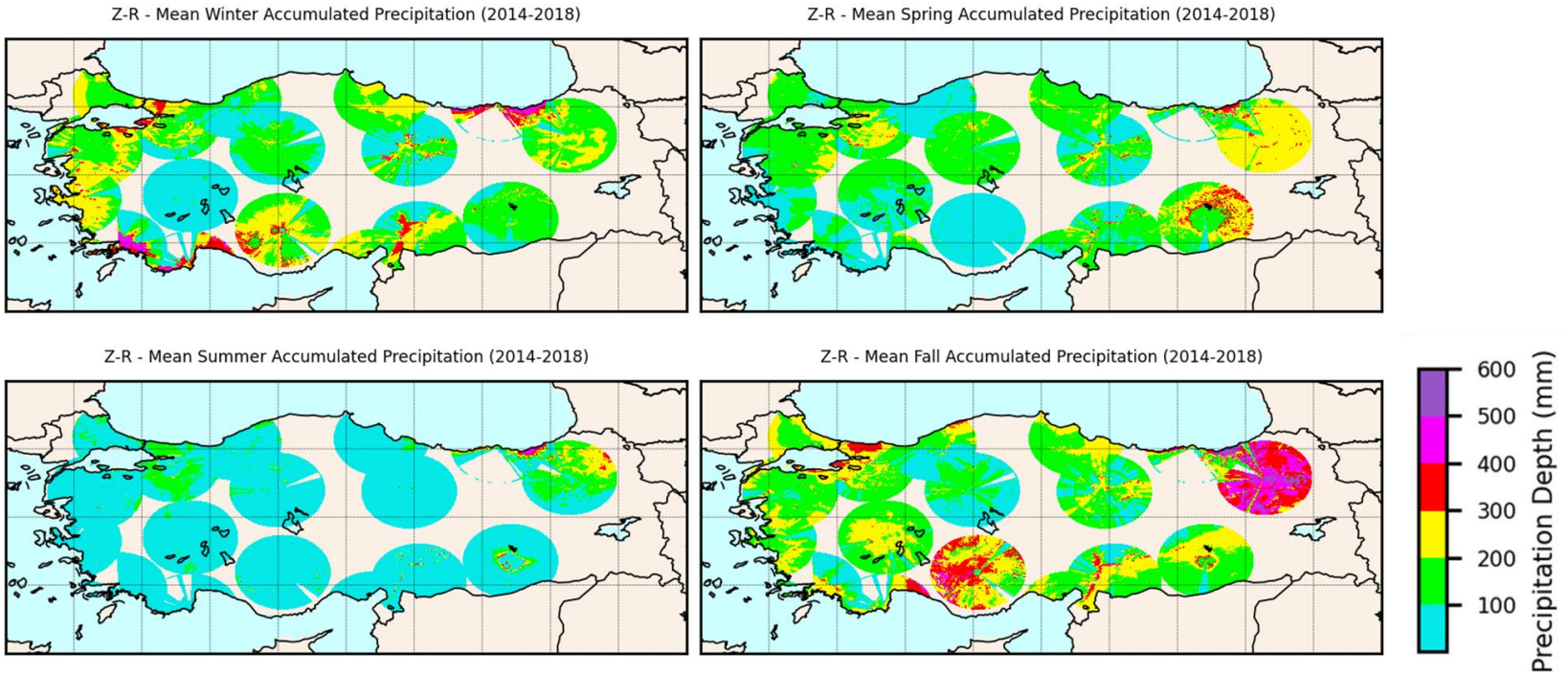

Figure 3.37 Seasonal composite maps for Z-R corrected radar estimations

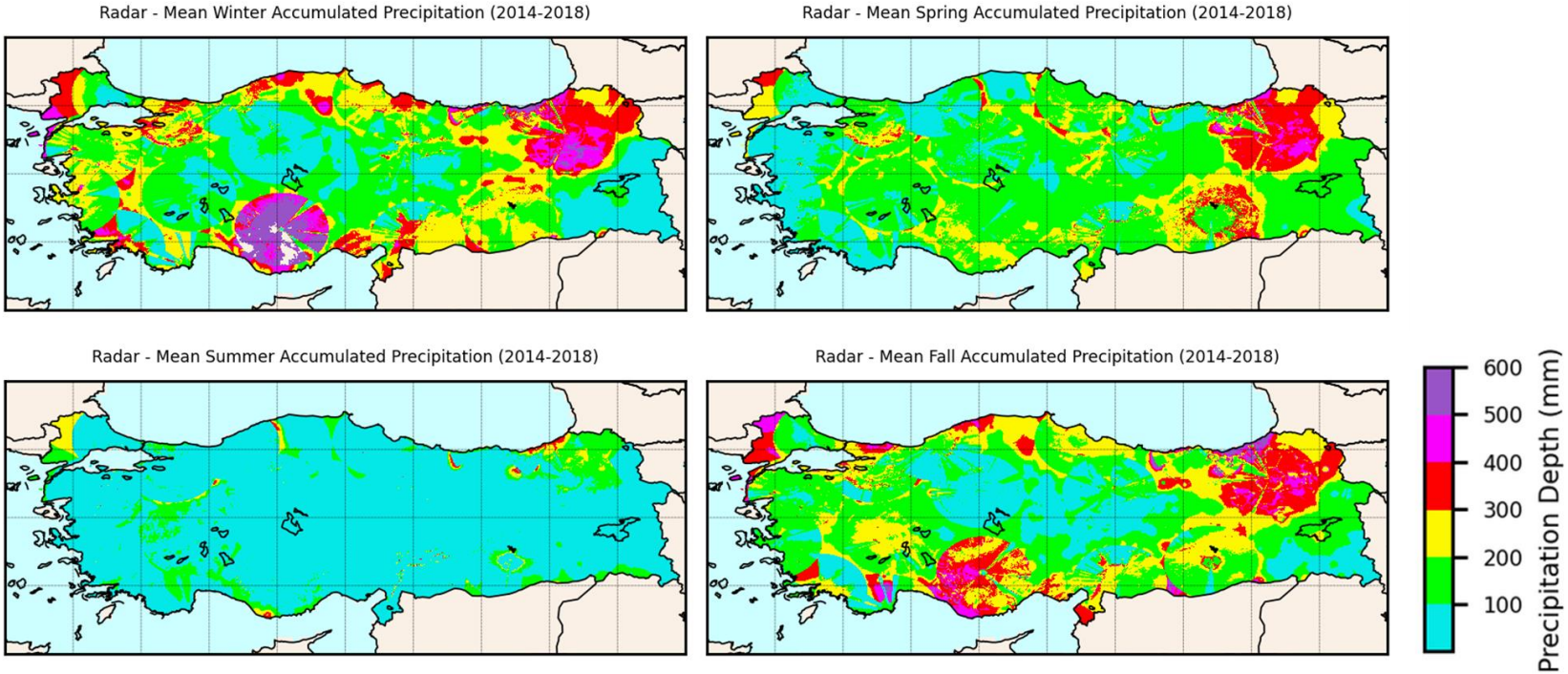

Figure 3.38 Seasonal interpolated composite maps for uncorrected radar (Radar) estimations

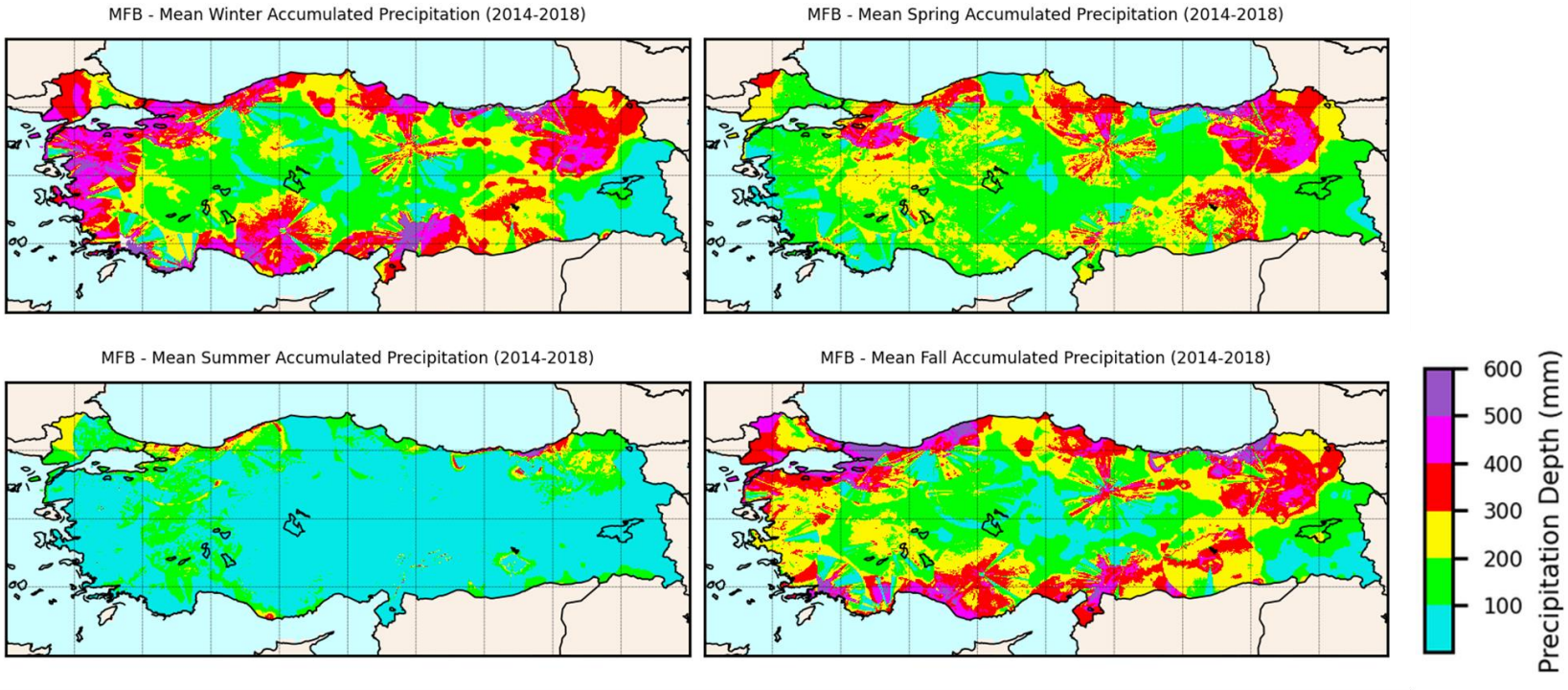

Figure 3.39 Seasonal interpolated composite maps for Mean Field Bias (MFB) corrected radar estimations

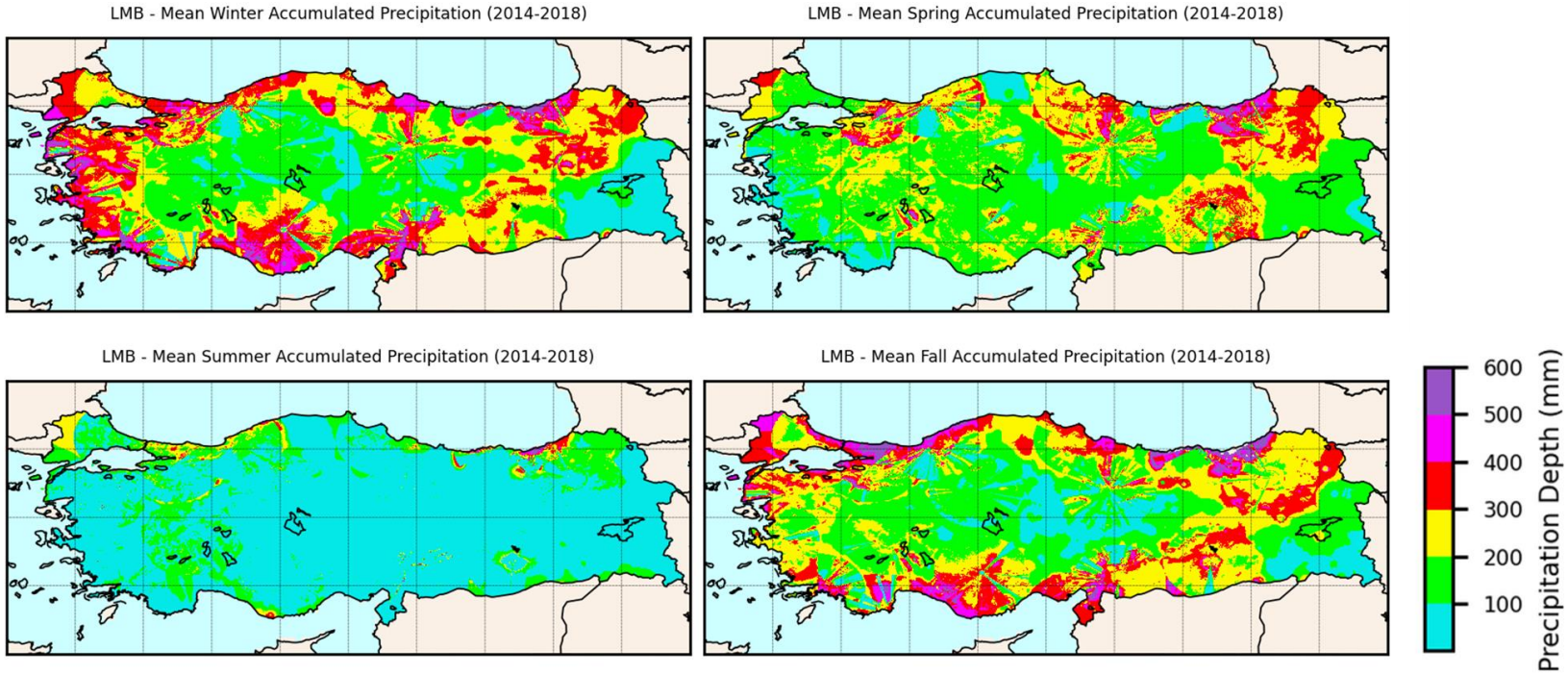

Figure 3.40 Seasonal interpolated composite maps for Local Multiplicative Bias (LMB) corrected radar estimations

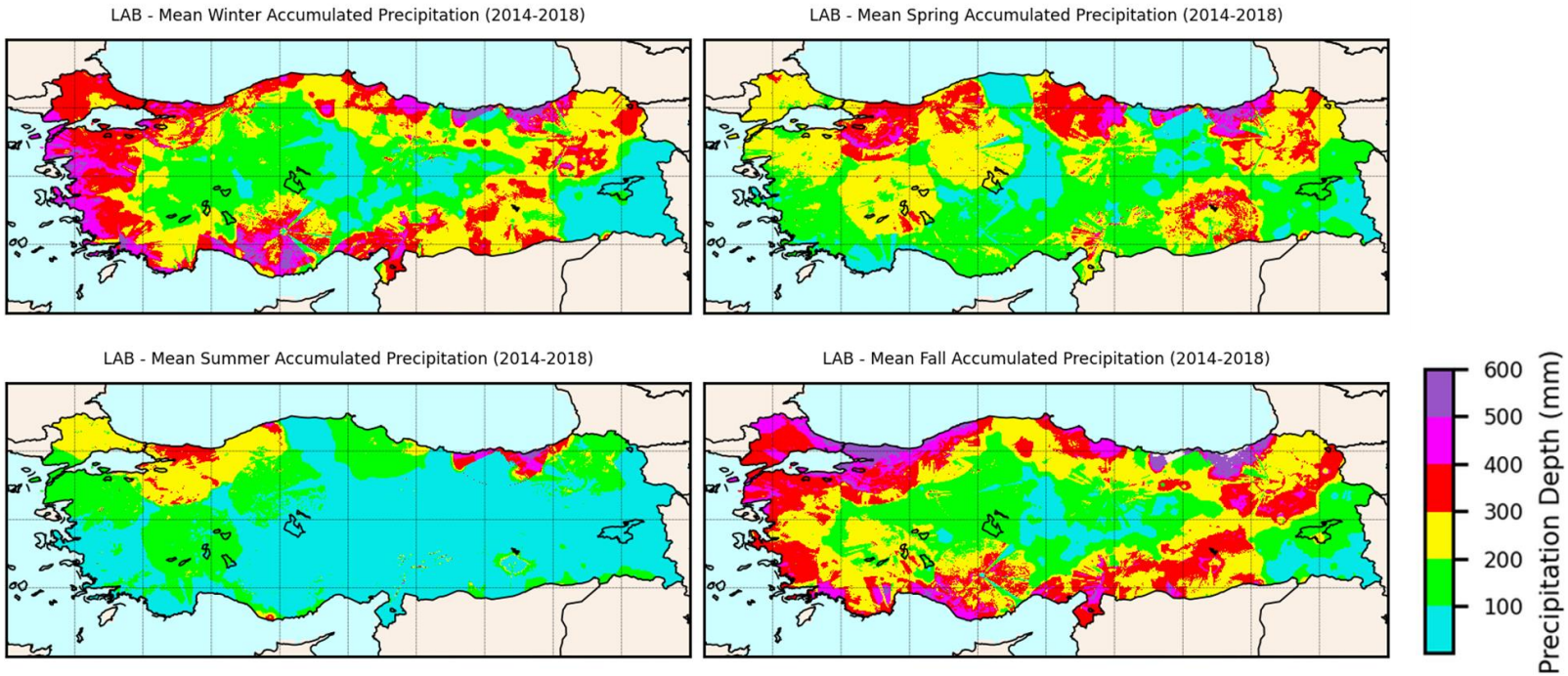

Figure 3.41 Seasonal interpolated composite maps for Local Additive Bias (LAB) corrected radar estimations

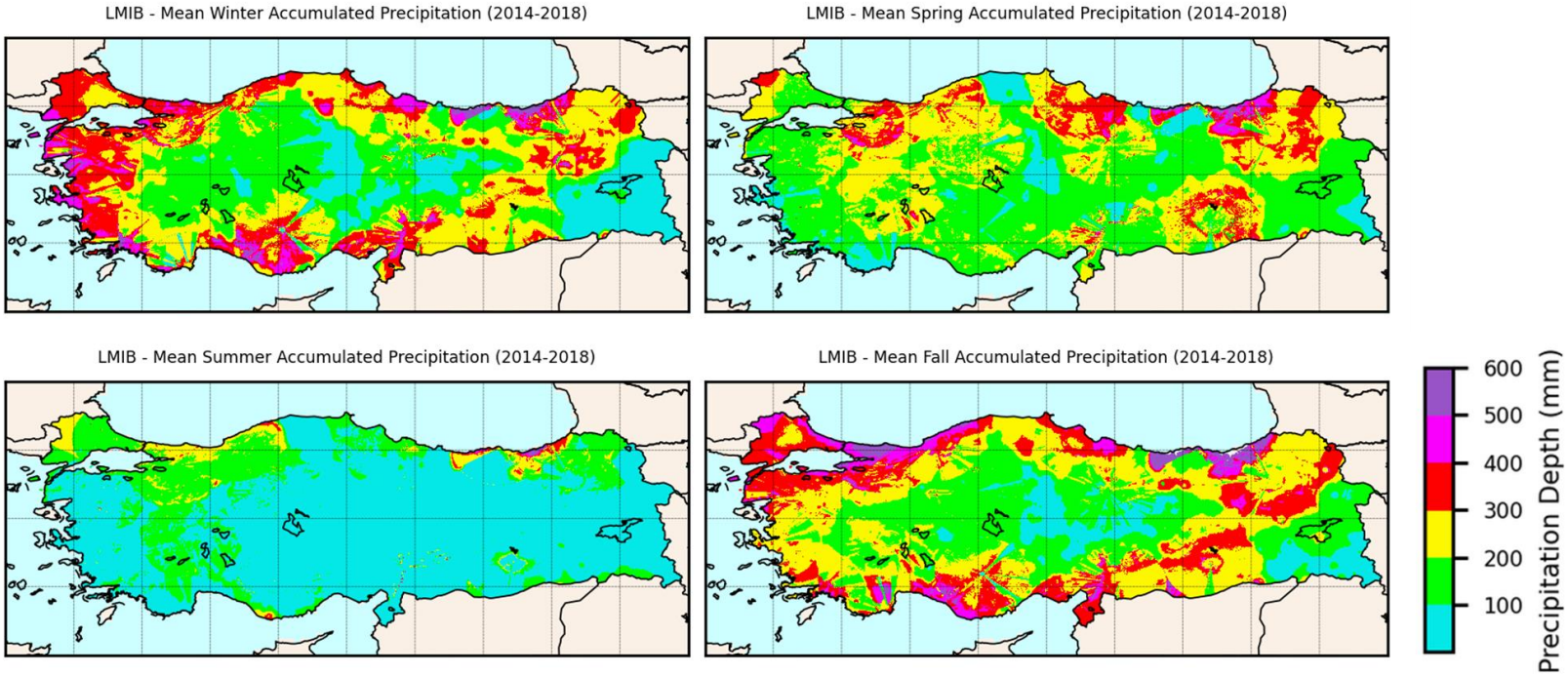

Figure 3.42 Seasonal interpolated composite maps for Local Mixed Bias (LMIB) corrected radar estimations

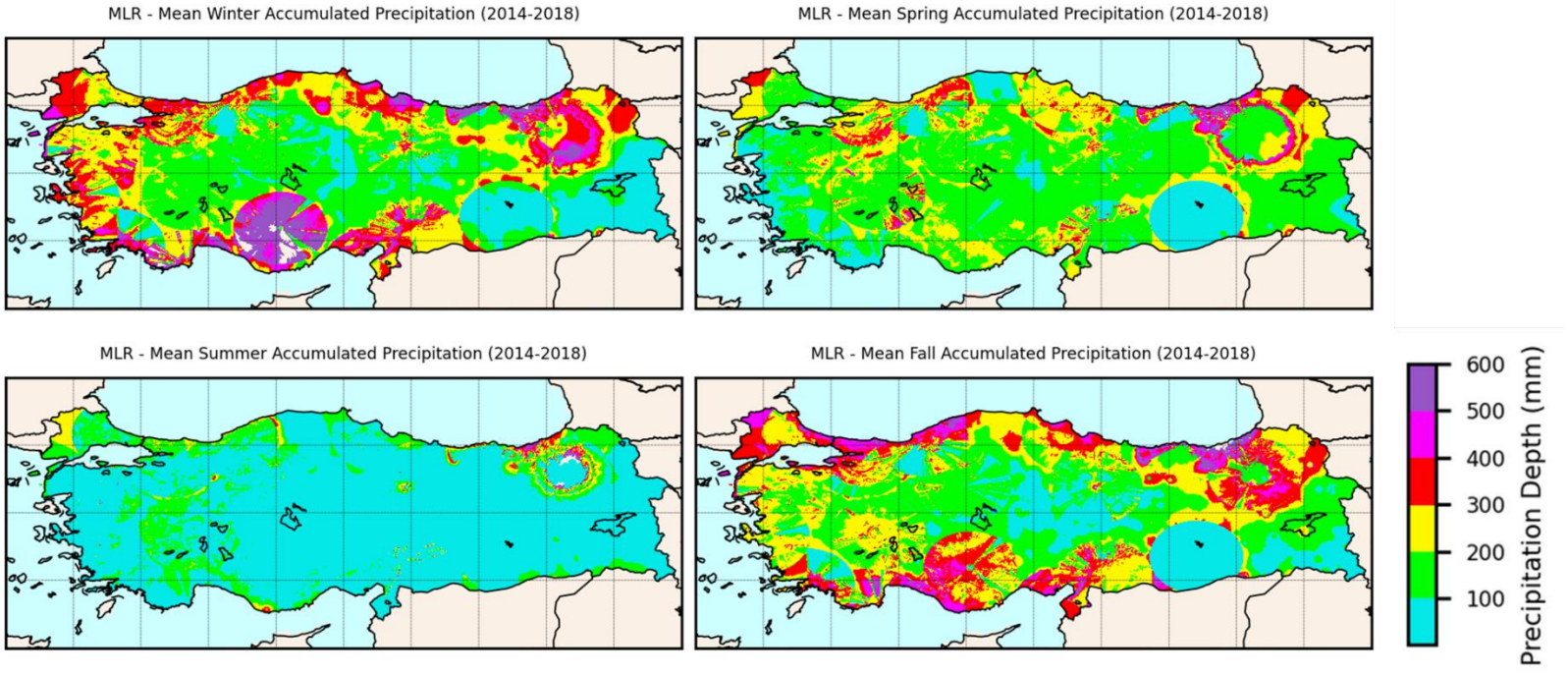

Figure 3.43 Seasonal interpolated composite maps for Multiple Linear Regression (MLR) corrected radar estimations

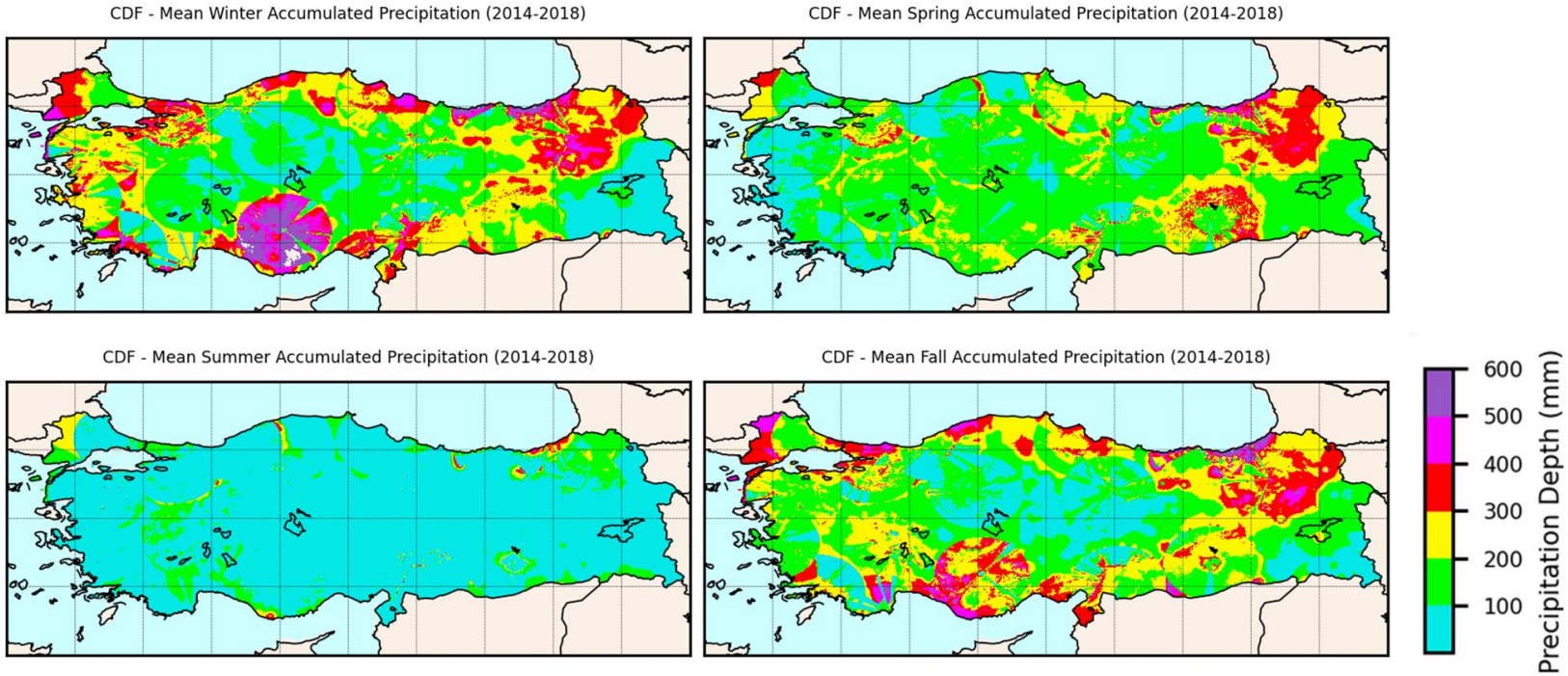

Figure 3.44 Seasonal interpolated composite maps for Cumulative Distribution Function (CDF) corrected radar estimations

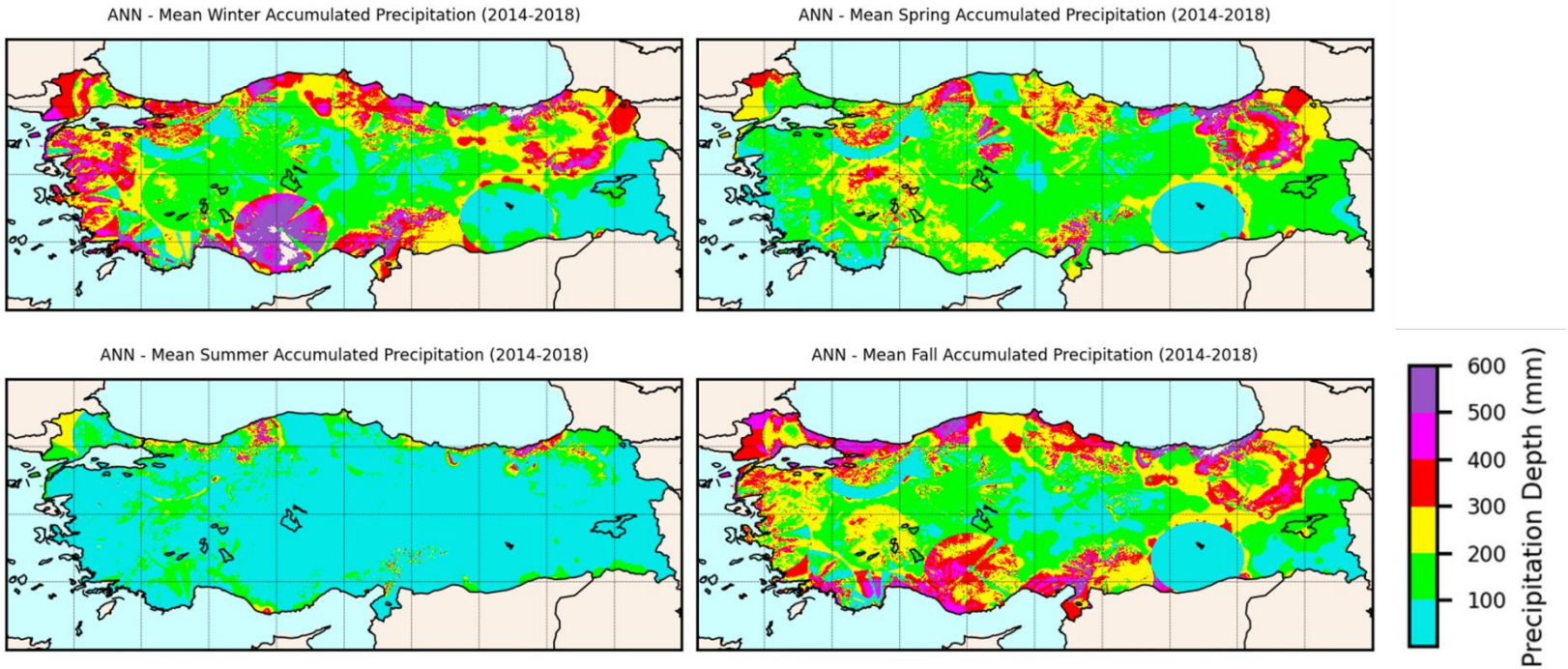

Figure 3.45 Seasonal interpolated composite maps for Artificial Neural Network (ANN) corrected radar estimations

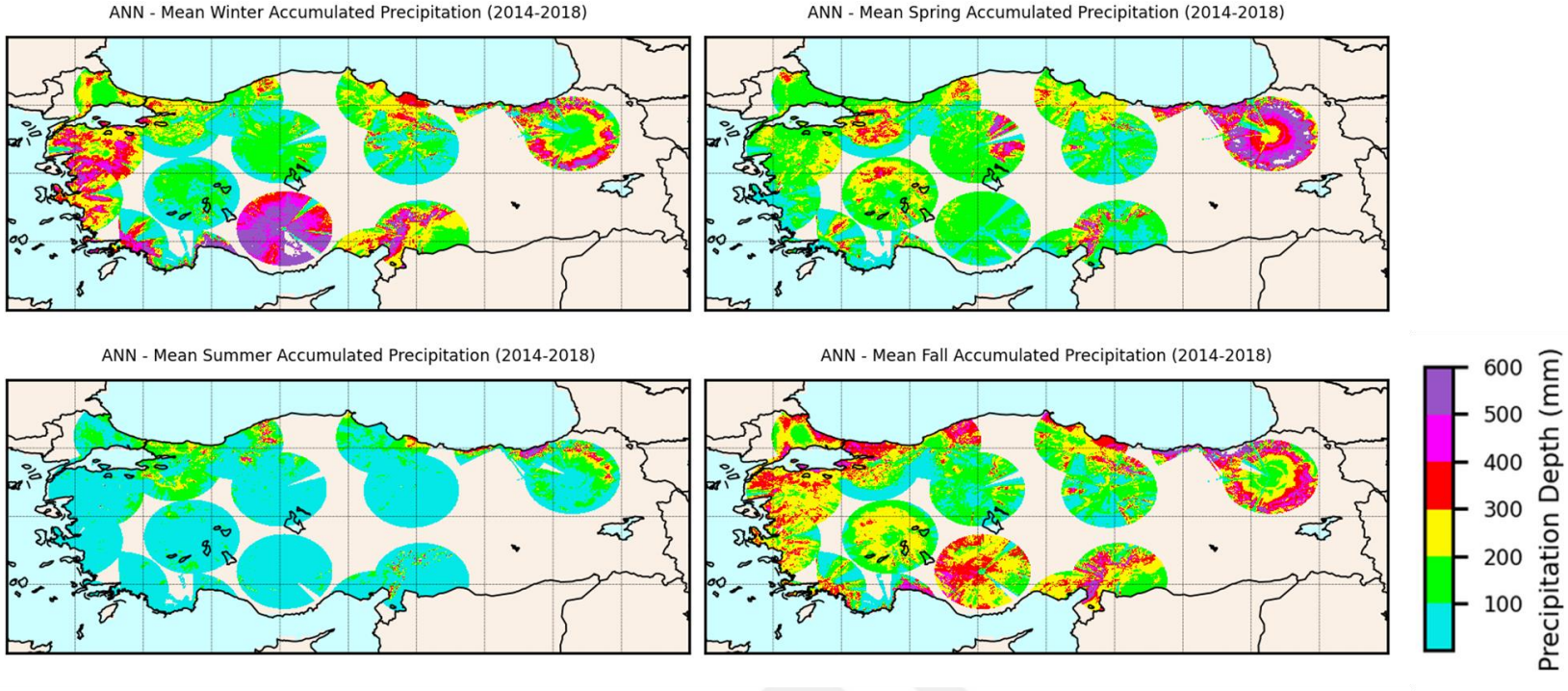

Figure 3.46 Seasonal composite maps for Artificial Neural Network (ANN) corrected radar estimations

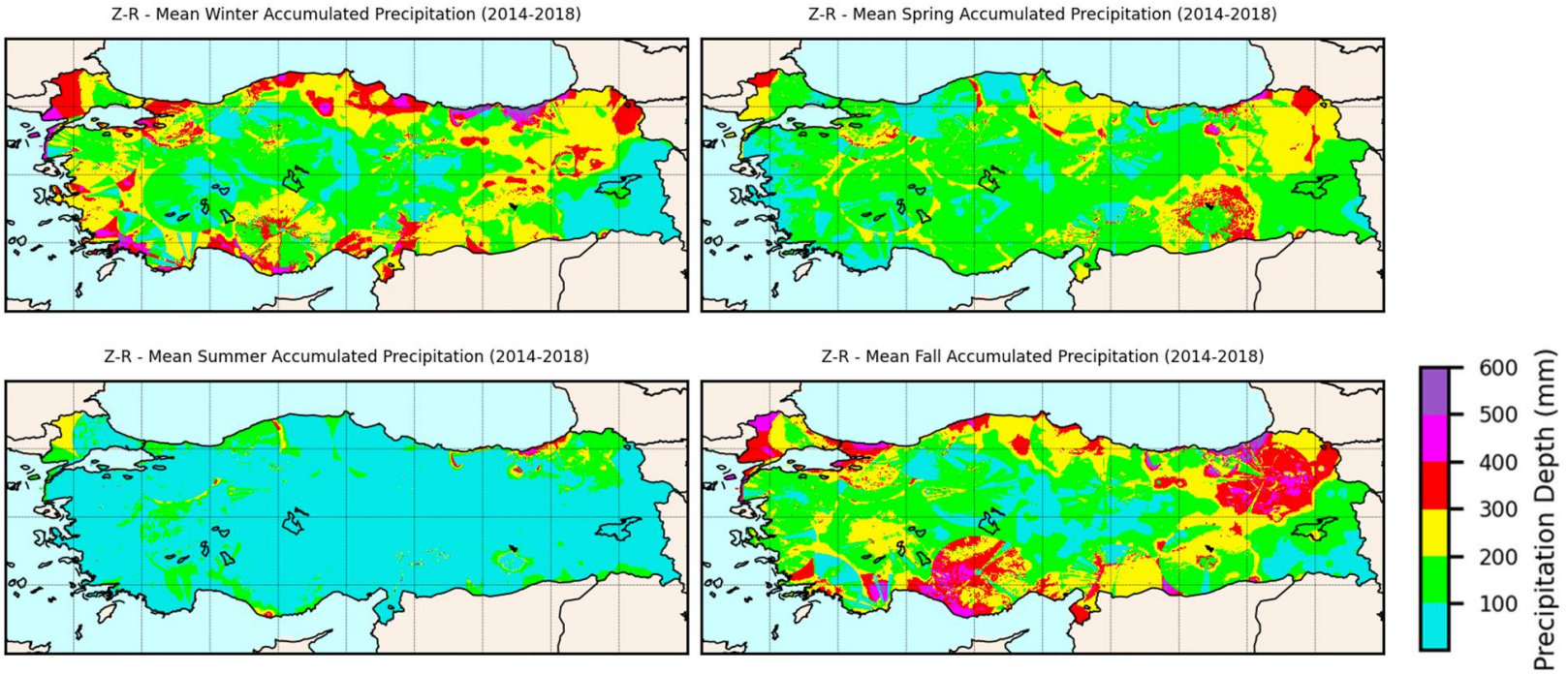

Figure 3.47 Seasonal composite maps for Z-R corrected radar estimations

3.3 Accuracy Estimation of the Bias-Corrected Radar Estimates

3.3.1 Intercomparison of Bias-Corrected Radar Estimates

Using the described error statistics (section 2.3.3), the accuracy of each bias correction method and its scatterplots over all radars are given in -3.49 The difference between these figures is the type of evaluated dataset. The datasets investigated in these figures are ordered by training and validation datasets, as described formerly in section 2.3.2. The error values are obtained from 5-years of data (2014-2018).

It can be observed that in the original radar data (Radar) the scatter intensity is relatively lower for values of less than 2.5mm/hr in the majority of the radars. However, for gauge observations of greater than 2.5mm/hr, substantial underestimation and scatter is more noticeable (except for Karaman radar; see 3.1.3). Moreover, in Radar, the number of radar-based estimates greater than 15mm/hr does not exceed 100 approximately. Nevertheless, the same number of observations occur in gauge values of greater than 20mm/hr. It is essential to mention that the radars are located in different climatic impact regions, and the mentioned values are approximate averages disregarding the location of the radars. Therefore, in heavy precipitation events (e.g., convective rainfall, hail) a very significant difference can be expected between the real precipitation intensity and the radar-estimated precipitation intensity. The bias correction methods have comparatively performed consistently either in training, or validation datasets. Although the validation stations shown in Figure 3.50-3.52, were not used to calibrate the radar estimations (i.e., assumed ungauged), the error values are analogous with the training results (Figure 3.48-3.49). For instance, the LAB method has resulted in a lower RMSE and ESD and higher COR values over all datasets (training and validation) for Ankara radar. This consistency gives us more confidence in choosing the best methodology for bias-correcting the radar estimations, especially in operational use.

Considering all radars, among the gauge adjustment methods, LAB has shown to perform better in cutting the scatter rate, minimizing the RMSE and ESD values, and increasing the COR. The LMIB method has a similar performance to LAB, but it provides higher accuracy in case the accuracy of the original data (Radar) is extremely low. For instance, over Karaman radar, LMIB has the highest accuracy among all methods both in the training and validation datasets. Nevertheless, long-term validation obtained from 17 radars indicates LAB can be reliably used as a reference method for improving the accuracy of radar-based estimates using the gauge-based observations in all radars situated in Turkey. Among the time-independent methods, it was shown that regression-based Z-R matching can be useful in minimizing the errors and increasing the COR (e.g., see Izmir-Muğla in Figure 3.52). MLR and ANN models perform well in compensating the underestimation problem but not satisfactory in reducing the RMSE and ESD values. However, they can overperform the simple MFB gauge adjustment method in individual radars (e.g., Antalya).

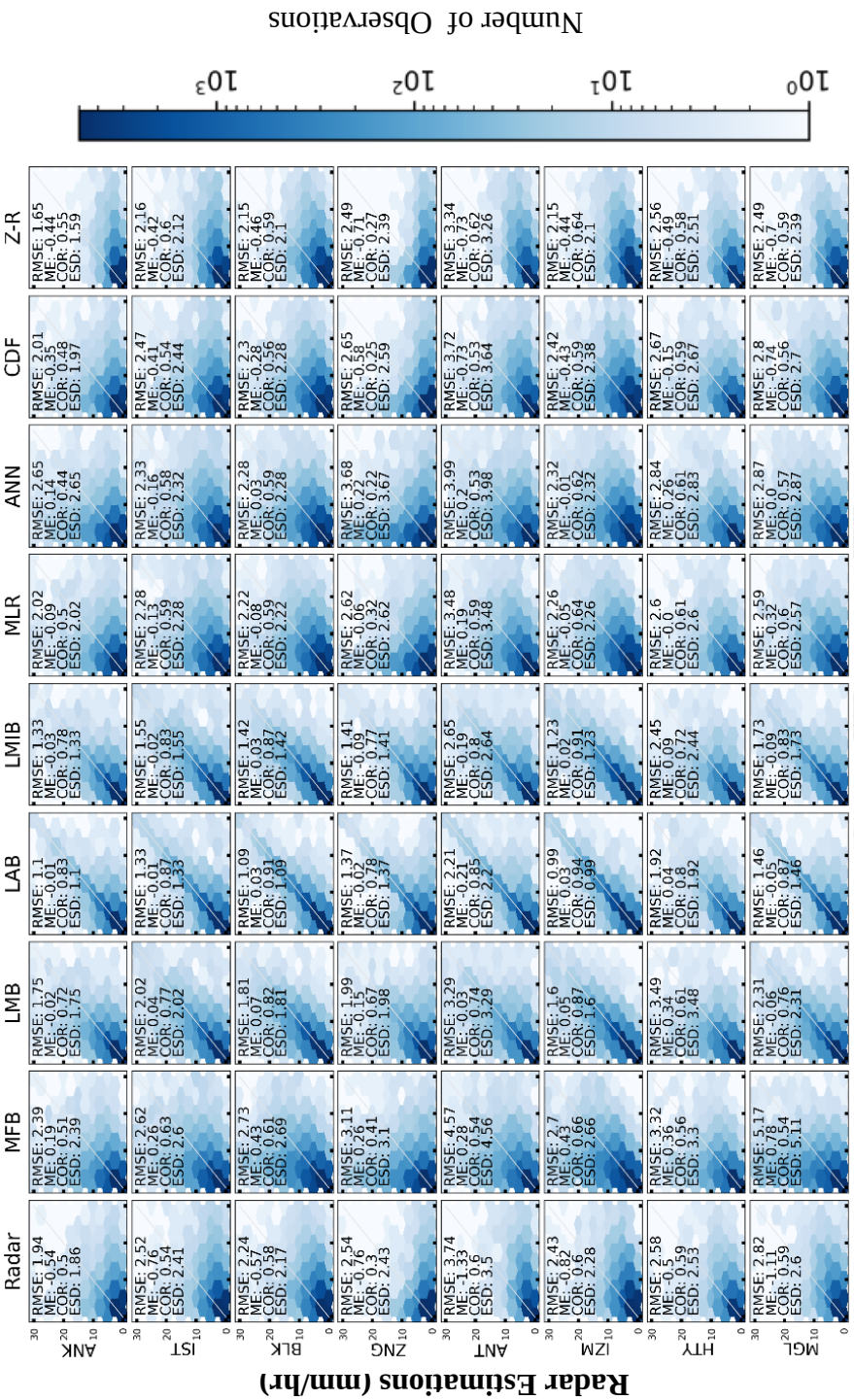

Figure 3.48 Plots showing the scatter and error metrics of all radars obtained from the training dataset

Figure 3.49 Plots showing the scatter and error metrics of all radars obtained from the training dataset (continued)

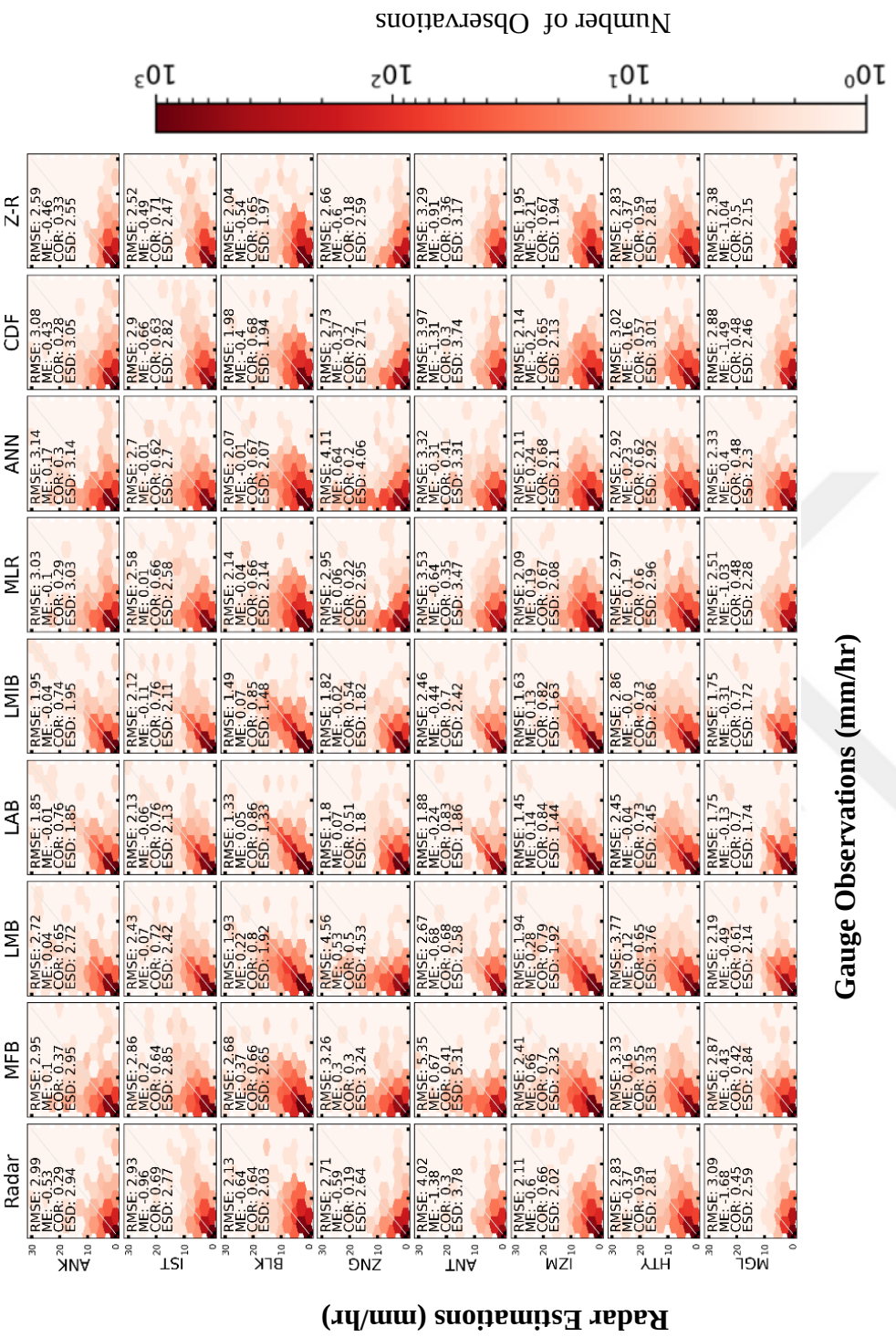

Figure 3.50 Plots showing the scatter and error metrics of all radars obtained from the validation dataset

Figure 3.51 Plots showing the scatter and error metrics of all radars obtained from the validation dataset (continued)

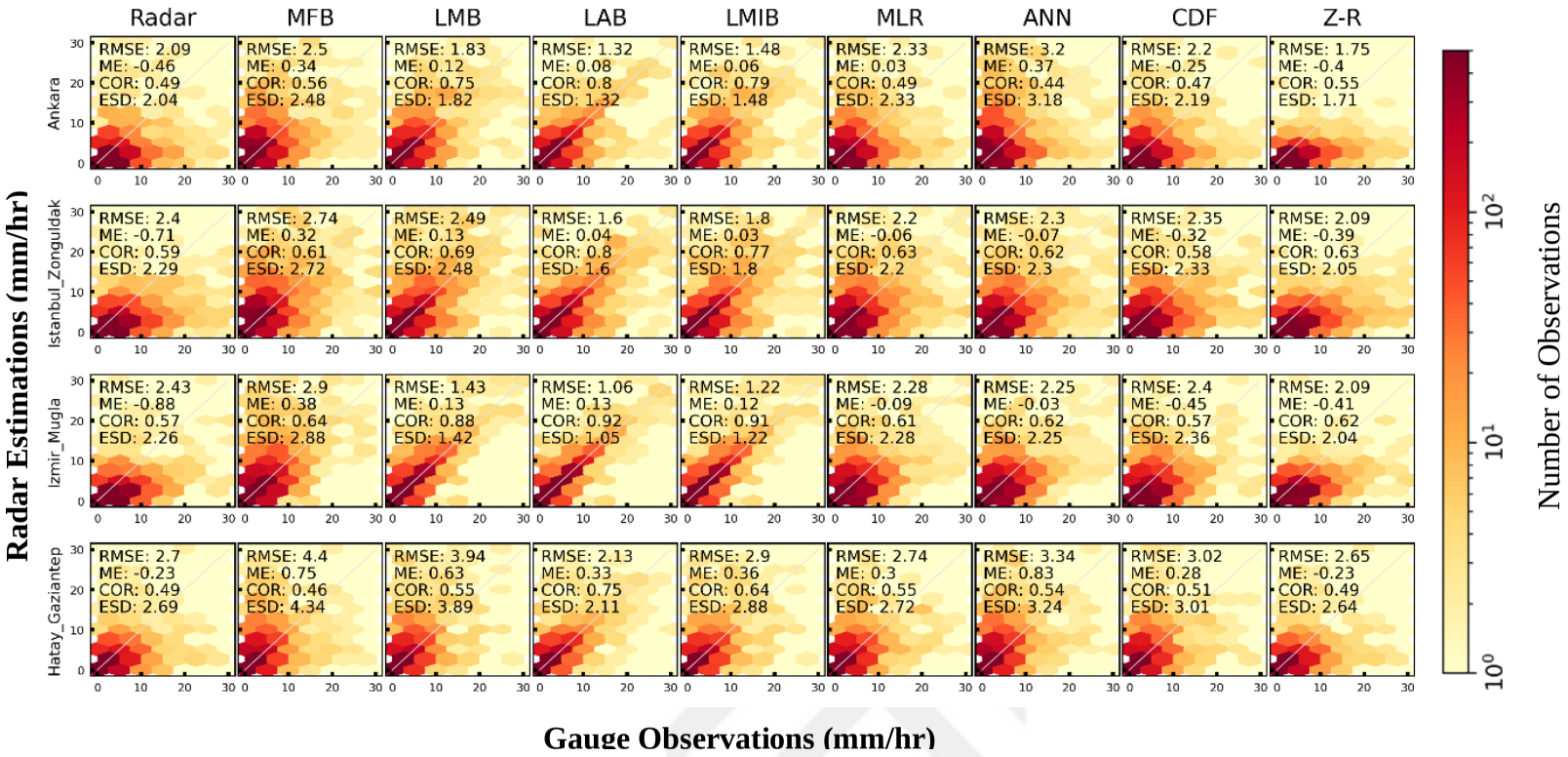

Figure 3.52 Plots showing the scatter and error metrics of all radars obtained from the additional validation dataset

3.3.2 Temporal Variation of Errors

Figure 3.53 represents ME of all methods averaged over all common radars in a long-term period (2014-2018). Karaman, Şanlıurfa, and Erzurum radars are excluded. The reason for the exclusion of these radars is the extreme systematic overestimation of Karaman radar, and insufficient long-term data from Şanlıurfa and Erzurum radars in the specified years. Moreover, over Erzurum radar, bright-band related errors are expected because of the elevation of the radar antenna which is located in a very high altitude and temperature may reach below zero over some months. Due to convective events in the summer, the original radar data (Radar) reveal the most significant underestimation during this season, whereas the amount of underestimation in other seasons is roughly 100% less and nearly stable. ME of all methods being closer to zero represents a significant improvement in balancing the underestimation problem compared with Radar.

Among the hourly gauge adjustment methods (shown with blue bars), the simplest MFB correction method reduces ME by 80% in summer, and by about 60% in the other seasons. Except for summer events, methods including additive bias (LAB and LMIB) have shown to be the most effective in eliminating the underestimation problem. In summer, LMB correction is shown to be the best alternative among the hourly gauge adjustment methods. Among the time-independent methods (shown with green bars), MLR and ANN are as nearly good as the hourly gauge adjustment methods. The difficulty in improving radar estimations in summer seasons can be seen in these methods as well. The simplest methods of all, Z-R based correction has also shown to reduce the ME as effective as MFB except for the summer season.

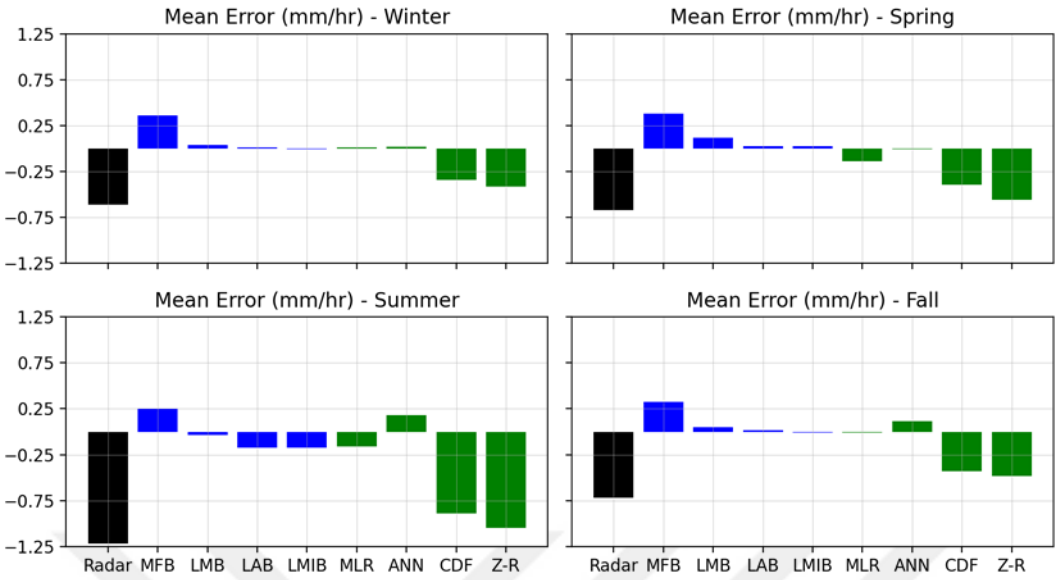

Figure 3.53 Temporal variation of the Mean Error (mm/hr)

As seen in Figure 3.54 and Figure 3.55, there is a minor difference between RMSE and ESD. This is because of the dominance of random errors, especially in the Summer and Spring months. As expected, because of the capabilities of gauge adjustment methods in suppressing both the systematic and random errors, they are more effective than time-independent methods in reducing RMSE and ESD quality metrics. However, time-independent methods still outperform MFB in random errors. The field-based rather than local assumption of error distribution in MFB is the main reason for not being successful in decreasing the RMSE and ESD.

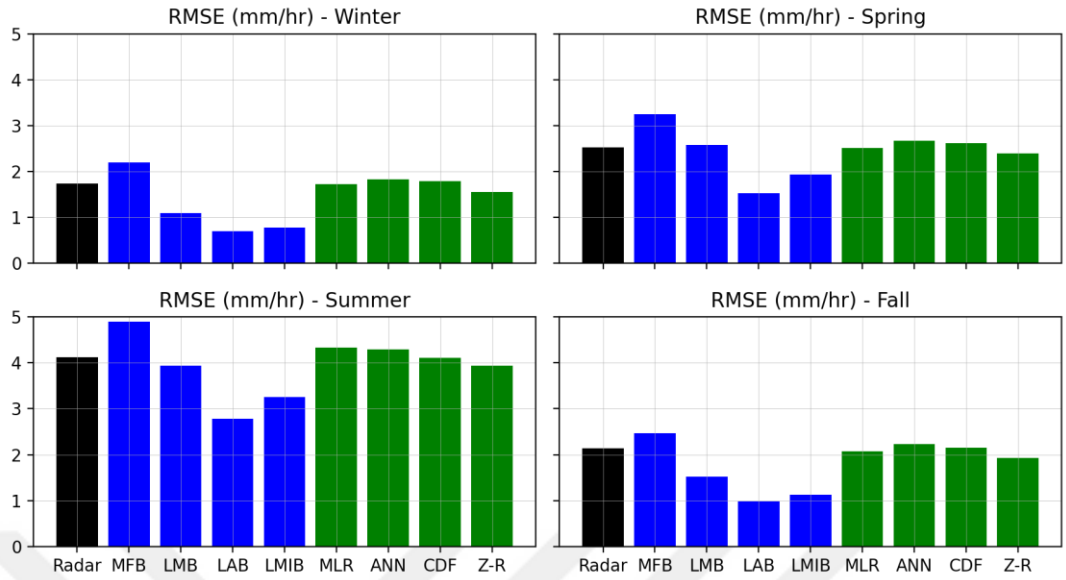

Figure 3.54 Temporal variation of the RMSE (mm/hr)

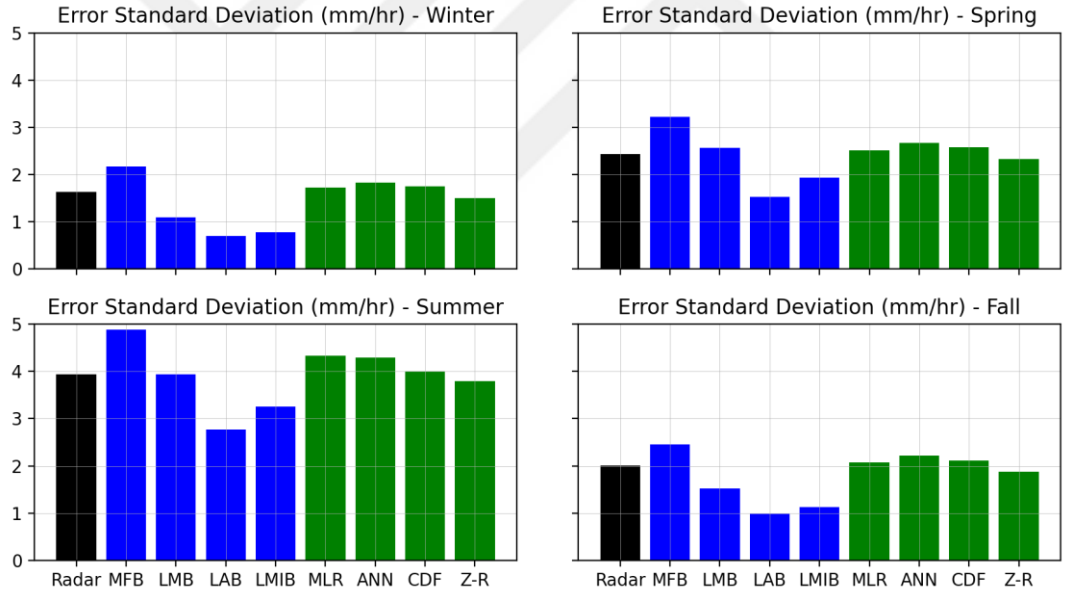

Figure 3.55 Seasonal variation of the Error Standard Deviation (mm/hr)

In Figure 3.56, it is shown that the COR of Radar is between 0.45 to 0.6 on average. It becomes the lowest in winter, which can be due to lower temporal representativity of radars in snowfall events due to horizontal advection (Lauri, Koistinen, and

Moisseev 2012). Gauge adjustment methods increased COR by up to 90% on average. Among time-independent methods, MLR and ANN slightly increased the COR. Nevertheless, because these correction methods are stationary through each season, they have no significant effect on the COR.

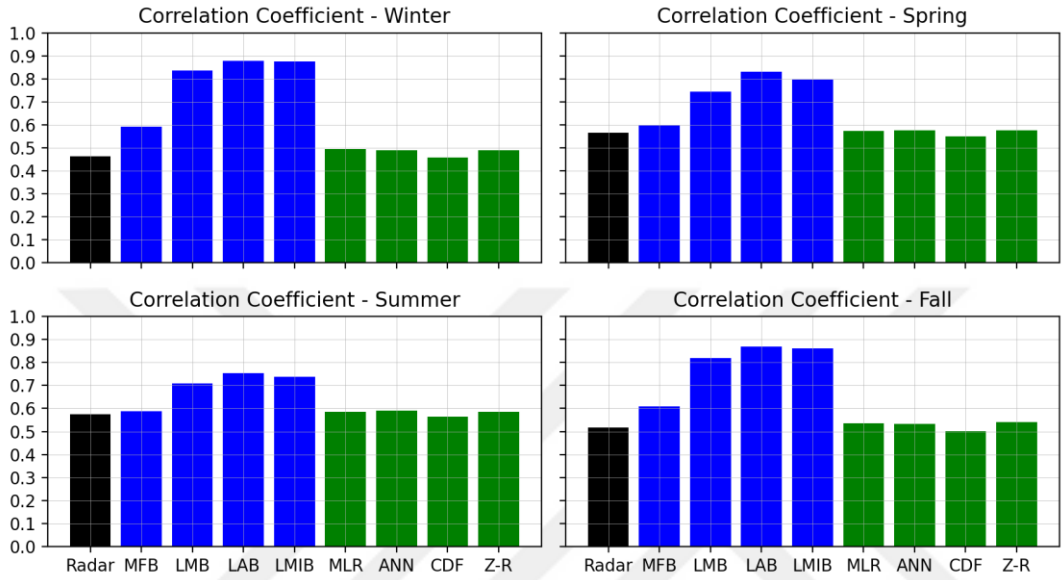

Figure 3.56 Seasonal variation of the Correlation Coefficient

3.3.3 Spatial Variation of Errors

In Figure 3.57-3.10, the spatial variation of ME is shown for Radar and all correction methods over four seasons. It can be observed that the radar estimations are generally lower than gauge observations in all seasons. The underestimation effects are highlighted in the summer months. The extreme overestimation problem in KRM is obvious and more stressed in winter and spring seasons. The reason behind this problem can be explored by meteorology specialists. All methods have increase ME from negative values closer to zero values. However, in time-independent methods, still ME values are shown to be lower than zero in summer months and over some radars (e.g., ANT).

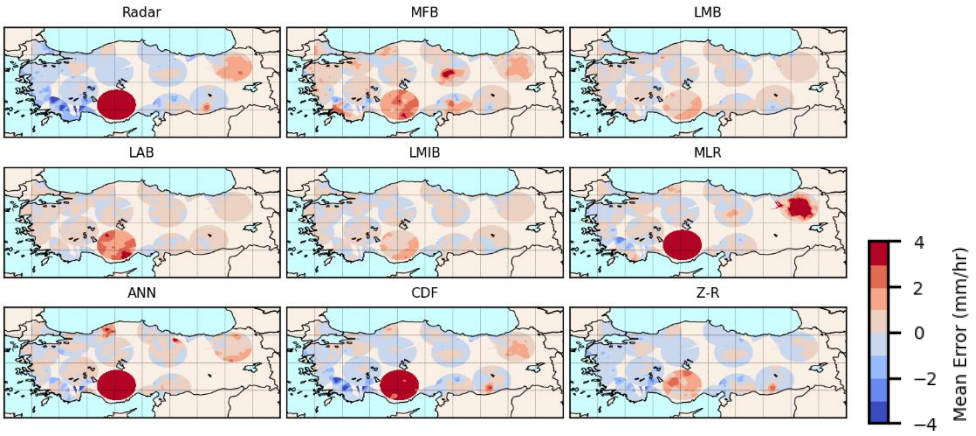

Figure 3.57 Spatial variation of ME (mm/hr) in winter

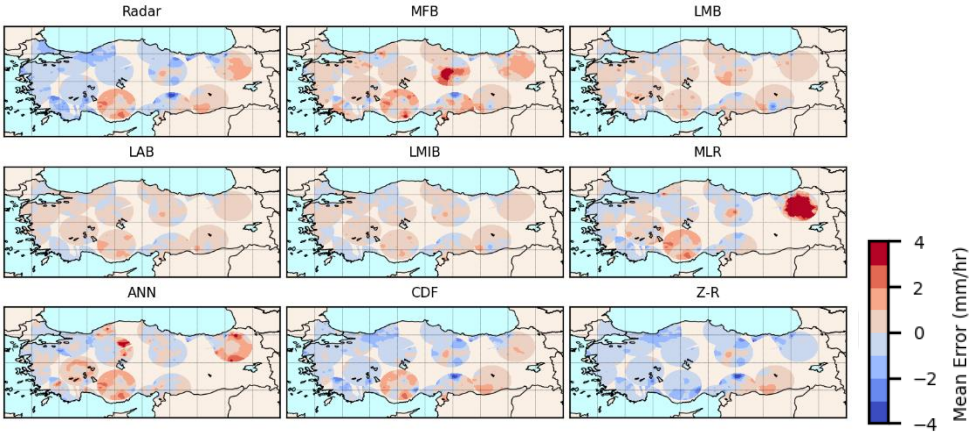

Figure 3.58 Spatial variation of ME (mm/hr) in spring

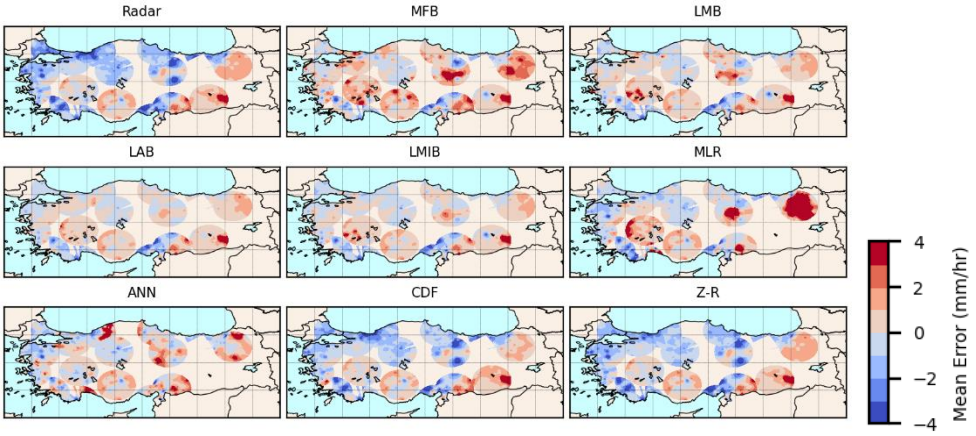

Figure 3.59 Spatial variation of ME (mm/hr) in summer

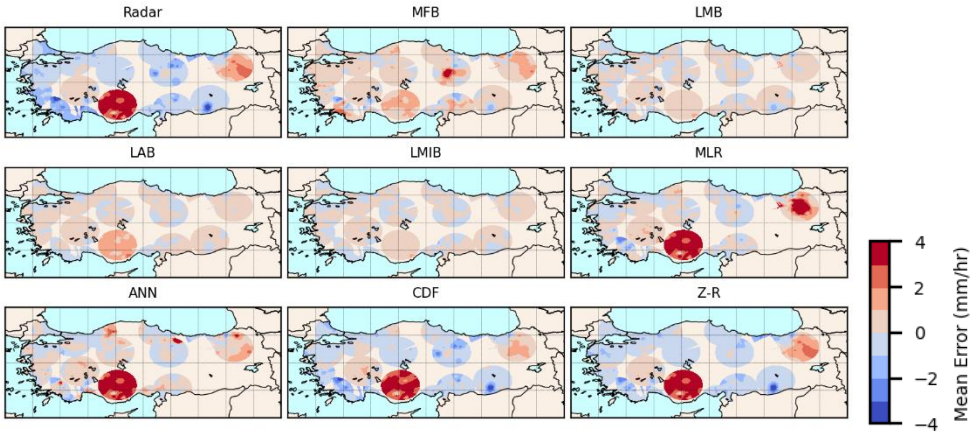

Figure 3.60 Spatial variation of ME (mm/hr) in fall

Figure 3.61-3.14 show the spatial variation of RMSE. In the spring and summer months, RMSE values are generally higher, especially in the coastal regions. The relative performances of the bias correction methods are shown by normalizing the RMSE by RMSE of the original radar (Radar) in Figure 3.65-3.18. The gauge adjustment methods are shown to have significantly reduced RMSE by an approximate factor of 0.75 in the coastal regions and 0.5 in the other regions. Time-independent methods have shown to outperform MFB in many cases, especially in the Spring. Generally, LAB correction performs relatively better than all methods. However, there is still a challenge in estimating the summer precipitation in the Mediterranean region due to the very high variability of precipitation in the summer. Both the nature of precipitation and relatively smaller numbers of gauges makes it hard to represent the precipitation using point-based observation and improve radar estimations.

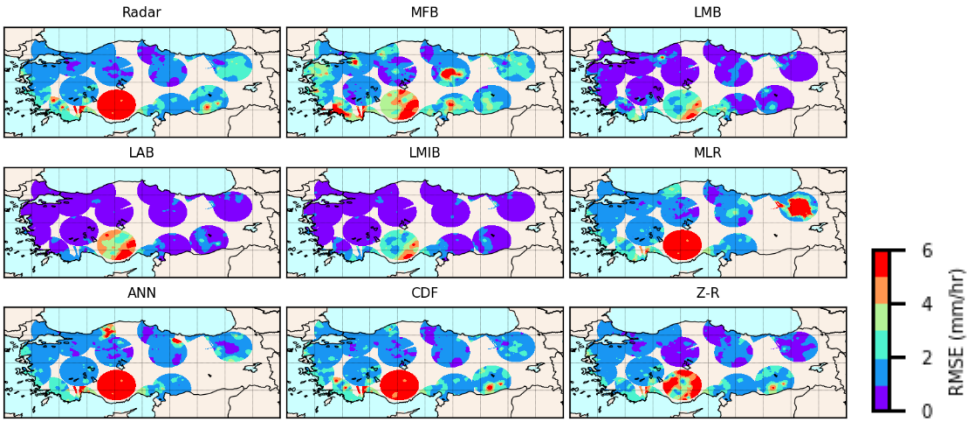

Figure 3.61 Spatial variation of RMSE (mm/hr) in winter

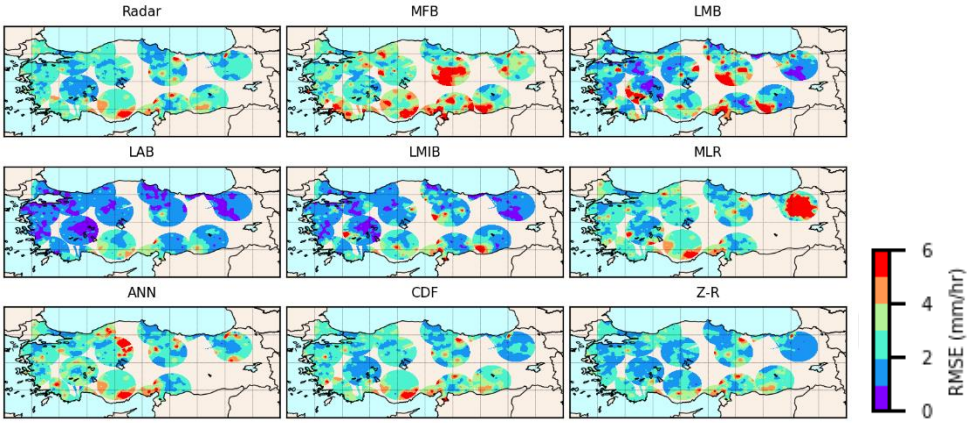

Figure 3.62 Spatial variation of RMSE (mm/hr) in spring

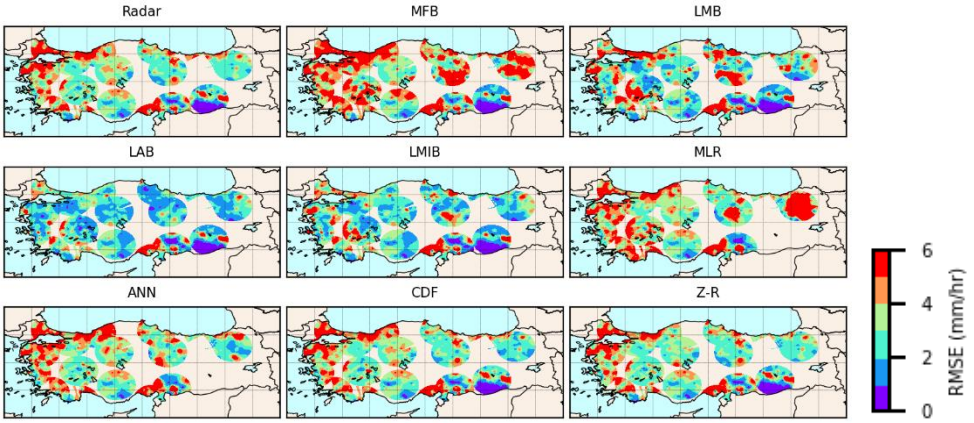

Figure 3.63 Spatial variation of RMSE (mm/hr) in summer

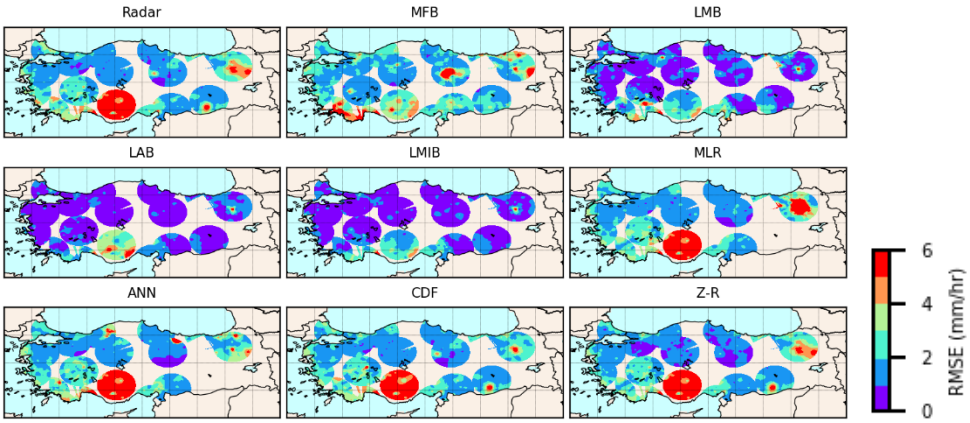

Figure 3.64 Spatial variation of RMSE (mm/hr) in fall

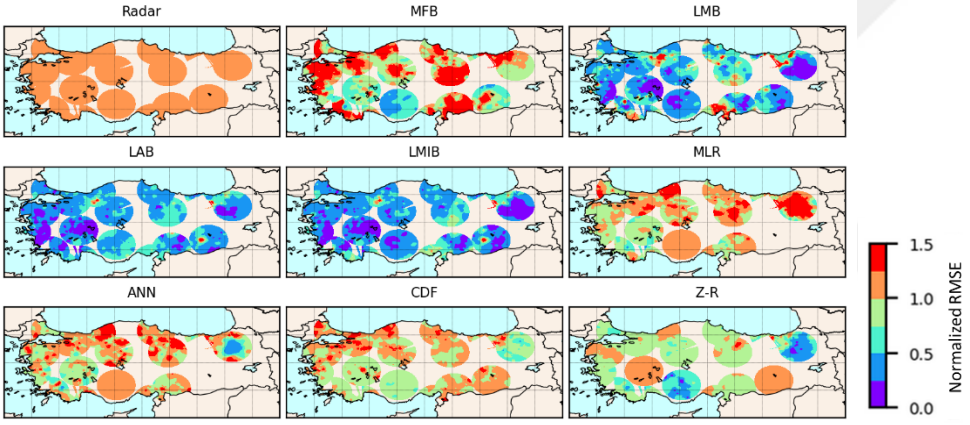

Figure 3.65 Spatial variation of Normalized RMSE in winter

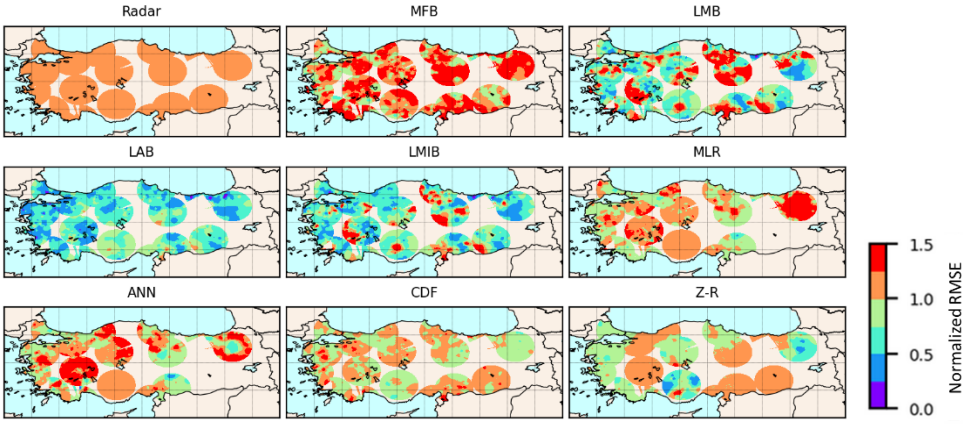

Figure 3.66 Spatial variation of Normalized RMSE in spring

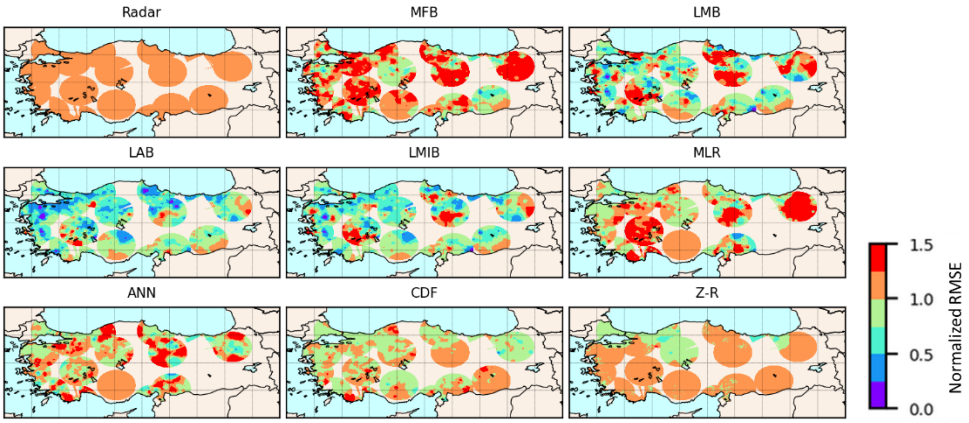

Figure 3.67 Spatial variation of Normalized RMSE in summer

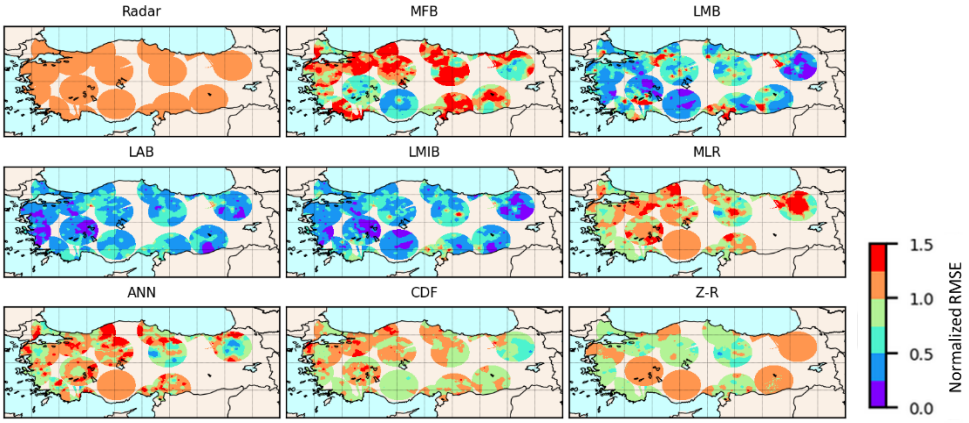

Figure 3.68 Spatial variation of Normalized RMSE in fall

CHAPTER 4

SUMMARY AND CONCLUSION

This chapter summarizes the main findings of the study, followed by conclusions drawn from the results section of the study.

4.1 Summary

A comprehensive radar network consisting of 17 C-band meteorological weather radars located over various regions have been installed in Turkey. Several studies have assessed the reflectivity and other radar-based products qualitatively. Yet, only a minority of them have focused on quantitative radar estimates. Even among these studies, they have been limited to a single methodology, radar location, and a limited number of precipitating events. One of the limiting reasons for the previous studies was the difficulty in accessing the radar data, which could only be read in the LINUX environment. The raw radar data was read in LINUX environment and stored in easily accessible formats in Windows environment. This data can be requested for access from GDM. The accessibility of these data will be an excellent opportunity for future studies. In contrast to the previous studies, the goal of this study is to analyze and develop various methodologies available in the literature, consisting of hourly gauge adjustment (MFB, LMB, LAB, LMIB) and time-independent bias correction (MLR, ANN, CDF, Z-R) and validate them on the radar network as a whole and over a long-term period.

The radar-based estimations were initially compared against about 1100 AWOS rain gauge observations. Furthermore, the performance of various bias correction methods, including gauge adjustment and time-independent methodologies, were cross-validated using independent validation gauges. Accordingly, a composite map

of both raw and statistically corrected radar data was composed based on all correction algorithms. The accuracy of this composite map was tested using 50 Triple-Collocated rain gauge stations over various regions. Finally, the accuracy of the corrected radar-based estimations was compared both seasonally and spatially over a long-term period. These analyses were followed by choosing a consistent methodology with the highest accuracy in producing a high-resolution radar-based precipitation map. The high-resolution precipitation maps produced in this study can be obtained from GDM. These maps will be a critical input in many future studies, such as the operational prediction of flash floods. Therefore, this research provides a significant contribution to the hydrology, meteorology, and water resources communities.

4.2 Conclusion

In the initial investigation of radar-based precipitation estimates, the radar estimations obtained from the majority of the radars have shown a generally good correlation (0.45-0.6) with the gauge-based observations (disregarding the time, location, and type of precipitating event). The lowest COR values belong to KRM, ERZ, and SRF. Most radars have an RMSE value between 2-4 mm/hr. KRM has the highest RMSE (near 10mm/hr). This shows there is a significant difference in this radar compared with the statistics of other radars, which could be due to hardware (e.g., transmitter malfunction) problems.

The most substantial limitation in the majority of the radars was shown to be the underestimation, which can happen due to beam blockage in regions with complex topography. In the scatterplots (Figure 3.48-3.54), it was shown that the underestimation rate is intensified in heavy rather than light precipitation events. An overall review of ME values indicates the underestimation of radars against ground observations in all radars except KRM and ERZ. The effect of beam blockage was investigated by measuring CBB-AV, which is the average CBB obtained from all elevation angles associated with each radar. It was shown that higher CBB-AV

results in lower percent biases, thus increasing the underestimation errors in radar-based estimations. Therefore, we used this parameter as a quality control factor in the final composite map and filtered out the radar-based estimations associated with CBB-AV of higher than 30%. Consequently, in the overlapping areas between two radars, the composite map uses the estimations from the radar, which has a CBB-AV rate of lower than this threshold. In overlapping areas where none of the radars pass this filter, the gauge-based observation interpolation is replaced in the composite map. CBB parameter was also used in measuring Hvmin, which was used as input in ANN and MLR models. Both the CBB-AV and Hvmin maps generated for the radar network in Turkey can be useful for operational decision making.

The relative performance of the bias correction methods was validated using four error statistics (ME, RMSE, COR, and ESD) over training and validation datasets using data obtained over five years (2014-2018). Confidence about the results obtained and selection of the best method among all methods was developed owing to the consistency of the error metrics over all mentioned datasets. The most significant difference in the performance of gauge adjustment and time-independent bias correction methods is the ability of the first set of methods to suppress the random errors. Although time-independent methods are stationary and do not change over time similar to gauge adjustment methods, they have shown to outperform simple field-based gauge adjustment method (MFB). Overall, local additive assumption of error distribution, LAB has shown to yield the best results among all eight methods by performing better in 16 out of 17 radars disregarding the season and type of precipitation. Based on results obtained from training and validation datasets, LAB can be reliably used as a reference method for improving the accuracy of radar-based estimates using the gauge-based observations in all radars situated in Turkey.

4.3 Recommendations for Future Research

The radar-based precipitation products are generated based on operational observation of weather by GDM and are not originally dedicated for research-based practices. Most of the decisions and changes made on the radar tasks, elevations, ranges, etc. are made based on operational policies according to the weather forecasting department. Thus, hardware/software limitations may affect the quality of the precipitation obtained by weather radars. However, the spatio-temporally higher resolution estimates provided by radars and the accuracy of precipitation obtained by both the bias-corrected radar product can carry a great potential which other gridded products may not. Radars have a limited area coverage [e.g., approximately about 70% of Turkey without considering the beam blocked areas, and 50% with considering the blocked areas (CBB-AV>=30%)]. However, when compared with other gridded precipitation products, the radar-based estimates yield much higher spatial resolution (up to 0.3 km). The best remote-sensing-based and NWP-based products can provide a spatial resolution of up to 10 and 3 km. Thus, intercomparison of the satellite-based and model-based products with the radar-based products over a region with a complex topography such as Turkey is suggested. Pursuing an in-depth comparison of these products may yield their biggest advantages and disadvantages over various regions and may give a better understanding in choosing the best alternative product which also can be used in the beam-blocked or blind areas in radar-based QPE.

The radar-based precipitation product used in this study is RAIN1, which is hourly accumulated precipitation estimation obtained by Marshall-Palmer's relationship as a default approach for reflectivity-precipitation conversion. For future studies, investigation of other radar-based products (e.g., CAPPI, RAW) is highly suggested. While RAIN1 data only provides 2-D precipitation estimates, RAW radar data provides 3-D reflectivity profile measured at various elevation angles. Such 3-D data can be used to better understand the effects of beam blockage over various elevation angles. Moreover, other reflectivity-based corrections such as attenuation correction

and clutter/echo filtering would be possible by using the RAW radar data, while current RAIN1 datasets have been only corrected using Doppler filtering and fast fourier transform correction that are implemented by the data-provider (Vaisala) built-in software. Utilizing and testing various polarimetric reflectivity algorithms such as KDP (specific differential phase) and ZDR (differential reflectivity) which can be implemented on multiple polarization radars (11 out of 17 C-band radars in Turkey are multiple polarization radars as shown in Table 1.1) is also suggested. These algorithms were not investigated in this study, and may provide more consistent estimates compared with normal radar reflectivity (Z).

In this study, eight bias correction methods were implemented and evaluated. However, other bias correction methods such as kriging is suggested to be investigated in the future studies. In addition to implementation of various other bias correction methods, the effects of rain gauge network density on the performance of these methodologies may also be investigated. Moreover, these bias correction methods were both generated and validated using gauge station data. However, indirect assessment of radar-gauge merged estimates may provide more information about the performance of these products. For example, utilizing the merged product in hydrologic (e.g., flow prediction), or hydraulic (e.g., water surface elevation prediction) models can also reveal the potential of radar-gauge merged and radar only precipitation estimates.

REFERENCES

Aditya Sai Srinivas, T. et al. 2019. "Estimating Rainfall Using Machine Learning Strategies Based on Weather Radar Data." *International Journal of Communication Systems* (November 2018): 1–11.

Afshar, M. H., and M. T. Yilmaz. 2017. "The Added Utility of Nonlinear Methods Compared to Linear Methods in Rescaling Soil Moisture Products." *Remote Sensing of Environment* 196: 224–37. http://dx.doi.org/10.1016/j.rse.2017.05.017.

Amjad, Muhammad, M Tugrul Yilmaz, Ismail Yucel, and Koray K Yilmaz. 2020. "Performance Evaluation of Satellite- and Model-Based Precipitation Products over Varying Climate and Complex Topography." *Journal of Hydrology* 584(February): 124707. https://doi.org/10.1016/j.jhydrol.2020.124707.

Anagnostou, Emmanouil N. 2004. "A Convective/Stratiform Precipitation Classification Algorithm for Volume Scanning Weather Radar Observations." *Meteorological Applications* 11(4): 291–300.

Arnaud, Patrick et al. 2011. "Sensitivity of Hydrological Models to Uncertainty in Rainfall Input." *Hydrological Sciences Journal* 56(3): 397–410.

Ayat, Hooman et al. 2018. "Calibration of Weather Radar Using Region Probability Matching Method (RPMM)." *Theoretical and Applied Climatology* 134(1–2): 165–76.

Barton, Yannick et al. 2020. "A Multi-year Assessment of Sub-hourly Gridded Precipitation for Switzerland Based on a Blended Radar—Rain-gauge Dataset." *International Journal of Climatology* (February).

Battan, Louis J. 1973. Quarterly Journal of the Royal Meteorological Society *Radar Observation of the Atmosphere*. University of Chicago Press. http://doi.wiley.com/10.1002/qj.49709942229.

Bech, Joan, Bernat Codina, Jeroni Lorente, and David Bebbington. 2003. “The Sensitivity of Single Polarization Weather Radar Beam Blockage Correction to Variability in the Vertical Refractivity Gradient.” *Journal of Atmospheric and Oceanic Technology* 20(6): 845–55.

Berne, A., and W. F. Krajewski. 2013. “Radar for Hydrology: Unfulfilled Promise or Unrecognized Potential?” *Advances in Water Resources* 51: 357–66. http://dx.doi.org/10.1016/j.advwatres.2012.05.005.

Bianchi, Blandine, Peter Jan Van Leeuwen, Robin J. Hogan, and Alexis Berne. 2013. “A Variational Approach to Retrieve Rain Rate by Combining Information from Rain Gauges, Radars, and Microwave Links.” *Journal of Hydrometeorology* 14(6): 1897–1909.

Blanchard, Duncan C. 1953. “RAINDROP SIZE-DISTRIBUTION IN HAWAIIAN RAINS.” *Journal of Meteorology* 10(6): 457–73. http://journals.ametsoc.org/doi/abs/10.1175/1520-0469%281953%29010%3C0457%3ARSDIHR%3E2.0.CO%3B2.

Brandes, Edward A. 1975. “Optimizing Rainfall Estimates with the Aid of Radar.” *Journal of Applied Meteorology* 14(7): 1339–45.

Calheiros, R. V., and I. Zawadzki. 1987. “Reflectivity-Rain Rate Relationships for Radar Hydrology in Brazil.” *Journal of Climate and Applied Meteorology* 26(1): 118–32. http://journals.ametsoc.org/doi/abs/10.1175/1520-0450%281987%29026%3C0118%3ARRRRFR%3E2.0.CO%3B2.

Chiang, Yen Ming, Fi John Chang, Ben Jong Dao Jou, and Pin Fang Lin. 2007. “Dynamic ANN for Precipitation Estimation and Forecasting from Radar Observations.” *Journal of Hydrology* 334(1–2): 250–61.

Collier, Christopher G. 2016. *Hydrometeorology (Advancing Weather and Climate Science) 1st Edition*. Wiley-Blackwell; 1 edition (July 25, 2016).

Crisologo, Irene. 2016. “How Mountains Can Affect Radar Signals.”

https://philippineradarnetwork.wordpress.com/2016/05/18/radar-beam-blockage/.

Crisologo, Irene, Robert A. Warren, Kai Mühlbauer, and Maik Heistermann. 2018. "Enhancing the Consistency of Spaceborne and Ground-Based Radar Comparisons by Using Beam Blockage Fraction as a Quality Filter." *Atmospheric Measurement Techniques* 11(9): 5223–36.

Cyr, Isabel. 2014. "Estimation of Z-R Relationship and Comparative Analysis of Precipitation Data from Colocated Rain-Gauge , Vertical Radar and Disdrometer." : 90.

Gabella, M., and E. Amitai. 2000. "Radar Rainfall Estimates in an Alpine Environment Using Different Gage-Adjustment Techniques." *Physics and Chemistry of the Earth, Part B: Hydrology, Oceans and Atmosphere* 25(10–12): 927–31.

Gabella, Marco, Jürg Joss, and Giovanni Perona. 2000. "Optimizing Quantitative Precipitation Estimates Using a Noncoherent and a Coherent Radar Operating on the Same Area." *Journal of Geophysical Research Atmospheres* 105(D2): 2237–45.

Gilewski, Pawel, and Marek Nawalany. 2018. "Inter-Comparison of Rain-Gauge, Radar, and Satellite (IMERG GPM) Precipitation Estimates Performance for Rainfall-Runoff Modeling in a Mountainous Catchment in Poland." *Water (Switzerland)* 10(11): 1–23.

Goudenhoofdt, E, and L Delobbe. 2009. "Evaluation of Radar-Gauge Merging Methods for Quantitative Precipitation Estimates." *Hydrology and Earth System Sciences* 13: 195–203.

Gunn, K. L. S., and J. S. Marshall. 1958. "THE DISTRIBUTION WITH SIZE OF AGGREGATE SNOWFLAKES." *Journal of Meteorology* 15(5): 452–61.

Gürbüz, Sevgi Zübeyde, and Uğur Oğuz. 2015. "Polarimetrik Radarlarda

Meteorolojik Olmayan Eko Ayırımı.” In *UZALMET 2015*, Antalya, 223–30.

Hazer, Aytaç, and Erkan Afacan. 2016. “ACHIEVEMENTS OF REFLECTIVITY - RAINFALL RATE CONVERSION COEFFICIENTS FOR 8 RADARS OF TSMS.” *ERAD*: 28.

Hazer, Aytaç, and Nurullah Kara. 2017. “Meteoroloji Radar Ağında , Z - R İlişkisindeki A ve B Katsayılarının Bulunması ve Bunların Radara Uygul Anarak Sonuçların Yer Gözlemi Yle Karşılaştırılması.” *Uzalmet*. http://uzalmet.mgm.gov.tr/tammetin/21.pdf.

Heistermann, M., S. Jacobi, and T. Pfaff. 2013. “Technical Note: An Open Source Library for Processing Weather Radar Data (Wradlib).” *Hydrology and Earth System Sciences* 17(2): 863–71.

Hunter, Steven M. 1996. “WSR-88D Radar Rainfall Estimation: Capabilities, Limitations and Potential Improvements.” *National Weather Service Office* 20: 26–36. http://www.srh.noaa.gov/mrx/research/precip/precip.php.

Jewell, Sharon A., and Nicolas Gaussiat. 2015. “An Assessment of Kriging-Based Rain-Gauge-Radar Merging Techniques.” *Quarterly Journal of the Royal Meteorological Society* 141(691): 2300–2313.

Jing, Wang et al. 2008. “Classification of Precipitation Radar Reflectivity Echo with Back-Propagation ANN.” *Proceedings - 2008 Pacific-Asia Workshop on Computational Intelligence and Industrial Application, PACIIA 2008* 2: 630–33.

Joss, J. 1970. *On the Quantitative Determination of Precipitation by Radar*. City-Druck, 1970. https://books.google.com.tr/books?id=njqnGwAACAAJ.

Kucera, Paul A., Witold F. Krajewski, and C. Bryan Young. 2004. “Radar Beam Occultation Studies Using GIS and DEM Technology: An Example Study of Guam.” *Journal of Atmospheric and Oceanic Technology* 21(7): 995–1006.

Larson, Lee W., and Eugene L. Peck. 1974. “Accuracy of Precipitation

Measurements for Hydrologic Modeling." *Water Resources Research* 10(4): 857–63.

Lauri, Tuomo, Jarmo Koistinen, and Dmitri Moisseev. 2012. "Advection-Based Adjustment of Radar Measurements." *Monthly Weather Review* 140(3): 1014–22.

Lazri, M. et al. 2012. "Identifying Convective and Stratiform Rain by Confronting SEVERI Sensor Multispectral Infrared to Radar Sensor Data Using Neural Network." *Sensors and Transducers* 145(10): 19–32.

Lee, J.-K., J.-H. Kim, and M.-K. Suk. 2015. "Application of Bias Correction Methods to Improve the Accuracy of Quantitative Radar Rainfall in Korea." *Atmospheric Measurement Techniques Discussions* 8(4): 4011–47.

Lengfeld, Katharina et al. 2020. "Use of Radar Data for Characterizing Extreme Precipitation at Fine Scales and Short Durations." *Environmental Research Letters* (June).

Liu, H., V. Chandrasekar, and G. Xu. 2001. "An Adaptive Neural Network Scheme for Radar Rainfall Estimation from WSR-88D Observations." *Journal of Applied Meteorology* 40(11): 2038–50.

Mahavik, Nattapon. 2017. "Bias Adjustments of Radar Rainfall during Seasonal March of the Summer Monsoon in the Middle Of." 12(4): 577–94.

Marshall, J. S., and W. Mc K. Palmer. 1948. "THE DISTRIBUTION OF RAINDROPS WITH SIZE." *Journal of Meteorology*.

McKee, Jack L., and Andrew D. Binns. 2016. "A Review of Gauge–Radar Merging Methods for Quantitative Precipitation Estimation in Hydrology." *Canadian Water Resources Journal* 41(1–2): 186–203. http://dx.doi.org/10.1080/07011784.2015.1064786.

Moghim, Sanaz, and Rafael L. Bras. 2017. "Bias Correction of Climate Modeled Temperature and Precipitation Using Artificial Neural Networks." *Journal of*

Hydrometeorology 18(7): 1867–84.

Morin, Efrat et al. 2003. “Estimating Rainfall Intensities from Weather Radar Data: The Scale-Dependency Problem.” *Journal of Hydrometeorology* 4(5): 782–97.

Overeem, Aart, Iwan Holleman, and Adri Buishand. 2009. “Derivation of a 10-Year Radar-Based Climatology of Rainfall.” *Journal of Applied Meteorology and Climatology* 48(7): 1448–63.

Ozkaya, Arzu, and Zuhal Akyurek. 2019. “Evaluating the Use of Bias-Corrected Radar Rainfall Data in Three Flood Events in Samsun, Turkey.” *Natural Hazards* (0123456789). https://doi.org/10.1007/s11069-019-03723-z.

Ozturk, Kurtulus, Firat Bestepe, and Mehmet Zeybek. 2012. “Improving the Accuracy of Time-Cumulated Radar-Based Rainfall Estimates in the Event of a Flood.” 1(1): 2012.

Öztürk, Kurtuluş, and Alper Çubuk. 2015. “Meteoroloji Radarlarında Kullanılan Farklı Yağış Hesaplama Yöntemlerinin Tutarlılık Analizi.” In *UZALMET*, , 260–70.

Öztürk, Kurtuluş, and Ali Ulvi Yilmazer. 2007. “Improving the Accuracy of the Radar Rainfall Estimates Using Gage Adjustment Techniques: Case Study for West Anatolia, Turkey.” *Atmospheric Research* 86(2): 139–48.

Öztürk, Kurtuluş, and Mehmet Zeybek. 2013. “Meteoroloji Radarları Yağış Veri Kalitesinin Yükseltilmesi.” In *UZALMET 2013*, , 160–76.

P. Yousefi, Kaveh et al. 2020. “Production of a High-Resolution Improved Radar Precipitation Estimation Map Using Gauge Adjustment Bias Correction Methods.” In *EGU2020*, EGU Sharing Geosciences Online.

Park, Shinju, Marc Berenguer, and Daniel Sempere-Torres. 2019. “Long-Term Analysis of Gauge-Adjusted Radar Rainfall Accumulations at European Scale.” *Journal of Hydrology* 573(November 2018): 768–77. https://doi.org/10.1016/j.jhydrol.2019.03.093.

Piman, T., M. S. Babel, A. Das Gupta, and S. Weesakul. 2007. “Development of a Window Correlation Matching Method for Improved Radar Rainfall Estimation.” *Hydrology and Earth System Sciences* 11(4): 1361–72.

Rabiei, E., and U. Haberlandt. 2015. “Applying Bias Correction for Merging Rain Gauge and Radar Data.” *Journal of Hydrology* 522: 544–57. http://dx.doi.org/10.1016/j.jhydrol.2015.01.020.

Rahimi, A. R. et al. 2006. 23 Journal of Atmospheric and Oceanic Technology *Attenuation Calibration of an X-Band Weather Radar Using a Microwave Link*.

Rosenfeld, D., D. Atlas, and D. A. Short. 1990. “The Estimation of Convective Rainfall by Area Integrals 2. The Height-Area Rainfall Threshold (HART) Method.” *Journal of Geophysical Research* 95(D3): 2161–76.

Rosenfeld, D., D. B. Wolff, and E. Amitai. 1994. “The Window Probability Matching Method for Rainfall Measurements with Radar.” *Journal of Applied Meteorology* 33(6): 682–93.

Sahlaoui, Zahra, and Soumia Mordane. 2019. “Radar Rainfall Estimation in Morocco: Quality Control and Gauge Adjustment.” *Hydrology* 6(2): 41. https://www.mdpi.com/2306-5338/6/2/41.

Schilling, Wolfgang. 1991. “Rainfall Data for Urban Hydrology: What Do We Need?” *Atmospheric Research* 27(1–3): 5–21.

Sekhon, R. S., and R. C. Srivastava. 1970. “Snow Size Spectra and Radar Reflectivity.” *Journal of the Atmospheric Sciences* 27(2): 299–307.

Shakti, P. C., Tsuyoshi Nakatani, and Ryohei Misumi. 2019. “The Role of the Spatial Distribution of Radar Rainfall on Hydrological Modeling for an Urbanized River Basin in Japan.” *Water (Switzerland)* 11(8): 6–8.

Sharifi, Ehsan, Reinhold Steinacker, and Bahram Saghafian. 2016. “Assessment of GPM-IMERG and Other Precipitation Products against Gauge Data under

Different Topographic and Climatic Conditions in Iran: Preliminary Results." *Remote Sensing* 8(2).

Sinclair, Scott, and Geoff Pegram. 2005. "Combining Radar and Rain Gauge Rainfall Estimates Using Conditional Merging." 22(February): 19–22.

Sokol, Zbyněk. 2003. "Utilization of Regression Models for Rainfall Estimates Using Radar-Derived Rainfall Data and Rain Gauge Data." *Journal of Hydrology* 278(1–4): 144–52.

Song, Yang, Dawei Han, and Miguel A. Rico-Ramirez. 2016. "High Temporal Resolution Rainfall Information Retrieval from Tipping-Bucket Rain Gauge Measurements." *Procedia Engineering* 154(June 2017): 1193–1200. http://dx.doi.org/10.1016/j.proeng.2016.07.525.

Suk, Mi-Kyung, Ki-Ho Chang, Joo-Wan Cha, and Kyung-Eak Kim. 2013. "Operational Real-Time Adjustment of Radar Rainfall Estimation over the South Korea Region." *Journal of the Meteorological Society of Japan. Ser. II* 91(4): 545–54.

Teschl, Reinhard, Walter L. Randeu, and Franz Teschl. 2007. "Improving Weather Radar Estimates of Rainfall Using Feed-Forward Neural Networks." *Neural Networks* 20(4): 519–27.

Tiron, Gina, and Steluţa Gosav. 2010. "The July 2008 Rainfall Estimation from Barnova WSR-98 D Radar Using Artificial Neural Network." *Romanian Reports in Physics* 62(2): 405–13.

Wang, Haijiang, Yuanbo Ran, Yangyang Deng, and Xu Wang. 2017. "Study on Deep-Learning-Based Identification of Hydrometeors Observed by Dual Polarization Doppler Weather Radars." *Eurasip Journal on Wireless Communications and Networking* 2017(1).

Wardhana, A, H Pawitan, and B D Dasanto. 2017. "Application of Hourly Radar-Gauge Merging Method for Quantitative Precipitation Estimates." In *IOP*

Conf. Series: Earth and Environmental Science, , 1–72.

Wei, Chih Chiang, and Po Yu Hsieh. 2020. "Estimation of Hourly Rainfall during Typhoons Using Radar Mosaic-Based Convolutional Neural Networks." *Remote Sensing* 12(5): 1–19.

WMO. 2008. 6th editio WMO-No. 168 *Guide to Hydrological Practices. Volume I: Hydrology–From Measurement to Hydrological Information*.

Xiao, Rongrui, V. Chandrasekar, and Hongping Liu. 1998. "Development of a Neural Network Based Algorithm for Rainfall Estimation from Radar Observations." *IEEE Transactions on Geoscience and Remote Sensing* 36(3): 716–24.

Yilmaz, Koray K. et al. 2005. "Intercomparison of Rain Gauge, Radar, and Satellite-Based Precipitation Estimates with Emphasis on Hydrologic Forecasting." *Journal of Hydrometeorology* 6(4): 497–517.

Zhang, Jian et al. 2011. "National Mosaic and Multi-Sensor QPE (NMQ) System Description, Results, and Future Plans." *Bulletin of the American Meteorological Society* 92(10): 1321–38.

Zhang, Jian, Youcun Qi, Carrie Langston, and Brian Kaney. 2012. "Radar Quality Index (RQI) - A Combined Measure for Beam Blockage and VPR Effects in a National Network." *IAHS-AISH Publication* 351(April): 388–93.

Zhang, Xuesong, and Raghavan Srinivasan. 2010. "GIS-Based Spatial Precipitation Estimation Using next Generation Radar and Raingauge Data." *Environmental Modelling and Software* 25(12): 1781–88. http://dx.doi.org/10.1016/j.envsoft.2010.05.012.